A Statistical Theory of the Epilepsies

by

Kuryan Thomas

Dissertation submitted to the Faculty of the
Virginia Polytechnic Institute and State University
in partial fulfillment of the requirements for the degree of
Doctor of Philosophy
in
Physics

APPROVED:

Samuel P. Bowen, Chairman

Richard A. Arndt

John R. Ficenec

Guy J. Indebetouw

L. David Roper

August, 1988
Blacksburg, Virginia

A Statistical Theory of the Epilepsies

by

Kuryan Thomas

Samuel P. Bowen, Chairman

Physics

(ABSTRACT)

A new physical and mathematical model for the epilepsies is proposed, based on the theory of bond percolation on finite lattices. Within this model, the onset of seizures in the brain is identified with the appearance of spanning clusters of neurons engaged in the spurious and uncontrollable electrical activity characteristic of seizures. It is proposed that the fraction of excitatory to inhibitory synapses can be identified with a bond probability, and that the bond probability is a randomly varying quantity displaying Gaussian statistics. The consequences of the proposed model to the treatment of the epilepsies is explored.

The nature of the data on the epilepsies which can be acquired in a clinical setting is described. It is shown that such data can be analyzed to provide preliminary support for the bond percolation hypothesis, and to quantify the efficacy of anti-epileptic drugs in a treatment program. The results of a battery of statistical tests on seizure distributions are discussed.

The physical theory of the electroencephalogram (EEG) is described, and extant models of the electrical activity measured by the EEG are discussed, with an emphasis on their physical behavior. A proposal is made to explain the difference between the power spectra of electrical activity measured with cranial probes and with the EEG. Statistical tests on the characteristic EEG manifestations of epileptic activity are conducted, and their results described.

Computer simulations of a correlated bond percolating system are constructed. It is shown that the statistical properties of the results of such a simulation are strongly suggestive of

the statistical properties of clinical data.

The study finds no contradictions between the predictions of the bond percolation model and the observed properties of the available data. Suggestions are made for further research and for techniques based on the proposed model which may be used for tuning the effects of anti-epileptic drugs.

Acknowledgements

I dedicate this work to my father and mother, Vetecheril Thomas and Aleyamma Kuryan Thomas, who instilled in me the desire to better myself through learning.

While doing my research and writing my dissertation, I had help from many friends and relatives. A list like this does not repay my debt to them, but it demonstrates that this dissertation would not be written without their support.

Thanks, therefore, in approximately alphabetic order to:

- Sam Bowen for his friendship and guidance. Every graduate student should have an advisor like Sam. We have many conversations on a wide range of topics, but I will always remember with particular gratitude the conversation we had on September 21, 1987. He also keeps a large supply of writing implements for people who forget to bring pens to meetings.
- Ms. Glenda Garner and the other staff of the Epilepsies Clinic at the Bowman-Gray School of Medicine at Wake Forest University, for providing me with large amounts of data from the clinic's databases.
- Dr. Jean Gotman of the Montreal Neurological Institute for providing the EEG data.
- John Earl Gray, the scholar from Oxford, for his books and conversations. He trounced me so soundly in chess that I quit playing chess and started doing my research.

- Jim and Janet Meyer for their support. With every conversation we have, we come closer to solving the world's problems.

- Jim Muth and Kelly Flynn, for their friendship. Jim taught me how to craft computer programs: before I worked with him, I wrote programs that I cannot bear to look at any more. Keep those functions short, Jim.

- Dr. J. Kiffin Penry and Martin Penry of Epilepsy Information, Inc. in Winston-Salem, North Carolina, and Abbott Laboratories of Chicago, Illinois, for purchasing all the computer hardware and software used on this project. I was provided *carte blanche* at the start of the program to buy any such equipment I wanted, and I was able with their help to assemble a microcomputer-based UNIX™ system. There is no better environment for creative research. Dr. Penry also made available to me his considerable expertise and experience in the treatment of the epilepsies.

- All the members of my committee for their tolerance during a difficult time for me.

- Dave Roper for serving on my committee and helping me with many problems, personal and computer-related (occasionally both).

- My brother Dr. Benku Thomas for a lifetime of his interest, humor, and support. Not to mention his Hewlett-Packard LaserJet II.

- Dr. Royce Zia for helpful discussions on nucleation theory and the dynamics of cluster formation in percolating systems, and for reviewing my dissertation and coming to my research defense on short notice.

- Christa Charlotte Hannelore Dolores, for everything.

Contents

List of Figures

List of Tables

Chapter 1

Introduction

This dissertation describes the statistical properties of the epilepsies and investigates the hypothesis that the epilepsies are a manifestation of the modern physical theory of percolation. The model proposed suggests that epileptic seizures are the appearance of spanning percolating clusters of electrical activity in the brain.

Percolation theory has its origins in the work of Hammersley [32] and has been applied to studies of disease propagation, semiconductor theory and various other fields. Two examples of percolation phenomena in nature are the study of water flowing through loosely packed soil (from which the theory's name derives) and the spread of fires in a sparse forest.

The epilepsies are defined by Delgado-Escueta *et al.* [18] as

> recurrent convulsive and non-convulsive seizures, which are caused by partial or generalized epileptogenic discharges in the cerebrum.

The effects of an epileptic seizure on a human vary from brief losses of consciousness, possibly with no outward signs, to violent muscular spasms, the popular impression of the "epileptic

fit." Most people with epilepsy can live a normal life with seizures controlled effectively by anti-epileptic drugs. But for the few who suffer from a chronic untreatable epilepsy, life can be very difficult. Research in the epilepsies is essential to improve the quality of life for such patients.

The motivation for this research is to combine the perspective of computational physics with the accumulated data from the medical studies of the epilepsies to create new theoretical constructs and tools that may ultimately lead to better treatment. Part of this dissertation will describe the data that are available to a physical science study of the epilepsies. Preliminary studies of the application of percolation theory to the epilepsies are then described.

Chapter 2

Background

In any discussion of the epilepsies, it is impossible to avoid numerous references to the anatomy of the central nervous system of the human and to the cellular mechanisms by which information is transmitted in the central nervous system. It is, of course, also necessary to be familiar with the vocabulary used by researchers in the epilepsies. This chapter presents an overview of these topics for physical scientists.

2.1 Neurology

2.1.1 The Central Nervous System

The Central Nervous System, or CNS, is the seat of all motor and sensory functions of the human being. It is divided into two main parts: the spinal cord, which acts as a central "trunk line" for nerves running from the brain to the rest of the body, and the brain itself. Because the epilepsies manifest themselves entirely in the brain, it is not necessary for the purpose at hand to discuss the structure of the spinal cord.

Macro structure of the human brain

The human brain is anatomically divided into the following sections [49]:

Medulla oblongata: Little more than a swelling at the top of the spinal cord, it is the seat of the automotor activities such as heartbeat.

Cerebellum: Two small elongated areas lying to the rear of the medulla oblongata. It receives signals from the equilibrium sensors in the middle ear, from the tactile sensors in the skin, and from the eyes. It is responsible for low level signal processing and for maintaining equilibrium.

Thalamus: A small egg-shaped region above the medulla through which all sensory nerve impulses are relayed on their way to the processing areas of the higher brain.

Cerebrum: This is the large hemispherical region of the brain that lies immediately below the skull, and is the seat of voluntary motor activity, sensory processing, and cognition. It is also responsible in humans for the higher functions of language processing, memory, and time and interval logic.

There are several terms commonly used to locate parts of the brain: They are summarized in Table 1.

The micro structure of the human brain

The cerebrum is comprised of two different types of tissue: white matter and grey matter. The grey matter is towards the surface of the brain, forming the region known as the cortex. This is the specific area responsible for the higher functions of human brains. The white matter lies interior to the grey matter and seems to be responsible for connecting parts of the cortex with different functions to each other [67].

Table 1: **Common positional terms and their definitions.**

Anterior	Towards the front of the body (i.e., towards the eyes).
Posterior	Towards the back of the body (i.e., away from the eyes).
Temporal	The part of the brain directly in from the ears.
Parietal	The part of the brain just above and behind the temporal area.
Frontal	The part of the brain directly behind the eyes.

On a microscopic level, the cerebrum is comprised of billions of nerve cells held together by a connective tissue known as the *glia*. The cerebral cortex consists of two types of neurons:

The pyramidal cells: These are cells that serve to transmit information from the grey matter to the white matter and back.

The local cells: Further divided into the stellate and Martinotti varieties, these cells are responsible for local interactions within the cortex.

2.1.2 Neurons

As described above, the cerebrum is made up of many billions of nerve cells, or neurons. Neurons comprise the electrical circuitry of the brain—they generate the electrical impulses responsible for all brain function, and they pass the activity on from one to another in a coordinated fashion.

Anatomy of neurons

Neurons are basically tree-shaped cells. A long *axon* extends outwards from the central nucleus, terminating in a branched set of *axon terminals*. On the opposite end of the nucleus from the axon are the *dendrites*. Connections from one neuron to another are made by *synapses*. There is a cleft separating one cell from another across the synapse, ranging from 2 to 20 nm [49]. Nerve impulses arrive at a synapse and are transmitted to the next neuron either electrically or chemically. This anatomy is most characteristic of the pyramidal cells. The stellate local cells are more "branchy," with no well-defined axon.

The branching surface of the neuron accounts for almost 90% of the surface area of a cell [63]. Branching surfaces are typically very close to the actual cell body: the number of branches $B_n(r)$ intersecting a sphere of radius r centered on the cell body is approximately [63]

$$B_n(r) \sim e^{-\lambda r}, \tag{2.1}$$

with $\lambda \simeq 350\,\mathrm{cm}^{-1}$.

The mechanism of neuron transmission

Neurons conduct electrical impulses using an electrochemical mechanism discovered by Hodgkin and Huxley [33]. A neuron lies embedded in a bath of ions. When the neuron is in a passive state (that is, not firing), it maintains a *resting potential* between the inside of its outermost membrane and its surroundings. This potential is on the order of 70 mV [49,94].

When an electrical impulse arrives at a synapse from a neighboring neuron, chemicals are released in the synaptic cleft. These chemicals diffuse across the cleft to the resting cell, where they affect the permeability of the membrane to Na^+ ions.

If the chemical composition of a synapse is such that the transmitter chemicals increase the permeability of the resting membrane to Na^+ ions, the synapse is said to be *depolarizing* or *excitatory*. In this case, the resting membrane begins to admit Na^+ ions from the surrounding ion bath, resulting in an increase in the concentration of positive ions inside the membrane. This in turn means that the transmembrane potential increases (becomes less negative). This is the excitatory postsynaptic potential, or EPSP. If there is a sufficient number of excitatory synapses all contributing their EPSP's to the resting neuron, the transmembrane potential in the resting neuron increases to a certain critical level, at which the cell membrane becomes almost completely permeable to Na^+ ions. The resulting incoming rush of Na^+ ions drives the potential across the membrane up to about 40 mV [49,94] with the inside positive with respect to the outside.

At this point, only a small area of neuron adjacent to the synapse is excited. Because of the difference in transmembrane potential between this area and the surrounding resting areas, small eddy currents begin to flow in the surrounding ion bath. These currents tend to depolarize the surrounding areas of the neuron, which in turn undergo a critical transition and become excited. By this time, the initially excited area adjacent to the synapse has

been restored to resting potential by the action of ion pumps inside the neuron which force out the Na^+ ions. In this manner, a pulse of positive transmembrane potential flows across the neuron, forming an electrical impulse. After a neuron fires, it cannot fire again for a period known as the *absolute refractory period.* This period lasts about 1 ms, which means that a neuron cannot fire at a rate larger than about 1 kHz [49].

Excitatory synapses generate chemicals such as acetylcholine, which tend to depolarize the neighboring resting neuron. Some synapses, called *inhibitory* or *hyperpolarizing* synapses, release chemicals such as γ-aminobutyric acid (GABA), which increase the permeability of neuron membranes to K^+ ions but not to Na^+ ions [49]. Because K^+ ions are more concentrated inside the neuron, the reduced permeability causes them to flow out of the neuron and to the surroundings, leaving behind the negatively charged protein molecules to which they were bound. This causes the transmembrane potential to decrease (become more negative). This is called an inhibitory postsynaptic potential or IPSP—inhibitory because it causes the resting neuron to become more resistant to the depolarizing effects of any EPSP's that may arrive at the same time.

In this way, EPSP's and IPSP's sum up at a resting neuron. If the EPSP's outweigh the IPSP's, the resting neuron fires and transmits the impulse on to its neighbors. Thus, a cell firing does not necessarily cause all of its neighbors to fire as well. Some neurons fire for the purpose of inhibiting their neighbors.

A detailed study of the cytochemistry of neuron transmission is given by Roberts [81], who also discusses the role of GABA as a neuron inhibitor.

2.2 The epilepsies

There is no such thing as "epilepsy." Rather, there are a group of symptoms, collectively called the epilepsies. They are symptoms of brain dysfunction that display two characteristic

features: paroxysmal and disorderly neuron activity (a *seizure*), and the ability of the affected neurons to recruit other neurons, resulting in a spread of the seizure [70,18]. The particular brain dysfunction that triggers the seizure can be anything from severe traumatic brain injury to extreme heat.

The important thing to note is that a seizure is not necessarily the result of an illness—even a "normal" person can have a seizure if extremely excited or exposed to adverse environmental conditions. Some drugs, such as penicillin, can also induce seizures.

The epilepsies are classified according to a scheme known as the International Classification of Epilepsies and Epileptic Syndromes [71]. More important to this work is the International Classification of Epileptic Seizures, which places different seizures into classes defined by the origin and extent of the seizures. Table 2 summarizes the classes, giving the acronyms for the seizures that will be used throughout this work.

The epilepsies are treated by administering anti-epileptic drugs (AED's). The typical treatment regimen consists of multiple daily doses of one or more AED's, taken throughout the day in varying amounts. This strategy is designed to keep up the level of AED in the bloodstream, on the theory that the more AED in the bloodstream, the more AED is getting into the brain. Physicians study the effects of the prescribed AED's and tune the dosages and timing of the drugs so that the treatment is deemed most effective.

Traditionally, a large battery of different AED's are administered. Each drug treats a different symptom of the illness. This method is falling out of favor, to be replaced by the more selective strategy of monotherapy [69]. Monotherapy involves prescribing just one drug that treats as many symptoms as possible—the benefits include better compliance because the patient has fewer drugs to remember to take, and a reduced load on the patient's kidneys.

AED's such as phenobarbital used in traditional treatments work by depressing the levels of brain activity. The unpleasant side-effects of such treatment include impaired motor and

Table 2: **The International Classification of Epileptic Seizures.** Adapted from [71].

Category	*Subcategories*	*Acronyms*
Partial[a]	Simple partial seizure[b]	SPS
	Complex partial seizure[c]	CPS
Generalized[d]	Absence	ABS
	Myoclonic jerk seizures	MJS
	Clonic seizures	
	Tonic seizures	
	Tonic-Clonic seizures	GTC
	Atonic seizures	
Unclassified	All other types	

[a]Involving only a local area of the brain.

[b]No loss of consciousness.

[c]Accompanied by loss of consciousness.

[d]Spread to involve diverse areas of the brain.

cognitive faculties [72]. These drugs have been abandoned by more progressive physicians in favor of more selective drugs such as carbamazepine and valproic acid, which act by influencing the levels of excitatory versus inhibitory chemicals in the brain [72]. Valproic acid, under the trade name Depakote, is showing much promise as a monotherapy drug [69].

Chapter 3

Percolation and the epilepsies

3.1 Percolation theory

3.1.1 Review of percolation theory applications

Since the original work on percolation theory by Hammersley [32], the theory has been applied to a wide range of phenomena which display critical transitions. For example, Jouhier *et al.* [38] have applied percolation theory to a statistical description of the sol-gel transition, while Grest and Cohen [30] have applied the theory to the liquid-glass transition. Outside the field of solid-state physics, Schulman and Seiden [86] have derived a model for the formation of galaxies using a directed bond percolation model. They show that the arms in spiral galaxies result from the critical percolation transition. Zallen [99] gives a list of physical phenomena that are percolative processes.

3.1.2 Theoretical overview of percolation

Kinds of problems that percolation theory is applied to

The simplest statement of the quest of percolation theory is this:

> Given a system consisting of a number of sites arranged in a lattice and some phenomenon that randomly involves more than one of the sites, how does the phenomenon spread through the lattice?

Take two examples:

- A forest of trees arranged in a two-dimensional square lattice, with the phenomenon being fire. If there exists some probability that the fire spreads from one tree to another, how does the fire spread through the forest? This is an example of *site* percolation, which deals with a phenomenon that acts on each site of the lattice.

- The percolation of water through a three-dimensional lattice of spheres. This is a reasonable model for the way in which water percolates through loosely packed soil. There is a certain probability that a channel exists between any two spheres, through which the water can flow. What is the path taken by water that is poured over the top of the assembly of spheres? Does any water make it all the way through the spheres? This example illustrates *bond* percolation, which attempts to describe the propagation of phenomena that are better described as a connection between two sites of the lattice. In this example, the connection is the existence of the channel.

Clerc *et al.* [10] give an excellent introduction (in French) to percolation theory and its predictions. Stauffer [92] gives a less detailed overview in English of the same material.

The predictions of percolation theory

When percolation theory is applied to problems such as those discussed above, it yields descriptions of the behavior of *clusters* on the lattice. Clusters are groups of nearest-neighbor sites in the lattice that are affected by the lattice phenomenon. For example, in a forest fire, a cluster consists of a set of nearest-neighbor trees all of which are burning. In the water percolation problem, a cluster consists of a group of nearest-neighbor particles all of which have channels between them.

The fundamental parameter of all percolating clusters is the *occupation probability* for site-percolating systems or the *bond fraction* for bond-percolating systems. (To avoid much duplication of terminology for both types of percolation, the discussion will be restricted to bond percolation.) The bond fraction p is simply the fraction of all sites in a lattice that are connected by bonds.

The first and most important prediction of percolation theory is that there exists a certain critical bond fraction p_c at which a cluster forms that spans the entire lattice (this is strictly true only for infinite clusters, as will be seen shortly). It can be shown [92,99] that the average cluster size (the average number of sites that are in a cluster—the "mass" of the cluster) in a percolating system obeys

$$\langle S \rangle \sim \frac{1}{|p - p_c|^{\gamma}} \tag{3.1}$$

as $p \rightarrow p_c$. The average cluster size on the lattice grows rapidly as a p approaches p_c.

What is somewhat surprising at first sight is that p_c need not be very large. Table 3 shows p_c for various lattice geometries, from which it is apparent that the more "complex" the lattice structure, the lower p_c gets.

Another important quantity in percolation theory is the *spanning distance* ξ. This is analogous to the average radius of a cluster, and is given by [92]

$$\xi = \frac{1}{|p - p_c|^{\nu}}. \tag{3.2}$$

Table 3: **p_c for various lattice geometries.** From [92]. Note that p_c depends on whether the percolation is site or bond.

Lattice	Site	Bond
Honeycomb	0.6962	0.65271
Square	0.59275	0.50000
Triangular	0.50000	0.34729
Diamond	0.428	0.388
Simple cubic	0.3117	0.2492
BCC	0.245	0.1785
FCC	0.198	0.119

When $p \sim p_c$, the spanning distance (or *correlation length*, as it is often called) exceeds the linear dimension of the lattice, resulting in the appearance of the infinite or spanning clusters.

3.1.3 The critical transition and beyond

The infinite cluster

When p exceeds p_c, there exists on an infinite lattice a spanning cluster—the mean cluster size has diverged. The measure of the spanning cluster in this region of p is the *order parameter*, P, also called the strength of the infinite cluster. It is the probability that any site on the lattice, chosen at random, is part of the infinite cluster. P obeys the general relationship [92]

$$P \propto (p - p_c)^{\beta} \tag{3.3}$$

for $p > p_c$.

The structure of the incipient infinite cluster

Equation 3.3 shows that just above p_c, the infinite cluster exists but does not involve a large fraction of the lattice sites. The structure of the cluster above p_c has been described by Mandelbrot [53] using his theory of fractal dimensions [54]. He shows that the fractal dimensionality of clusters when p is far above p_c is the dimensionality of the lattice itself. But for p just above p_c, the clusters are of lower dimensionality than the lattice in which they are embedded. Stanley and Coniglio [91] give a value of 2.5 for the dimensionality of a weak cluster on a three dimensional lattice. They show that the fractal dimension of the cluster goes as

$$D_c \sim d - \frac{\beta}{\nu}, \tag{3.4}$$

Another approach to the structure of the incipient cluster has been that of Pike and Stanley [77]. They performed a Monte Carlo simulation of a bond percolating square lattice and discovered that the incipient cluster is defined by three types of bonds which they term red, blue, and yellow. Red bonds form a backbone of the incipient cluster: breaking the red bonds causes the cluster to drop into subcritical behavior. Blue bonds also lie in the backbone of the cluster, but lie in "blobs" on the backbone (that is, breaking all but one blue bond in a blob converts the last remaining blue bond to a red bond). Finally, yellow bonds are those that dangle off the backbone and do not contribute to the spanning property of the incipient cluster. Conceptually, one may say that red bonds and blobs of blue bonds are the bonds that actually connect different parts of the lattice to each other and make the cluster a spanning cluster, while yellow bonds simply add mass to the cluster. See Figure 1 for a visual representation of the different types of bonds.

Pike and Stanley show that the mean number of red bonds is a critical quantity diverging at p_c with an exponent γ_R which they calculated as 1 for the square bond-percolating lattice. As will be seen later, this concept is of considerable importance in applying percolation theory to an understanding of the epilepsies.

Kirkpatrick and Swendsen [41] show computer-generated pictures of the incipient cluster and its backbone for various values of p. Coniglio [12] has studied the structure of the incipient cluster using a quenched dilute s-state Potts model.

3.1.4 Finite lattices

When percolation theory is applied to finite-sized lattices, some of the results are not as clear cut as they are for infinite lattices. Percolation theory has yielded to real space renormalization [80], and the behavior of finite lattices is derived through numerical simulations by Clerc *et al.* [11].

The results indicate that the critical transition does not occur at so well-defined a point as

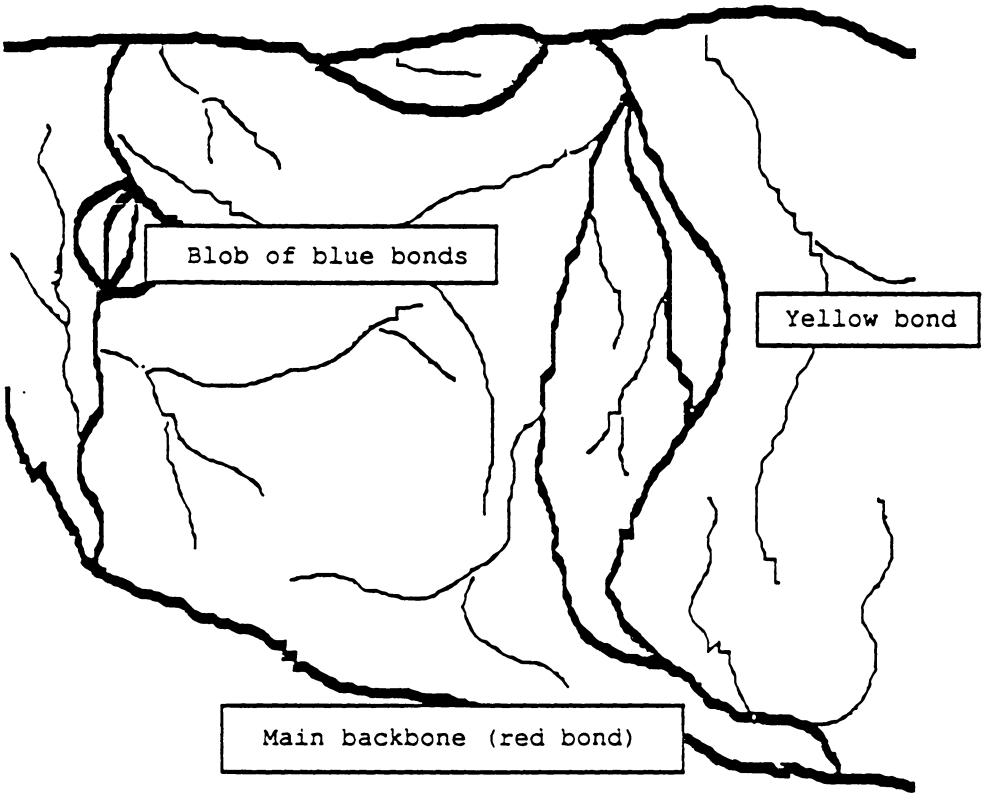

Figure 1: **The structure of the incipient cluster.** Pike and Stanley [76] show that the number of red bonds, which make up the backbone of the spanning cluster, diverges as $p \rightarrow p_c$.

for infinite lattices. The strength of the infinite lattice behaves as [92,11]

$$P = L^{-\beta/\nu} F\left[(p - p_c)L^{1/\nu}\right], \tag{3.5}$$

where L is the linear dimension of the lattice and β and ν are given by Equations 3.3 and 3.2. F is a scaling function chosen by renormalization requirements: if $p \gg p_c$, then $F\left[z = L^{1/\nu}(p - p_c)\right] \sim z$ so that $P \sim (p - p_c)^{\beta}$. For $z \sim 0$, that is, $p \sim p_c$, Equation 3.4 requires the volume of the spanning cluster to go as $L^{d-\beta/\nu}$. But the volume of the spanning cluster is just PL^d, which requires $F(z = 0) \sim 1$. Finally, for $p \ll p_c$, $F \sim 0$.

What the behavior of F means is that when $p \ll p_c$, the finite system is not affected by its boundaries, and behaves like an infinite system. Similarly, when $p \gg p_c$, the strength P of the spanning cluster is independent of the finite linear dimension L of the lattice. Only when $p \simeq p_c$ does the finite system differ appreciably from the infinite system. Clerc *et al.* [11] show that one of the differences is that there is a non-zero probability that a spanning cluster exists in a finite lattice when $p < p_c$. They show that the probability R that a spanning cluster exists at a bond fraction p is given by

$$R(p, L) = \Phi\left[(p - p_c)L^{1/\nu}\right] \tag{3.6}$$

where L is the linear dimension of the lattice and Φ is a scaling function that increases from 0 to 1 as its argument goes from $-\infty$ (far below p_c) to $+\infty$ (far above p_c). Stauffer [92] summarizes in English the findings of Clerc *et al.*

3.1.5 The power of percolation theory

Table 3 and Equations 3.1, 3.3, and 3.2 display the unifying power of percolation theory. Nowhere in any of these is there any assumption about the details of the percolative process. In fact, renormalization group theory has shown [52,92] distribution of the number of clusters of size s as a function of the bond fraction p satisfies the scaling equation

$$n_s(p) = s^{-\tau} f\left[(p - p_c)s^{\sigma}\right] \qquad (p \to p_c, s \to \infty) \tag{3.7}$$

for *any* percolative process. τ and σ depend on the dimensionality of the lattice, but not on the details of the actual site-site interaction, or even on the geometry of the lattice [19]. This property is known as the *universality* principle. (The universality over lattice geometries is true only for percolating systems that share the same type of interaction, e.g., nearest neighbor. Such groups of systems are said to form a *universality class.*) The details of the scaling function f do depend on the lattice geometry, but not on the details of the interaction.

τ and σ are related to the exponents γ and β in Equations 3.1 and 3.3 by the equations [92]

$$\beta = \frac{\tau - 2}{\sigma} \tag{3.8}$$

$$\gamma = \frac{3 - \tau}{\sigma} \tag{3.9}$$

Table 4 lists the critical exponents for two and three dimensional lattices, and lists the fractal dimension of the clusters below, at, and over the percolation threshold.

Thus, percolation theory is capable of unifying many diverse and seemingly unrelated phenomena, as the introductory section to this chapter illustrates. The behavior of a percolating system is governed by a few characteristic exponents, and the relationships between the exponents are simple enough that when some particular lattice exponent is derived, the others are immediately available. What makes percolation particularly attractive is that the statistical behavior of the lattice clusters does not depend on the nature of the interaction that forms the clusters in the first place. If a general idea of the scaling laws is all that is desired, it is not even necessary to know the geometry of the lattice. In an application such as the one discussed in this work, this can make the difference between understanding something, even if only on a statistical level, and understanding nothing at all.

However, as will be seen when percolation theory is applied to an understanding of the epilepsies, deriving even one of the exponents presupposes experimentally obtained data of a sufficiently high quality that statistical analyses can extract the exponents. Unfortunately, this is rarely the case in any biological system.

Table 4: **Percolation exponents for two and three dimensions.** Note that the exponents are constant for all lattice geometries of any given dimension, at least for the same universality class. Adapted from [92].

Exponent	$d = 2$	$d = 3$
β	5/36	0.4
γ	43/18	1.8
ν	4/3	0.9
σ	36/91	0.45
τ	187/91	2.2
$D_c(p < p_c)$	1.56	2
$D_c(p = p_c)$	91/48	2.5
$D_c(p > p_c)$	2	3

3.2 Application of percolation to the epilepsies

The characteristic property of any percolative system is the critical transition from finite cluster size to infinite (or, in the case of finite lattices, spanning) clusters. The onset of an epileptic seizure may also be viewed as a critical transition of the brain from the normal state to the seizure state. It seems reasonable, therefore, to postulate that the brain is a percolating system: specifically, it appears to be a bond percolating system, or possibly as a correlated bond percolating system, with the lattice composed of the billions of neurons and the bond being the existence of an excited connection between two neurons. This assumption views the seizure as being caused by the existence of an excitatory cluster in which random or periodic signals can propagate to widely diverse regions of the brain and thence to the rest of the nervous system. In this picture, the actual neural discharges during a seizure represent a different phenomenon from the formation of the clusters.

3.2.1 The brain as a percolating system

If indeed the epileptic brain is a percolative system, it becomes necessary to model the epilepsies in terms of clusters of bonded neurons, clusters being the basic unit of currency in percolation theory. Studies have shown that the electrical state of the brain changes in response to mental state [42,47]. There is also an entire field of neurology devoted to the changes of the brain's electrical activity in response to external stimuli, called evoked potentials [48,84,85]. This observation led to the postulation that the changes of brain activity are in fact changes in the sizes of clusters of active neurons. As will be seen, this postulation shows promise in explaining the statistics of the epilepsies.

Within this model, the normal brain is seen to be a system with some fraction of the possible number of bonds being excited. This fraction is p, the bond excitation fraction. Under normal circumstances, p is some small number representing clusters of neurons that are activated for the purpose of maintaining brain activity. For example, a waking adult

might have active clusters in the anterior lobe of the brain, responsible for vision, as well as in the temporal lobe, responsible for language, and the frontal lobe, responsible for higher cognitive activity. Clearly, p depends on the level of activity of the brain. It seems reasonable that fewer neurons are activated in a sleeping person than in a waking person, especially because sensory input in a sleeping person is not processed even though the signals are received in the brain. For the normal brain, the overlap of active clusters in the different parts of the brain is characterized by little or no overlap an interference.

3.2.2 Variation in p and its effect

It is probably impossible to track the exact variations in p for a system so complex as the human brain. It is possible to make general statements about the variation in p: as noted above, p is lower during sleep, and presumably when the brain is highly taxed, such as in a very emotional or stressful situation, p is high. A reasonable assumption is that p varies more or less randomly throughout the day, with some sort of diurnal variation superimposed on the random excursions. To approximate the temporal variation a two-parameter Gaussian probability distribution of p is proposed:

$$\varrho(p) = A \exp\left[-\frac{(p-\bar{p})^2}{\Delta p^2}\right] \tag{3.10}$$

with A being the standard normalization constant, and where the average $\bar{p}$ and variance Δp model the temporal variations.

In most people, the variation in p is presumably relatively narrow (Δp is small), and the average bond fraction $\bar{p}$ is kept to small values. The brains of epileptics, however, would seem to have chemical or electrical compositions that conspire to occasionally push p above the critical threshold, p_c, for the brain. That is, in such people,

$$\bar{p} + \Delta p \geq p_c. \tag{3.11}$$

When this occurs, the brain undergoes a critical transition.

3.2.3 Seizures as critical transitions

The critical transition in a percolating brain, as in any other percolating system, is the formation of spanning clusters. When translated to the central nervous system, this implies the formation of clusters that span areas of the brain responsible for diverse activities. The clusters in the area responsible for auditory processing, for example, might grow to encompass the area responsible for olfactory response.

Early in the seizure, the spanning cluster is still relatively weak (or, in the language of Mandelbrot [53], of low fractal dimension). Relatively little crosstalk between areas exist, and using the model of Pike and Stanley [77], discussed in Section 3.1.3, the number of red bonds is small. The seizure is of the localized variety: most of the mass of the seizing cluster is made up by bonds between neurons in a small area. A flood of inhibitor such as GABA from the synapses may break a number of these red bonds, causing the spanning cluster to collapse rapidly. But if p keeps on increasing, the spanning cluster becomes stronger and involves more areas of the brain (see Equation 3.3). In clinical terms, the seizure has generalized. Eventually, the spanning cluster becomes so strong as to involve sites in the motor areas of the brain, causing the characteristic tonic-clonic muscular activity of the GTC seizure. In its simplest form, these percolation ideas describe the different stages of a seizure quite well, but cannot explain the detailed dynamics of neuron recruitment and generalization of seizures.

One of the consequences of a percolation model of seizures is that the stronger the cluster, the longer the seizure should last. This can be seen in a qualitative way by using the Pike and Stanley model. As the cluster grows ever stronger, the number of red bonds grows. To stop the seizure, it becomes necessary to break up more of these bonds, and assuming a constant time to break one bond, the time to collapse the cluster increases. A later section will derive a prediction for the distribution of seizure durations based on such a model.

The overshoot of p into the critical area may be brought about by any number of factors.

Many seizures appear to be brought about by strong stimuli such as flashing lights, strong emotional excitement, or the presence of certain chemicals [49]. These kinds of seizures are easily explained by the percolation model as rapid increases in p brought about by the stimuli. The idiopathic, or unexplained, seizures are more difficult to dispose of. It seems reasonable that there has to be *some* cause for these seizures, and indeed idiopathic seizures can be statistically categorized into areas like "waking" seizures (in which the seizure occurs when the patient wakes). A waking seizure is probably an overshoot of p as the brain transits from its sleeping state to its waking state. However, one of the recurring problems facing any physical theory of biological systems is the variability of these systems. It is nearly impossible to construct a statistical theory of any biological system that can account for every single observation.

3.2.4 The model is reasonable

Several aspects of this model are in qualitative agreement with the literature on the epilepsies. The model of generalization proposed in the previous section agrees well with clinically observed manifestations of partial seizures that generalize [15]. One of the more interesting physiological phenomena that accompany a seizure is that of an "aura." These are precursors to the seizure, during which the patient experiences hallucinations. Strange smells or visual blurring may precede the actual seizure. Using the percolation model, this can be explained by considering the way in which the spanning cluster forms. As the focus of the seizure recruits more neurons into the spanning cluster, the cluster begins to involve the pyramidal cells which connect different parts of the brain to each other. Neural activity in one part of the brain spreads in an uncontrolled way to other parts, and it may be that neural activity which originates in the olfactory processing system begins to cause spurious activity in the auditory system, for example, which could create an auditory hallucination.

Seizures that are generalized from the onset are presumably caused by a global increase in p all over the brain, rather than a local increase that spreads to recruit other areas. Thus, the

percolation model can qualitatively account for some phenomenology of epileptic seizures.

More evidence is provided by studies that have examined the way in which masses of epileptic neurons in the central nervous system induce seizures. Wyler and Ward [98] have deduced a model for the mechanism by which malfunctioning neurons can recruit aggregates of other neurons into a seizing cluster. There exists a type of neuron, which they call a Group 1 neuron, which spontaneously begins to fire in an uncontrolled manner. Group 1 neurons then recruit so-called Group 2 neurons, and when the whole mass of hyperactivated neurons reaches a certain critical mass, a seizure is triggered. This terminology is strongly reminiscent of percolation theory.

Percolation theory cannot make any statement about the way in which these Group 1 neurons spontaneously misbehave or go about recruiting other neurons. This electrochemical mechanism has been studied by Calvin [8]. He shows that the ability of abnormal neurons to recruit others is strongly influenced by the ratio of excitatory to inhibitory synapses.

In another study, Roberts [81] discusses the role of reduced inhibitory-neuron efficacy in seizures, and shows support for the idea that a loss of inhibitory neurons at a seizure focus accounts for the higher epileptogenic susceptibility at such a site. This clearly corresponds to an increase in p at the center of the site.

Chapter 4

Statistics of clinical data

Two types of data were available to this research program. Clinical observations of epileptic patients provided statistics on the time distribution, duration, and other properties of seizures, while computer-recorded databases of brain electrical activity provided similar data on the microscopic manifestations of the epileptiform brain. This chapter will concentrate on the clinically obtained data.

4.1 Description of data

A quick note: graphs of almost all the data available to this research program are reproduced in Appendix A. In that appendix, graphs are shown for ten different patients. The graphs display the distribution of seizures by time of day, by day of week, and by duration of seizures. There are also graphs showing the distribution of seizure-free intervals by interval length. At the beginning of Appendix A, there is a catalog describing the graphs and how they are arranged.

4.1.1 How the data were obtained

The clinical observations of epileptic patients were obtained from the Bowman-Gray School of Medicine of Wake Forest University in Winston-Salem, North Carolina. The epilepsies research program there maintains a clinic for the treatment of the epilepsies, and patients are requested to maintain a seizure calendar. Patients (or their parents or guardians) record the date and time of any seizure, its duration, and make a guess at the type of the seizure. At the same time, clinical staff maintain records of the patient's weight history, prescription schedules, and results of laboratory tests for blood antiepileptic drug (AED) levels.

4.1.2 What data were available

Each patient record consists of four files: the seizure calendar, weight history, AED prescription history, and AED blood-level measurements. The seizure calendar records the date, time, and duration of each seizure event, along with a guess at the type of the seizure (see Table 2). The weight history file contains a record of the patient's weighings: its sole purpose is to determine weight-normalized dosage levels. The AED prescription history records the prescriptions of AED's administered to the patient in absolute milligrams (this must be then normalized to milligrams per kilogram of body weight). And finally, the AED blood-level records contain the results of laboratory tests which measure how effectively the patient is absorbing the prescribed AED's into the bloodstream.

All four files are generated by a database program, and are in text (ASCII) format, making the debugging of analysis programs much easier.

4.1.3 The quality of the data

Not all the clinical data are of the same quality. The weight and prescription records are obviously error-free, while the AED blood-level measurements are quite accurate.

The seizure calendar is the most important record for a statistical research program such as this, and unfortunately, it is not very accurate. The date of the seizure event is probably quite accurate as long as the seizure occurred during normal waking hours, but the time and duration data are of poor quality. Patients who have epileptic seizures that cause loss of consciousness are aware that a seizure occurred only when they recover consciousness and discover a discontinuity in time. They may have no idea how long it lasted or when it started. Frequently, the patient has no idea of the duration or time of the seizure, and the clinical staff makes a guess at these data based on previous records [22]. However, records filled in by the staff are marked as such, and can be eliminated from statistical surveys. On the other hand, data from patients (often children or mentally handicapped people) whose calendars are maintained by relatives may be quite accurate.

4.1.4 What kinds of data can be derived from the raw data

As part of the grant from Abbott Laboratories which supported this research, a program was developed to analyze the raw data available to clinicians. The program can produce the following analyses from the raw clinical data:

- Number of seizures on each day over a period of days.
- Average number of seizures per day over a period of weeks.
- Number of seizure-free intervals as a function of the interval over a period of days or weeks.
- Number of seizures on each day of the week over a period of days or weeks.
- Number of seizures at various times of the day over a period of days or weeks.
- Number of seizures as a function of seizure duration over a period of days or weeks.
- Prescribed dosages of up to two drugs at a time.

- Measured blood levels of up to two drugs at a time.

It is hoped that the availability of such an analysis tool will inspire neurologists, statisticians, or physicists to experiment with the data in the same fashion as was done for this dissertation, and perhaps to spot trends or correlations that were missed in this research study.

4.1.5 The variability of the data

As has been pointed out earlier, a formidable problem faces any statistical theory of a biological system—the variability of the data available. Even when the data are of good quality, the systems being studied are so complex that it is a source of some wonder that any trends are observable. As an example, consider the fact that so unpredictable a system as the human central nervous system always reacts in a predictable way in the knee-jerk reflex. Deducing this reaction from a mass of data that categorizes the reaction of a human being to a large variety of stimuli is no small task.

To gain some understanding of the variability of the data available to this study, look at Figures 32 through 51, in Appendix A. The first few graphs show the daily time distribution of seizures for several patients. Some patients experience most of their seizures in the daytime, others at night, and still others seem to have no discernible trends. Next come a series of graphs displaying the weekly distribution of seizures for the same patients. This could go on at some length, but the idea is probably obvious: data from studies such as this vary widely in the best of circumstances, and the generally poor quality of data makes analysis even harder.

4.2 The statistics of epileptic seizures

4.2.1 Seizure-free intervals

The first statistical tests carried out on the clinically obtained data were to discover if the probability of having a seizure in some interval of time is affected in any way by the previous seizure history of the patient. If there was an effect, it would suggest that there exists some sort of a relaxation mechanism by which the probability of having a seizure gradually increases from zero to one, and then drops back to zero immediately after the seizure. In fact, this is not the case.

If the probability of some statistical event is independent of the events that have preceded it, the probability distribution for that event is a Poisson distribution [66]. In other words, the probability of there being k events in t units of time is

$$P(k,t) = (\lambda t)^k \frac{e^{-\lambda t}}{k!}. \tag{4.1}$$

(Here, λ is the average rate of these events per unit time.) In particular, the probability of having no events in some interval t is

$$P(0,t) = e^{-\lambda t}. \tag{4.2}$$

Thus, as the length of the interval increases, the probability of there being no event decreases exponentially.

If the *seizure-free interval* is defined as the time between two consecutive seizures, it is a characteristic of all the data analyzed in this study that the distribution of seizure-free intervals is an exponentially decreasing function of interval. That is, the number of seizure-free intervals of a certain length decreases exponentially as the length increases. Figure 2 shows this decrease for one patient. See Appendix A for data on more patients.

In a more detailed analysis, Binnie *et al.* [5] came to the same conclusion. They studied three sources of data: counts of epileptiform discharges (see Section 5.3) in the EEG's

of several patients, seizure calendars maintained by patients in a drug-efficacy test, and seizure calendars of mentally retarded patients in a long-term health care facility (records were maintained by the staff). They applied several statistical tests to these data, all of which indicated a Poisson distribution of seizure-free intervals. Their studies were over long enough intervals that they were able to note some variations from a true Poisson distribution. For example, some patients displayed significant periodicity of seizure rates. This may indicate that the assumption that $p(t)$ is Gaussian is not strictly accurate for some patients if a sufficient mass of data can be studied. Or perhaps the Gaussian distribution is modulated by a weakly periodic function, causing $\bar{p}$ and Δp to vary periodically.

The conclusion, therefore, is that the occurrence of a seizure in a patient is not dependent on the occurrence of any past seizures. This provides some evidence for the earlier assumption that the bond fraction p is normally distributed over time, with the caveats noted above.

4.2.2 The effects of AED's on seizure statistics

As discussed previously, this statistical study assumes that the diurnal variation of p is small and p can be assumed constant over a day. The variation in p from day to day is too complex to be modeled accurately, and is assumed to be a random distribution with a Gaussian form (Equation 3.10).

AED's presumably affect p in different ways. If the criterion for a seizure is that p exceeds p_c, then both $\bar{p}$ and Δp can affect the seizure rate (see Equation 3.11). In this section, a simplified theory is derived for determining the effect of an AED on the parameters of the distribution of p. Because the seizure rate is easily measured clinically, it will be used as the measurable quantity.

If the seizure rate is a Poisson process, then Equation 4.2 holds for the probability of there being no seizures in one day. Further, if $p(t)$ is the function governing the variation of p

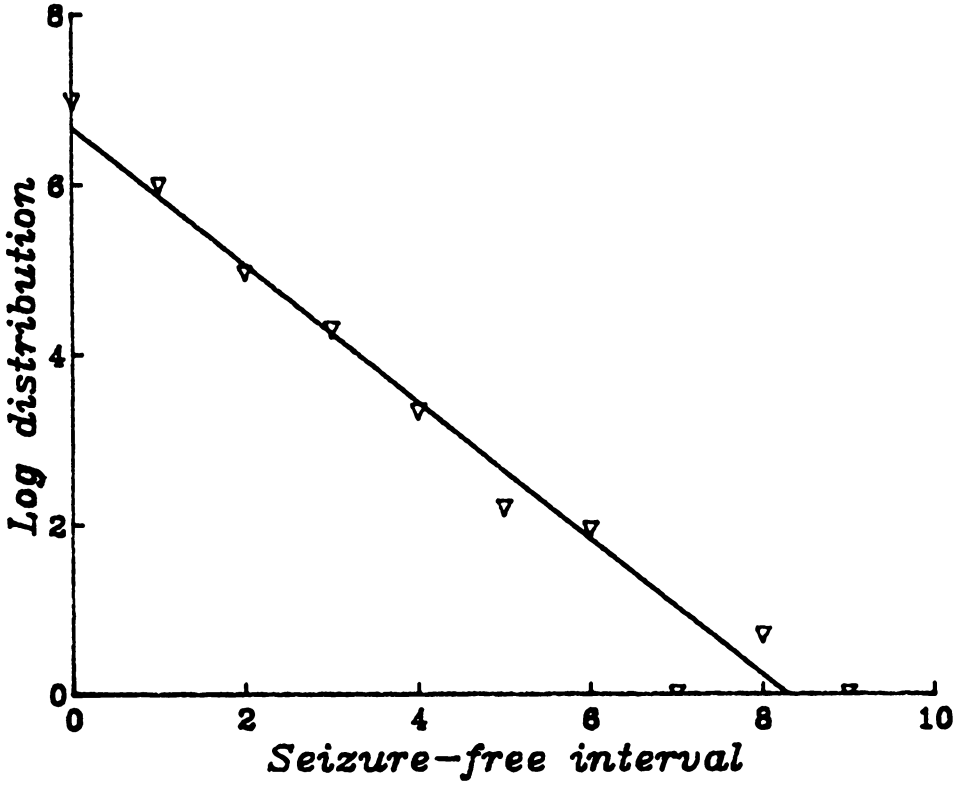

Figure 2: **The distribution of seizure-free intervals.** The exponential decrease in the number of seizure-free intervals with interval indicates that the onset of a seizure is a Poisson process. Note that the y-axis is logarithmic.

with time, then

$$e^{-\lambda t} = \frac{\int_0^t p(t)\Theta(p - p_c)\,dt}{\int_0^t p(t)\,dt} \tag{4.3}$$

because the probability of no seizures in some interval is just the area under the $p(t)$ curve for $p > p_c$ divided by the area under the entire $p(t)$ curve. Here, $\Theta(x)$ is the step function:

$$\Theta(x) = \begin{cases} 1 & x \geq 0 \\ 0 & \text{otherwise} \end{cases} \tag{4.4}$$

If we assume Equation 3.10, this yields

$$e^{-\lambda t} \simeq 1 - \frac{\Delta p\, p_c}{2\sqrt{\pi}\,(p_c - \bar{p})\bar{p}} \exp\left[\frac{-(p_c - \bar{p})^2}{\Delta p^2}\right] \tag{4.5}$$

using the simplification

$$1 - \mathrm{erf}(x) = \frac{1}{x\sqrt{\pi}} e^{-x^2} \qquad x \to \infty. \tag{4.6}$$

Equation 4.5 yields $\bar{p}$ and Δp if p_c is known. The effect of AED concentration can now be modeled by assuming that an AED decreases $\bar{p}$ and Δp as the AED concentration c increases. Let f_1 be the fractional decrease in $\bar{p}$ that would be obtained if $c \to \infty$, and f_2 be the corresponding fractional decrease in Δp. Then,

$$\bar{p}(c) = \bar{p}_0 \frac{1 + (1 - f_1)c/K}{1 + c/K} \tag{4.7}$$

$$\Delta p(c) = \Delta p_0 \frac{1 + (1 - f_2)c/K}{1 + c/K} \tag{4.8}$$

where K is the concentration at which increasing c no longer has any effect and $\bar{p}_0$ and Δp_0 indicate values at $c = 0$.

Thus, a treatment program could derive estimates of $\bar{p}_0$ and Δp_0 using Equation 4.5, and then use Equations 4.7 and 4.8 to control the parameters of $\varrho(p)$.

4.2.3 Distributions of seizure durations

A reasonable assumption is that a seizure eventually terminates because inhibitor such as GABA (γ-aminobutyric acid) diffuses through the seizing area of the brain, hyperpolarizing the synapses and restoring the system to a subcritical state. Support for this model comes from Roberts [81], who shows that a deficiency in GABA levels can cause the characteristic synchronized firing of seizing neurons—it appears reasonable that generation of GABA or some other neural inhibitor can reverse the process and restore normalcy [65].

If the collapse of the seizure requires all the bonds in the spanning cluster to be broken, then the seizure terminates when the inhibitor has spread to cover the volume filled by the spanning cluster. Assuming that the inhibitor spreads using a simple diffusion mechanism, the distance over which the inhibitor diffuses in time τ is

$$d = D\tau^{1/2}. \tag{4.9}$$

The number of neurons s in a seizing cluster is given by Equation 3.3 as

$$s = N\alpha(p - p_c)^{\beta} \tag{4.10}$$

where N is the number of neurons in the region of the brain. But

$$s = \frac{\nu_0 \pi d^3}{6} \tag{4.11}$$

where ν_0 is the number density of neurons. Thus, from Equation 4.9,

$$s = \frac{\nu_0 \pi D^3 \tau^{3/2}}{6}. \tag{4.12}$$

Equating 4.10 and 4.12,

$$b\tau^{3/2\beta} = (p - p_c) \tag{4.13}$$

$$b = \left[\frac{\nu_0 \pi D^3}{6N\alpha}\right]^{1/\beta}. \tag{4.14}$$

Consider the conditional probability distribution $\varrho_s(p)$ for a seizure when the bond fraction is p.

$$\varrho_s(p) = \frac{2}{\Delta p\sqrt{\pi}} \frac{\Theta(p - p_c) \exp\left[\frac{-(p-\bar{p})^2}{\Delta p^2}\right]}{1 - \mathrm{erf}(y)} \tag{4.15}$$

where

$$y = \frac{p_c - \bar{p}}{\Delta p} \tag{4.16}$$

Making the transformation

$$p - \bar{p} = p - p_c + (p_c - \bar{p}), \tag{4.17}$$

$\varrho_s(p)$ becomes

$$\varrho_s(\tau) = A \exp(-b^2\omega^2 - 2by\omega) \tag{4.18}$$

$$\omega = \tau^{3/2\beta} \tag{4.19}$$

Thus, a distribution of $\log(\varrho_s)$ is expected to be some sort of a polynomial in τ.

It is important to recognize the limitations of a simplistic model such as this. First, the work of Pike and Stanley [77] (see Section 3.1.3) makes it clear that it is not necessary to break all the bonds in the seizing cluster, merely to break the red bonds. As the strength of the seizing cluster increases, more of the bonds become red bonds and the approximations made above become more valid. It would appear that Equation 4.18 is more valid for seizures that have had time to develop, such as generalized tonic-clonic seizures.

Another limiting assumption is that the inhibitor starts to diffuse from a single point and spreads radially out through the cluster. It is not obvious *a priori* that this is a reasonable model, and more complex models should also be studied. Inhibitors are generated in several synaptic clefts simultaneously and presumably do not require as much time to engulf the seizing cluster as is implied by Equation 4.9.

The model also implies a spherically symmetric seizing cluster. Again, this is probably reasonable when the cluster is strong (i.e., $p \gg p_c$ and the fractal dimension D_c of the

cluster approaches 3), but certainly at $p \simeq p_c$, the cluster is not spherically symmetric (in fact, it is not even three-dimensional).

Despite all these limitations, there is modest agreement between Equation 4.18 and experimentally observed data. See Figure 3 and Appendix A.

4.2.4 Estimates of the percolation exponent β

Equation 4.18 can be used to derive a crude estimate of the value of β. First, rewrite Equation 4.18 as

$$\log\left(\frac{\varrho_s(\tau)}{\varrho_s(\tau_0)}\right) = -p(\omega^2 - \omega_0^2) - q(\omega - \omega_0), \tag{4.20}$$

with

$$p = b^2 \tag{4.21}$$

$$q = 2by \tag{4.22}$$

and A has been eliminated by dividing $\varrho_s(\tau)$ by $\varrho_s(\tau_0)$, τ_0 being some arbitrarily chosen duration. For simplicity of notation, let

$$\varrho_s'(\tau) = \frac{\varrho_s(\tau)}{\varrho_s(\tau_0)} \tag{4.23}$$

$$\omega' = \omega - \omega_0 \tag{4.24}$$

$$\omega'' = \omega^2 - \omega_0^2 \tag{4.25}$$

If there exists some discrete set of points

$$(\tau_i, \varrho_s'^{(i)}) \qquad 0 \le i \le n,$$

then the constants p and q can be determined by minimizing

$$S = \sum_{i=0}^{n} (\log \varrho_s'^{(i)} + p\omega_i'' + q\omega_i') \tag{4.26}$$

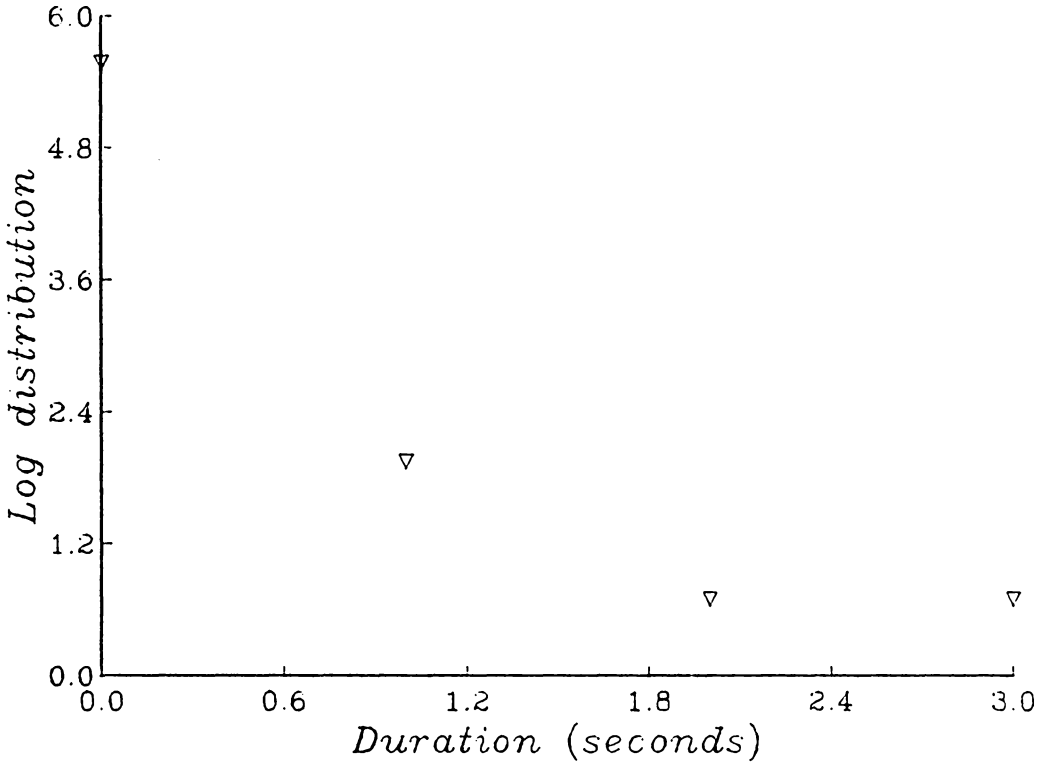

Figure 3: The distribution of seizures with duration. There is a measure of agreement with the parabolic shape predicted by Equation 4.18.

with respect to p and q. That is, by solving the simultaneous equations

$$\frac{\partial S}{\partial p} = 0 \tag{4.27}$$

$$\frac{\partial S}{\partial q} = 0. \tag{4.28}$$

Thus, the technique for obtaining β consists of solving Equations 4.27 and 4.28 for p and q for a range of values of β (each value gives a different set of ω_i''s). For each value of β, Equation 4.26 gives the value of S, and the value of β which yields the minimum S is close to the value that satisfies Equation 4.18. The values of β so computed for ten patients are listed in Table 5. Considering the poor quality of the data, it may be significant that the values are so close to each other.

4.2.5 Correlations of data

Visual inspections of the distributions of seizures as functions of the time of day and the day of the week appeared initially to show that there were strong correlations in some patients. Most patients appeared to have clearly defined periods of the day in which most seizures occurred, and some patients seemed to have most of their seizures on particular days of the week. See Figures 42 through 51 in Appendix A, which show the distributions of seizures as functions of the day of the week for ten patients involved in this study. Similarly, Figures 32 through 41, also in Appendix A, show distributions of seizures as functions of the time of the day for the same ten patients. The interval over which the data were sampled varies from patient to patient—each patient's data were sampled over the entire period during which he or she participated in the experimental treatment program at the Bowman Gray School of Medicine.

The hypotheses that seizures are distributed non-randomly as functions of the time of the day and the day of the week were tested using a χ^2 goodness-of-fit test [66]. The results are shown in Table 6. In that table, α_{DOW} is the confidence level for accepting the hypothesis

Table 5: **Values of β computed from clinical data using the least-squares technique.** Note that the values are close to each other. The types of seizures suffered are also listed

Patient	β	*Seizure types*
BH	1.2	ABS
CA	2.0	GTC, CPS
ES	2.5	SPS, GTC, CPS
JC	4.0	GTC, CPS
JM	4.0	SPS, GTC, CPS
KD	2.0	GTC, CPS
MAH	2.0	GTC
RK	3.0	GTC, CPS
TV	3.0	GTC, CPS
WC	4.2	CPS

that the seizure distribution is a non-random function of the day of the week. Similarly, α_{TOD} is the confidence level for accepting the hypothesis that the seizure distribution is a non-random function of the time of the day. The actual values of the χ^2 distribution are also given in the same table. The results show that there is in fact a strong correlation between seizure frequency and time of day. That is, most patients do have their seizures in well-defined periods of the day. This is strong indication of a daily periodic variation in the bond fraction p. However, few patients seem to have their seizures on any particular day of the week. It would appear that the stress of the working week has little or no effect on the seizure frequency, which suggests that the daily variation of $\bar{p}$ will be of importance for further studies but that day-to-day correlations are less important.

4.2.6 Distributions of seizure rates

One measure of a patient's seizure history appears never to be examined by treatment programs: the distribution of the average daily seizure rates. Using the percolation model, this distribution would measure the size of the "tail" of $\varrho(p)$, that is, the part of $\varrho(p)$ for which $p > p_c$. Higher daily seizure rates result when $\bar{p}$ is close to p_c, and lower seizure rates occur when $\bar{p} \ll p_c$. Figures 4 through 6 display these distributions for one patient as the concentration of the AED phenyltoin is varied.

It appears from these graphs that the average daily seizure rate has a clear average value and a variance. The effects of AED concentration on the seizure rate distribution is for the most part what is to be expected: higher concentrations cause lower mean $\bar{p}$ and Δp.

It must be stated here that some patients do not have so clearly defined a response to increasing levels of AED. Sometimes the mean daily seizure rate is higher for higher concentrations of AED. Many of these inconsistencies can be resolved by considering the stage at which the patient is in the treatment program, as will be explained shortly.

Figures 7 through 10 show the effects of increasing the concentration of various AED's on

Table 6: χ^2 confidence intervals for seizure distributions.

Patient ID	χ^2_{DOW}	α_{DOW}	χ^2_{TOD}	α_{TOD}
BH	34.26	>99.5%	373.22	>99.5%
CA	6.25	<90%	452.45	>99.5%
ES	11.06	>90%, <95%	306.19	>99.5%
JC	3.87	~ 10%	360.85	>99.5%
JM	20.41	>95%	527.47	>99.5%
KD	13.33	>95%, <97.5%	24.86	<90%
MAH	9.09	~ 90%	243.11	>99.5%
RK	7.28	<90%	119.67	>99.5%
TV	17.67	>99%	568.67	>99.5%
WC	1.30	~ 2.5%	531.62	>99.5%

the patient's average daily seizure rate. The data show that these AED's act by reducing the maximum number of seizures per day suffered by the patient. Some AED's seem to have no effect on the seizure rate: this could be because the patient is refractory (i.e., not responsive to medication). Some of the apparent inconsistencies in the data have been traced to the method by which AED's are administered. Doses of one AED are gradually lowered as doses for another are increased. As one AED dose decreases, the seizure rate will increase even though the AED being tracked has increasing concentration. In addition, Equations 4.7 and 4.8 are true in the steady state, i.e., when the drug has had enough time to permeate the brain tissue. Some of the large seizure rates at high doses that are apparent in Figures 7 through 10 have been traced to high initial doses of drugs administered to control seizures when the patient first joined the program.

On the whole, though, those AED's which have any effect at all seem to follow, at least semi-quantitatively, the forms predicted by Equations 4.7 and 4.8.

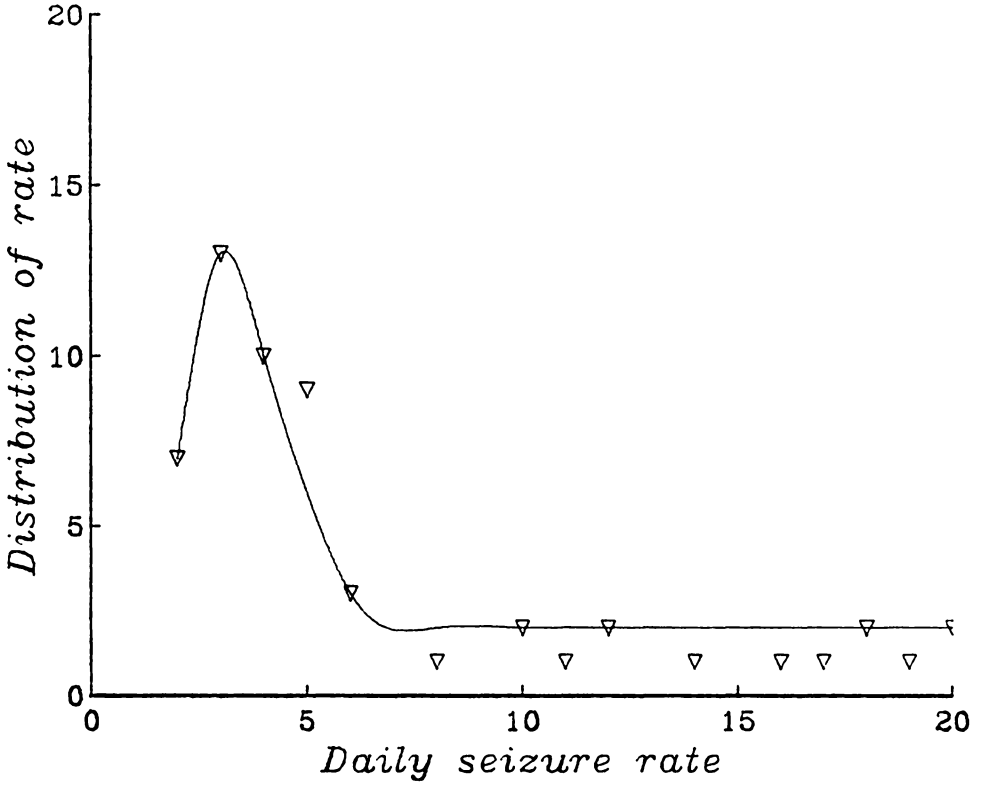

Figure 4: **The distribution of daily seizure rates for patient DM with 4 μg/kg of phenyltoin in the bloodstream.** The x-axis shows the daily seizure rate, and the y-axis shows the number of days on which a particular seizure rate occurred.

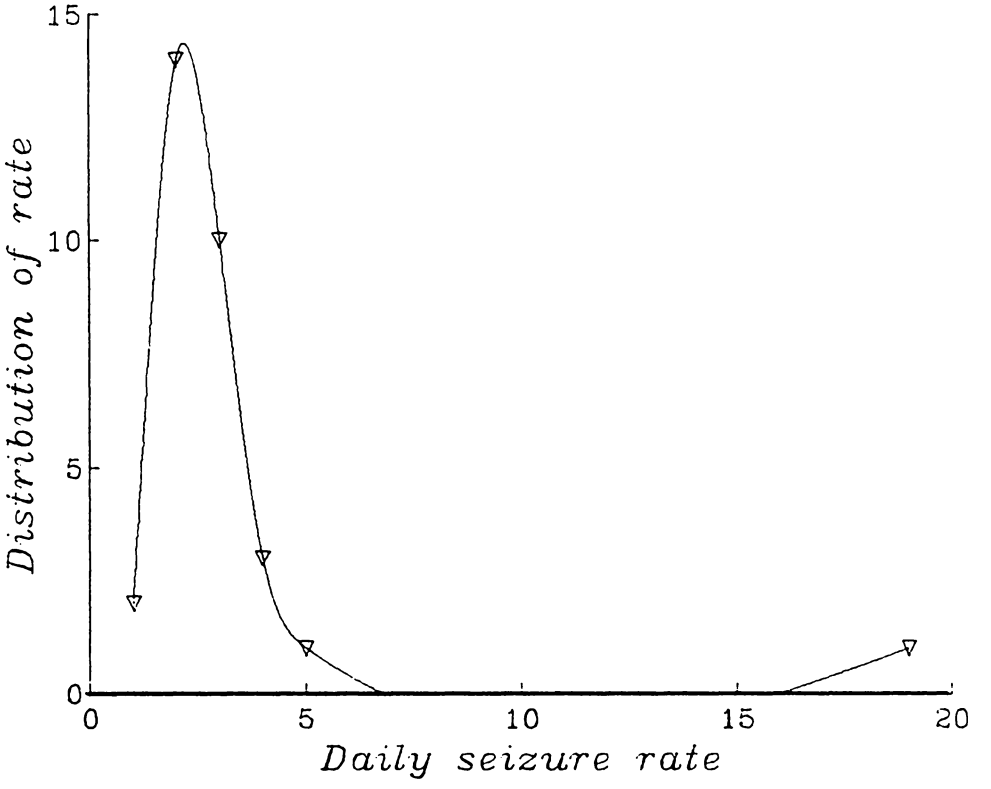

Figure 5: **The distribution of daily seizure rates for patient DM with 8 μg/kg of phenyltoin in the bloodstream.** The x-axis shows the daily seizure rate, and the y-axis shows the number of days on which a particular seizure rate occurred.

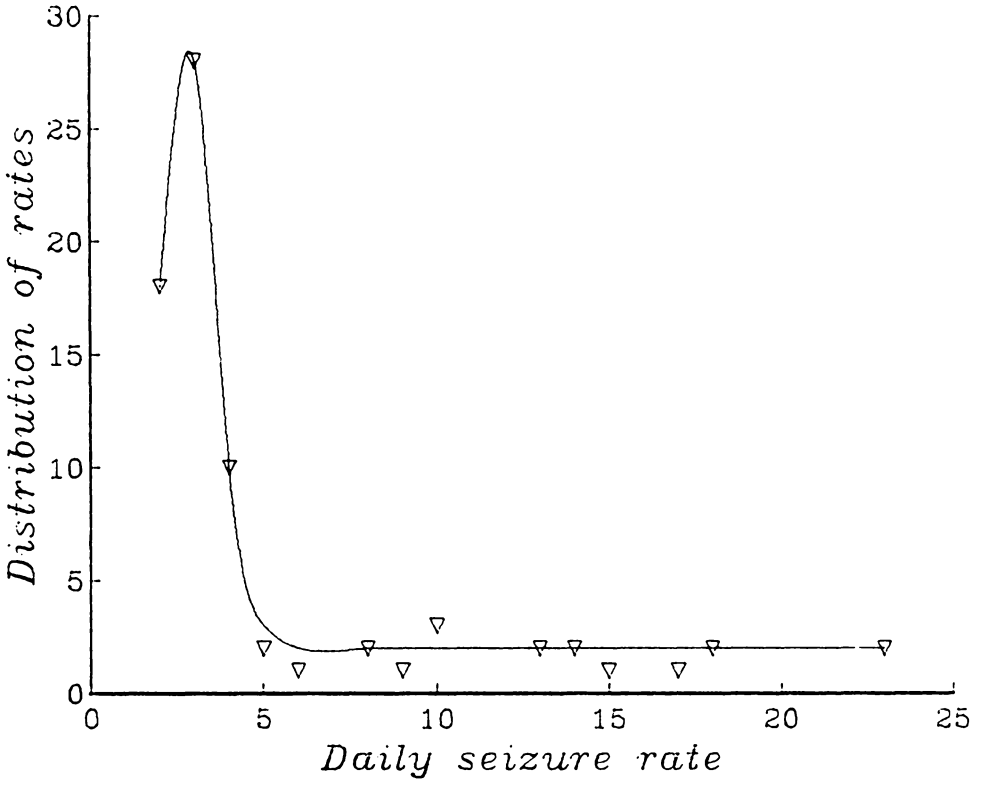

Figure 6: **The distribution of daily seizure rates for patient DM with 15 μg/kg of phenyltoin in the bloodstream.** The x-axis shows the daily seizure rate, and the y-axis shows the number of days on which a particular seizure rate occurred.

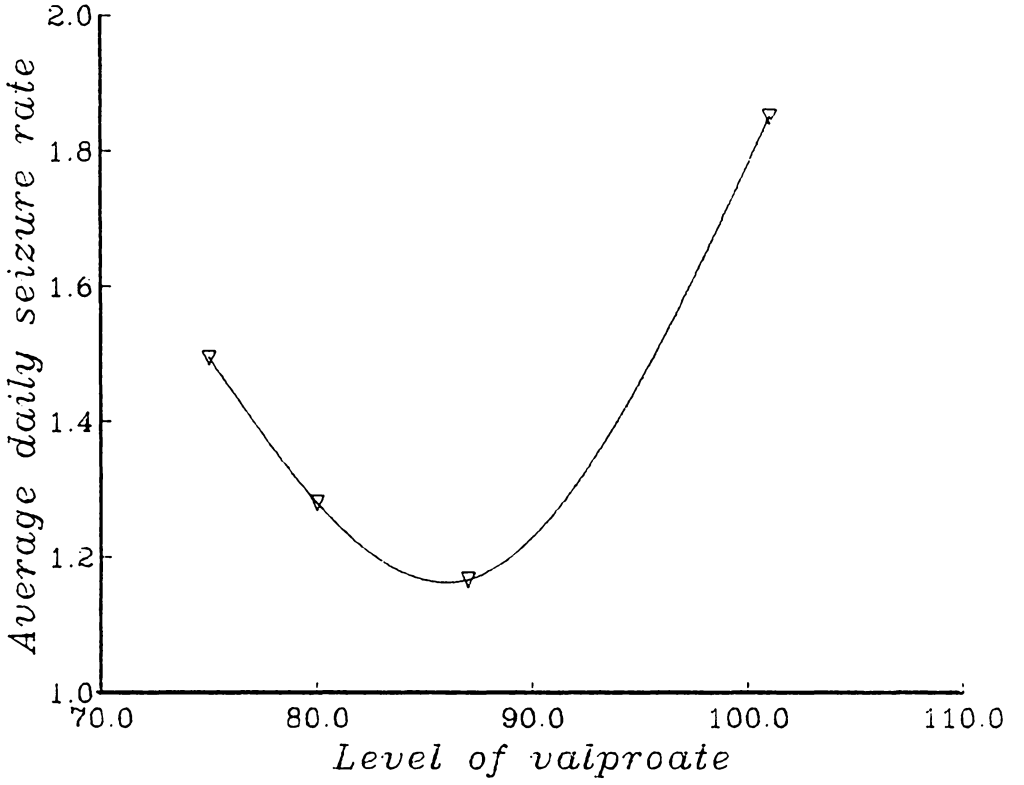

Figure 7: The effect of the AED valproate on patient RK.

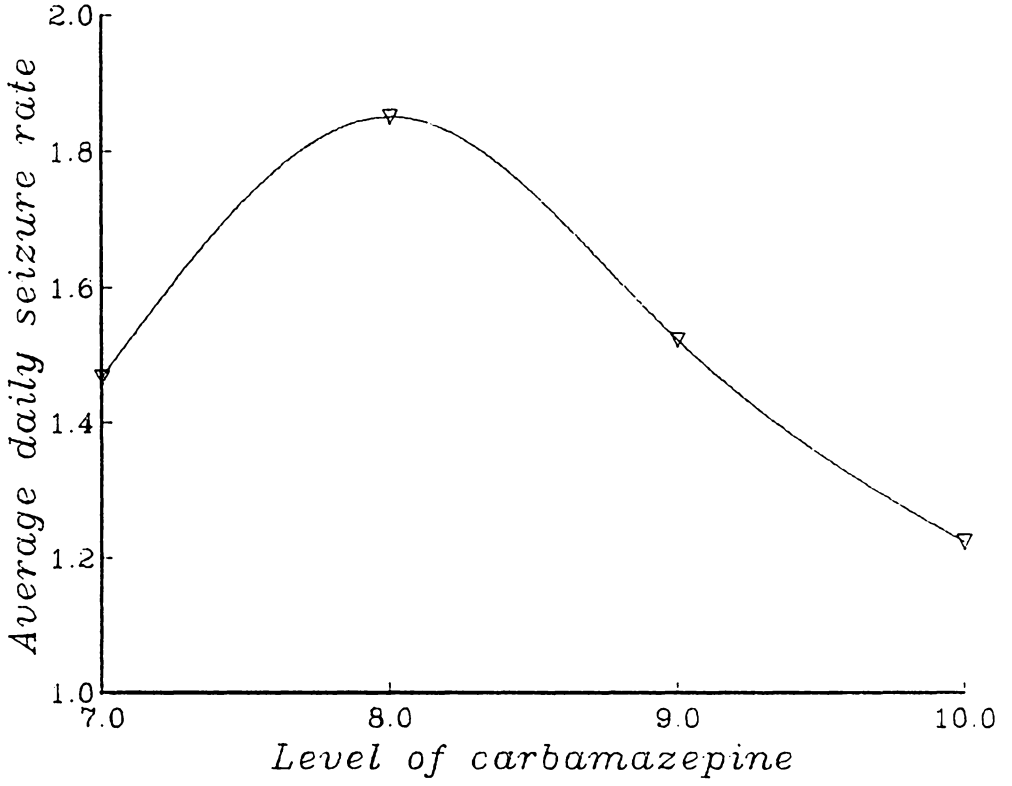

Figure 8: The effect of the AED carbamazepine on patient RK.

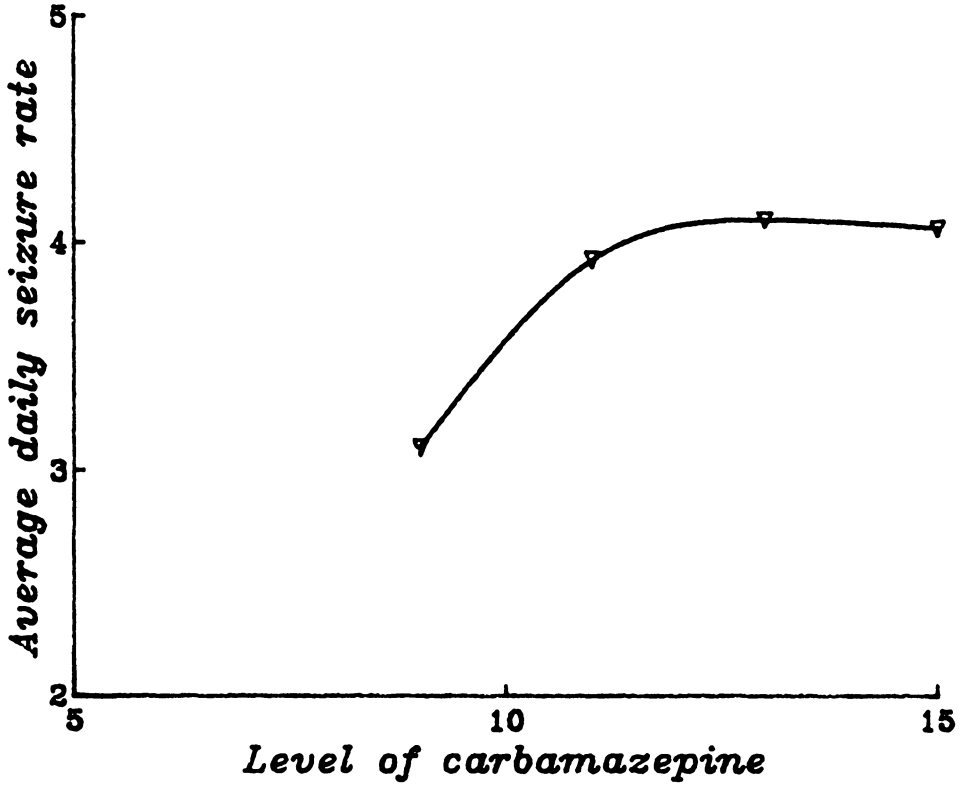

Figure 9: **The effect of the AED carbamazepine on patient DM.**

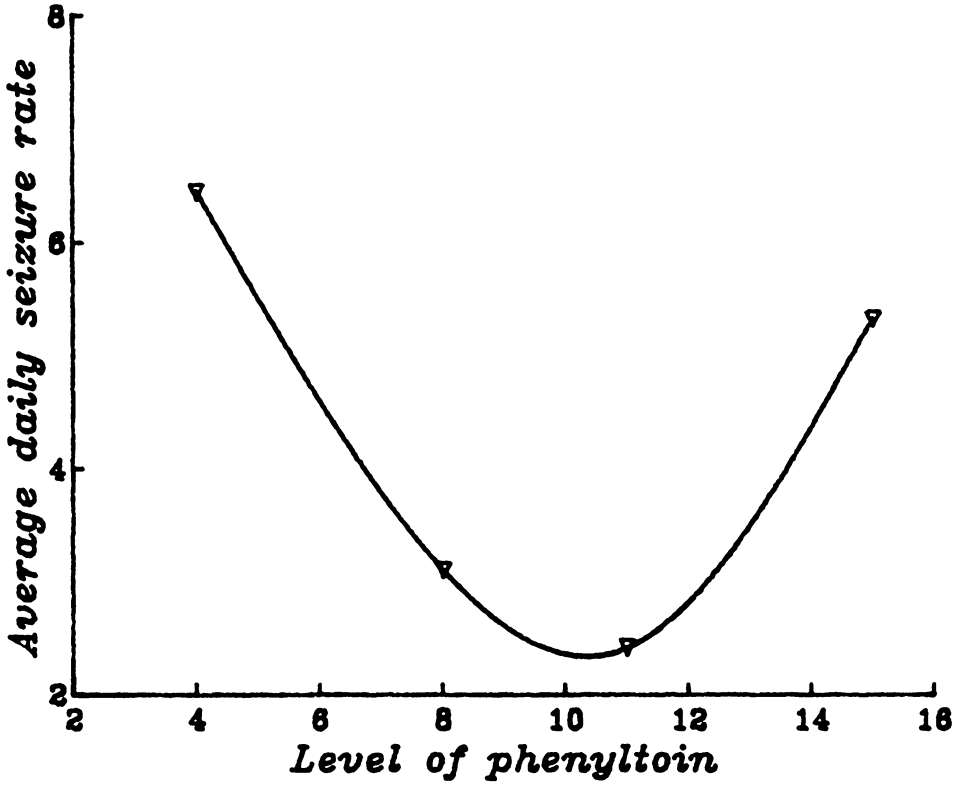

Figure 10: **The effect of the AED phenyltoin on patient DM.**

Chapter 5

The EEG

The electroencephalogram (or EEG) was invented by Hans Berger over half a century ago [4]. It has since gained widespread use as a tool in the study of brain activity [40] and in the diagnosis of the epilepsies [15]. Yet it remains the object of much speculation as to its physical origins, its relation to the actual electrical activity inside the brain, and its proper use for research and diagnosis. This chapter will present an overview of the electrical activity of the brain as discovered by researchers using the EEG, describe some of the work already done in attempting to explain the origins of the EEG, and then describe some of the statistical properties of the EEG.

5.1 Overview of EEG techniques

The EEG is basically a highly sensitive voltmeter, capable of accurately recording voltage differences of about $1\,\mu$V varying at frequencies up to 1 kHz [42]. The main instrument consists of an amplifier that can simultaneously transcribe the changing voltage differences onto a continuous roll of paper, yielding a "hard" copy of several hours worth of voltage measurements. The input to the device comes from several electrodes made of a good

conductor like silver, which are attached to the scalp of the patient at various points on the head. The electrodes are typically attached with a conductive paste.

There are several configurations or *montages* used by EEG operators in mounting the electrodes, but they break down into two classes—bipolar, in which the electrodes measure the voltage drop between successive electrodes, and single reference or monopolar, in which each electrode measures the voltage drop between that electrode and a reference electrode, usually mounted on the ears or the nose [79]. See Figure 11.

Modern techniques of EEG do not dispense with the traditional electrode technology or montages, but instead concentrate on replacing the recording device with a computer [27,28]. This is not as easy as it may sound—the EEG generates large quantities of data, which tax the mass storage capability of even modern computers. Typically, the raw EEG data are reduced by some technique before being stored on disk or tape. Even so, the reduced EEG data provided by the Montreal Neurological Institute for this study comprised ten million bits of information *for each patient* over 8 to 10 hours.

5.2 The electrical activity of the brain

The first use of the EEG was to study the electrical activity of the brain, and this section will present an overview of the findings of such studies. Note, however, that this should not be taken as an exhaustive study of the field: the number of studies devoted to the electrical activity of the brain is large. The overview is intended to give a flavor of the type of knowledge that has been discovered.

5.2.1 Spontaneous electrical activity

If an observer were to examine the Fourier transform of the EEG of a normal human, she would find that it breaks up into several peaks of maximum spectral power (see Figure 12).

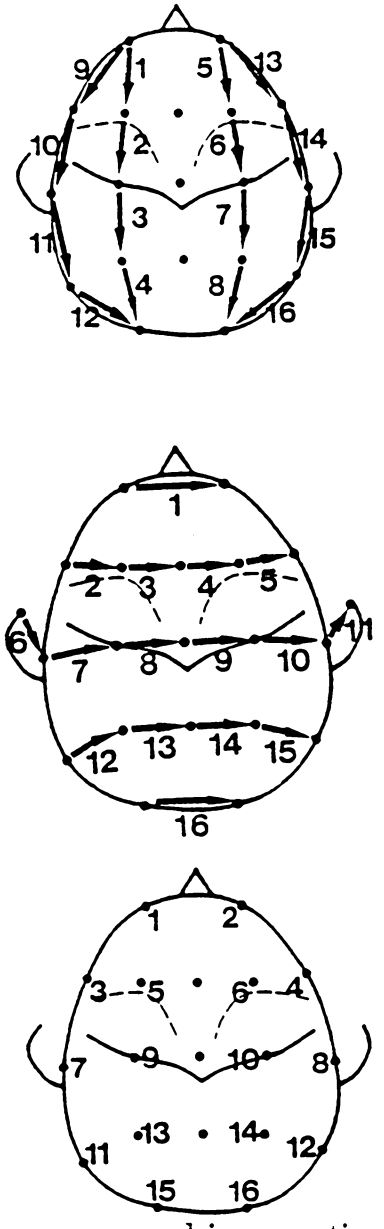

Figure 11: **Standard montages used in mounting EEG electrodes.** The first two are bipolar montages and the third is a monopolar montage. The arrows show the voltage drops measured by each electrode. Taken from [78].

Each of these peaks represent the activity of the brain in various rhythms. These rhythms are typically given lower-case Greek letter identifiers.

The α rhythm is the strongest peak in the Fourier spectrum, with a peak at about 10 Hz. This rhythm is observed primarily in the posterior region of the brain, and appears to be related to the visual apparatus in the brain. It disappears when the eyes are open, so it may be said that it represents the visual system "idling." The frequency of the α rhythm increases gradually with age, ranging from about 1.5 Hz at birth to about 10 Hz after 22 years [40]. Most humans display an asymmetry of α activity between right and left brain hemispheres, with the right side showing the higher voltages [40].

Occasionally there is a μ rhythm superimposed on the α activity. It can be distinguished from the α by the fact that it does not vanish when the eyes are opened. Keeping the body immobile enhances the μ rhythm [9].

The β rhythm is the next observable peak of electrical activity, centered at about 20 Hz. The amplitude of this activity is low, typically about 20 μV.

Finally, θ and δ waves show up at the onset of sleep. They are usually dominant in the posterior regions of the brain. There are certain other manifestations of sleep, called σ rhythms or sleep spindles. These are rounded spiky traces in the EEG which appear as the person falls into light sleep.

5.2.2 Evoked responses

The subject of evoked responses or evoked potentials has been studied extensively. A good review article is Low's [51]. The study of evoked potentials allows researchers to quantify the way in which the brain reacts to various external stimuli. The technique consists basically of connecting a person to an EEG and exposing him to a variety of stimuli such as sharp sounds, flashing lights, or somatic (touch) stimuli. The EEG records the resulting transient activity in the brain.

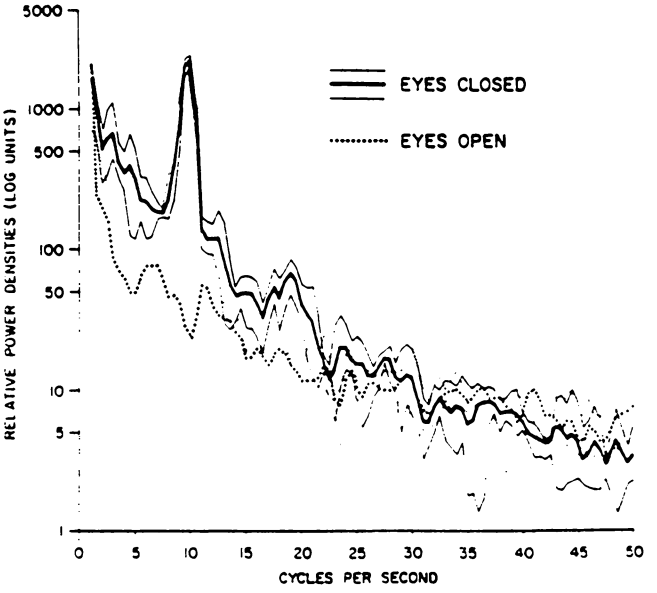

Figure 12: **The frequency spectrum of the normal EEG.** The outer curves show the maximum observed variations in the Fourier transform, and the dark curve shows the average. The α and β rhythms are quite visible. The graph is taken from [41].

The repeatability of these evoked responses can be quite good if the right precautions are taken to filter out background EEG noise [51]. Typically, the work on evoked potentials has concentrated on trying to break down the characteristic response of the brain to different stimuli into separate components, and then attempting to trace the sources of these components [17,31,44,58,85,84]. Much of the motivation for understanding the physical origins of the EEG has come from attempts to decode the event potentials evident in the EEG.

For the purposes of this study, it is worth noting that event potentials indicate that the assumption that the state of brain activity is related to the number of excited neurons is indeed a reasonable assumption. This does presume that the EEG measures in some way the number of active neurons in the brain, which is a theory that has some support [1,59,93].

5.3 The EEG as a diagnostic aid

The EEG is the most widely used tool for the diagnosis of the epilepsies. The brain's evoked responses to stimuli such as flashing lights or hyperventilation can reveal abnormalities that are indicative of the presence of epileptiform activity. But by far the most suggestive indication of such activity are the "spikes and slow waves" or SSW's.

Spikes are electrical manifestations that by definition last 70 ms or less [15]. The amplitudes of these spikes are greater than the background EEG activity, and are typically followed by a slow wave of the opposite polarity and lasting about 200 ms.

Different types of epilepsies have characteristic manifestations in the EEG [61].

The tonic clonic seizure starts off as a series of SSW's which show a loss of synchronization among the channels. At the same time, the EEG shows activity in all channels at about 20–40 Hz. This activity gradually slows in frequency until it reaches about 4 Hz, and then stabilizes. When the seizure ends, there is a long period of flatness in

the EEG, with very little activity present. This post-seizure flatness lends credence to the hypothesis that the bond fraction p has been lowered greatly by regulatory mechanisms in the brain.

The absence seizure has one of the most recognizable and repeatable EEG manifestations. The seizure starts off as desynchronization between the channels and activity at about 4 Hz. It quickly slows down to 3 Hz and then stabilizes. As the seizure ends, the frequency decreases until finally synchronization between the channels is regained. The activity is present in all channels. Absence seizures in older persons tends to show slower frequencies and lower amplitudes.

The complex partial seizure shows little similarity in EEG traces from seizure to seizure. This is not surprising when one considers the wide range of clinical symptoms. Nevertheless, the SSW's are still observable.

5.4 The physical origins of the EEG

Ever since Berger's original work on the EEG, there has been much work on trying to correlate the electrical activity picked up by the EEG at the scalp with the electrical activity of the brain. Brazier's [7] was the first paper to apply the knowledge gained by physicists about electromagnetism to an understanding of the EEG. She was also the first researcher to propose the current dipole theory of the EEG. This section will review this model and proceed to catalog the work of other researchers in the field. It is hoped that such a catalog will show researchers in the physical sciences that there is much physics and chemistry to be understood in this field, and will allow them to find the relevant work in the vast amount of existing literature on the EEG.

5.4.1 The current dipole model

Brazier [7] proposed that the origins of the EEG were in the minute currents that are set up by the excitatory and inhibitory postsynaptic potentials (EPSP's and IPSP's—see Section 2.1.2). The basic idea, to be expounded upon shortly, is that a polarized synapse causes ions in the ion bath that permeates the brain to move. Such ion currents from aggregates of synapses then add up to form a current that flows through the scalp. Before a complete exposition on this theory is given, a widely held misconception among EEG researchers must be addressed.

Since the original dipole model paper of Brazier, many papers have appeared which seem to assume that the EEG problem is one of *electrostatics*. That is, that there exist within the brain *charge* dipoles, and that the EEG picked up on the scalp is a potential field. This is clearly impossible, because the brain is embedded in an electrolytic fluid which acts as a conductor. Not an excellent conductor like copper (resistivity $\rho = 2 \times 10^{-6}\,\Omega\,\mathrm{cm}$), but a conductor nevertheless ($\rho = 350\,\Omega\,\mathrm{cm}$ in the cortex [63]). The potential $\Phi(r)$ at a distance r from a charge q in a conducting medium is given by

$$\Phi(r) = \frac{q}{4\pi\epsilon r} e^{-r/r_d}, \tag{5.1}$$

where r_d is the Debye shielding distance and ϵ is the dielectric constant of the material [35]. For brain tissue, $r_d \sim 1\,\text{Å}$ [63], and it is clear that it would be impossible to detect the effects of electrostatic dipoles deep in the brain. The analogy between the current due to a static current dipole and the potential due to a static charge dipole is fortuitous in that the results derived by some researchers can be applied with a change of perspective.

The current dipole model is based on empirical evidence obtained from microprobe studies [93], in which tiny electrolytic probes are inserted into the brain in an attempt to correlate surface EEG effects with bulk electrical activity. The work has established that the current dipoles in the brain are set up by the postsynaptic potentials. When a synapse either depolarizes or hyperpolarizes in response to neurotransmitters, the principle of charge

conservation requires that charges must flow in the surrounding ion bath. If the discussion is confined to positive charge for the moment, then charge must be sourced at a synapse if the synapse is hyperpolarizing (becoming more negative) and sunk at a synapse if the synapse is depolarizing (becoming less negative). The complementary source or sink appears to be in the membrane walls of the neuron (recall the discussion in Section 2.1.2 on the mechanism of synaptic transmission).

This does not fit well with the classical model of a dipole as being a current source/sink pair separated by a distance. One end of the "dipole" is well localized at a synapse, but the other "end" is in effect distributed over the entire body of the neuron. But at a sufficiently large distance the dipole approximation becomes more valid. In particular, aggregates of neurons tend to appear at such distances as forming dipoles.

The currents due to many such dipoles cause a bulk current to flow in the fluid surrounding the brain. Eventually, this current will show up at the scalp. Thus, the EEG is measuring *Ohmic* potential drops, not static potentials with respect to infinity [73,74]. The analogy made earlier between an EEG and a voltmeter is seen to be quite accurate. Data from studies on the relation between EEG voltage amplitudes and distance between electrodes [21] confirm this view. With this model, it becomes clear why attempts to find a "true ground" for the EEG are doomed. All such attempts, for example using a toe, will inevitably result in picking up massive amounts of extraneous noise from other current sources in the body, such as the heart [15].

That currents must flow tangentially through the resistive scalp, setting up Ohmic potential drops measured by the EEG, is required by the charge conservation principle. The scalp is a two dimensional conductor covering the skull. Beyond the scalp is a poor conductor, so charges injected from the brain through the skull into the scalp must flow away from such scalp sources and through the scalp to remotely located sinks, where the charges are returned through the skull into the brain. In three dimensions,

$$\vec{\nabla} \cdot \vec{J} = 0 \tag{5.2}$$

because of charge conservation. The $\partial\rho/\partial t$ term can be neglected because of the relatively high conductivity—all currents are much slower than the conduction screening response to fields, which has a characteristic time of $1/\sigma$.

In two dimensions,

$$\vec{\nabla}\cdot\vec{J} = \frac{\partial J_x}{\partial x} + \frac{\partial J_y}{\partial y} \tag{5.3}$$

with J_x and J_y being the components of $\vec{J}$. Using

$$\vec{J} = \sigma\vec{E} \tag{5.4}$$

$$\vec{E} = -\vec{\nabla}\Phi, \tag{5.5}$$

one obtains

$$-\frac{1}{\sigma}\vec{\nabla}\cdot\vec{J} = \frac{\partial^2\Phi}{\partial x^2} + \frac{\partial^2\Phi}{\partial y^2} \tag{5.6}$$

as the familiar relation between the Laplacian of the potential and the current density. It is this potential Φ that the EEG measures. Nunez [63] points out that this equation can be solved by a finite difference method [78] to yield the surface current density from EEG measurements.

Nicholson [59] has derived a model for the potential distribution inside the brain due to a large number m of neural sources and sinks.

$$\sigma\left(\frac{\partial^2\Phi}{\partial x^2} + \frac{\partial^2\Phi}{\partial y^2} + \frac{\partial^2\Phi}{\partial z^2}\right) = -I_m(x,y,z) \tag{5.7}$$

where

$$\int_V I_m\, d^3x = \sum_{i=1}^{m}\int_{M_i}\vec{J}_m\cdot d\vec{s} \tag{5.8}$$

where $\vec{J}_m$ is the transmembrane current and M_i is the surface area of the i'th neuron. Equation 5.7 assumes that the conductivity σ is isotropic; Nicholson derives the model for the more general case of anisotropic conductivity.

5.4.2 A review of research on dipole models

Research on the dipole models of the EEG, as in most other areas of research, falls into two general categories: "theoretical," attempting to refine the dipole models themselves, and "applied," using the dipole models in attempts to localize the sources of electrical activity in the brain.

The earliest and definitive work on constructing a dipole model is by Brazier [7]. Using a physical model of current dipoles in a conducting medium, she was able to correlate the EEG of an epileptic patient to two epileptic foci. Following her lead, many refinements were made to the model. Geisler and Gerstein [23] used a "three-sphere" model of the head, in an attempt to take into account the different conductivities of the cerebrospinal fluid, the skull, and the scalp. Kostopoulos and Gotman [43] derived an algorithm for computer derivation of neuron activity from the EEG.

Such theoretical analyses for the most part concentrated on refining models that are based on the EEG. In a departure from that norm, Perrin [74] and Pernier [73] propose that the EEG is basically flawed in that it measures voltages instead of currents. They propose that the EEG be replaced by a new technique they call surface current density mapping. Since the actual phenomenon being measured is the flow of current, it indeed appears to make more sense to measure current rather than voltages. As Perrin and Pernier point out, the current density technique has the added advantage that there is no need for an artificial reference for voltages. This allows topographic maps of current density to be generated by a computer.

These theoretical models solve the problem of deriving a surface EEG distribution when the localization and extent of the internal current dipoles is known. The inverse problem is of course more applicable to an understanding of brain mechanisms. Much research has been devoted to this topic, with varying degrees of success. A review of localization techniques is given by Kavanagh [39]. Many such techniques rely on assuming some reasonable distribu-

tion of static current dipoles and then iteratively solving the equations for scalp potential distributions. Moller *et al.* [58] and Deiber *et al.* [17] give the results of attempts to localize evoked potentials.

As computers and software became more sophisticated, so did the models for dipole localization. The assumption of stationary dipoles was abandoned, and more complex models with rotating dipoles came into favor. Scherg and von Cramon [84,85] derived a model for the brain-stem auditory evoked potential (BAEP). They used an iterative technique that assumed several dipoles whose centers are fixed but which rotate. The agreement to observed data is good.

Another new approach to dipole localization of the BAEP is the "3-channel Lissajou trajectory" technique [37,36,89]. This uses three orthogonally placed electrodes to record the BAEP. The three channels are plotted synchronously yielding a three-dimensional Lissajou trajectory of the scalp potentials due to the BAEP. This trajectory can be analyzed to yield the temporal behavior of the BAEP source dipoles.

Kraut *et al.* [44] used a variant of the finite-difference technique proposed by Nunez [63] to derive the dipole sources of the flash visual evoked potential.

The EEG is not the only tool used in these localization studies. Currents in the brain must give rise to magnetic fields, and the magnetoencephalogram (MEG) is coming into vogue as a diagnostic and research tool. Wikswo and Roth [96] derive techniques for localization of source dipoles using the MEG.

5.5 The power spectrum of the EEG

One of the findings of researchers attempting to correlate the internal electrical activity of the brain with the EEG is that the Fourier transform of the EEG tails off at much lower frequencies than does the Fourier transform of the intracranial activity. That is,

much higher frequency components can be found in the intracranial activity than in the EEG. This can be seen qualitatively by examining Figure 12 and comparing this with the absolute refractory period for neurons, given in Section 2.1.2. If the maximum neuron firing frequency is 1 kHz, it seems strange that there is almost no EEG activity above 50 Hz.

Apparently, this discrepancy has led to much confusion in the field of EEG research. Nunez [63] attacks the findings of studies that have concluded that the resistive properties of living tissue are radically different from those of inanimate matter (as a rational skeptic, Nunez shares with this author a reluctance to discard hundreds of years of research in physics which has shown that the physical properties of matter are the same throughout the universe). These studies used external current generators to measure the resistive properties of the tissue, and Nunez shows that they all fell victim to a misunderstanding of the nature of the electrolytic capacitance of the electrodes.

It is proposed here that the same electrode capacitance can account for the discrepancy between the power spectra obtained from cranial probes and that obtained from EEG. The particular effect responsible for the attenuation of higher frequencies is the double-layer capacitance. When a conducting electrode is placed in an electrolytic solution, there is a capacitance effect caused by the concentration of ions around the electrode (recall that the EEG electrodes are attached to the scalp using an electrolytic paste). This double layer capacitance has been shown to be virtually independent of the nature of the ions that occupy the double layer or of the potential applied to the electrode, and has a value of about $17\,\mu\mathrm{F\,cm^{-2}}$ of electrode area [6]. Using an electrode radius of 0.4 cm [79], one arrives at a double-layer capacitance of $17.1\,\mu\mathrm{F}$. With a typical electrode impedance of about $1000\,\Omega$ [79], the time constant $\tau = 1/RC$ of the electrode is about 58.5 Hz. That is, the power transmitted through the electrode at 60 Hz is lower by a factor of $1/e$ than the power transmitted at DC or 0 Hz. The same loss is not evident in intracranial probes because these typically have a very small cross-sectional area, with a proportionately lower capacitive effect.

It should be noted that this effect can account only for the overall loss in transmitted power as frequency increases. Some researchers have found that there is a bandpass filter effect as well, with some frequencies transmitted better than other almost equal frequencies. Pfurtscheller and Cooper [76], for instance, show that a bandpass effect in the β frequencies can be accurately modeled with a recursive multipole filter.

There is a wealth of research findings on the power spectrum of the EEG. Autret *et al.* [3] discovered an asymmetry in the power spectra of right and left hemispheres of the brain when motor activity occurs, and Leung [48] discusses the effects of various drugs and chemicals on the power spectrum of the rat EEG. Nuwer [64] uses differences between the power spectra of epileptiform and normal EEG's to localize the focus of epileptic activity in the brain. Others [16,83] propose methods to quickly compute the power spectrum of the EEG, allowing researchers to monitor in real time the effects of various stimuli to the EEG.

5.6 The statistics of EEG data

Part of this research effort involved an attempt to subject EEG data to the same sort of statistical tests which were applied to clinically obtained data. The results were not as fruitful, but they are presented here with the hope that other researchers may find something in them that was missed in this study.

5.6.1 The origin of the data

The data on EEG were made available by Dr. Jean Gotman of the Montreal Neurological Institute. The data were read by analog-to-digital converters attached to the EEG, reduced by a computer using an algorithm derived by Gotman [27], then recorded in machine-readable form on 9-track magnetic tape.

The reduction technique is a sequential pattern recognition procedure, rejecting the large proportion of the data which contains no epileptiform activity (defined as spikes and slow waves). The rejected data has a high probability of containing no such activity [28]. The portions of the data which are not rejected are subjected to more refined tests, and the algorithm proceeds by winnowing out uninteresting information in this sequential fashion.

First the EEG activity is reduced into sequences of segments, with a segment being defined as a section of signal between two consecutive extremes of amplitude. Thus, the rising part of a spike forms a segment, as does the falling part of a spike. Taking sequences of segments reduces the effect of having a high frequency noise superimposed on a slower wave, and tends to favor the lower frequency brain activity over the higher frequency activity generated by muscle movement. A wave is defined as two consecutive sequences with opposite polarity (one going up and the other down, for example). Each part of the wave (up- or down-going) is defined as a half-wave.

A weighted average of the background amplitude is computed every 1/3 second. The weighting is added to prevent true spike activity from contributing to the background average. The amplitude of a half wave is computed as the ratio of its absolute amplitude to the average background amplitude. The durations of each half wave and the second derivative at the peak of the wave are also computed. Thus, the technique reduces all spikes and sharp waves to triangles, characterized by an attack portion (going up for spikes and down for slow waves), a decay portion, and amplitudes and durations for each portion.

A wave is accepted as epileptiform if it meets all the following criteria:

- The ratio of absolute wave amplitude to background amplitude is 4 or larger.
- The durations of each half wave must be less than or equal to a value derived empirically and based on the amplitudes of the half waves. The second half wave has a larger rejection value because spikes and slow waves tend to have a sharp "attack" followed by a slower decay.

- The amplitudes of the half-waves are compared to the second derivative of the wave at its peak. The larger the amplitude, the sharper must the wave be to be declared an epileptiform spike.
- The total duration of the wave must be larger than or equal to 35 ms. This is necessary to reject muscle noise.

When a wave is accepted as epileptiform, its parameters are written to tape, along with the time at which it was seen.

5.6.2 The statistics of spike-free intervals

In a manner analogous to the definition of seizure-free intervals, one may define the spike-free interval as the elapsed time between two consecutive epileptiform events in the EEG of a patient. It would seem reasonable that if the gross manifestation of epileptiform activity, i.e., seizures, are Poisson distributed then epileptiform activity must itself be Poisson distributed.

However, this is not the case. Using the fact that the time of each event is recorded by Gotman's program, Figure 13 was generated, showing the distribution of spike-free intervals as a function of interval length. It is not clear why this discrepancy occurs. The EEG spike free data seem to follow a normal distribution more than a Poisson distribution. There appears to be a "preferred" spike free interval, suggesting a periodicity in the spike occurrence. As mentioned earlier, Binnie *et al.* [5] also observed a periodicity in EEG spike and slow wave activity.

5.6.3 The statistics of the spike rate

The average spike rate $\bar{\lambda}$ was computed over the entire EEG recording period. This was computed by counting up the number of epileptiform events in some interval and then

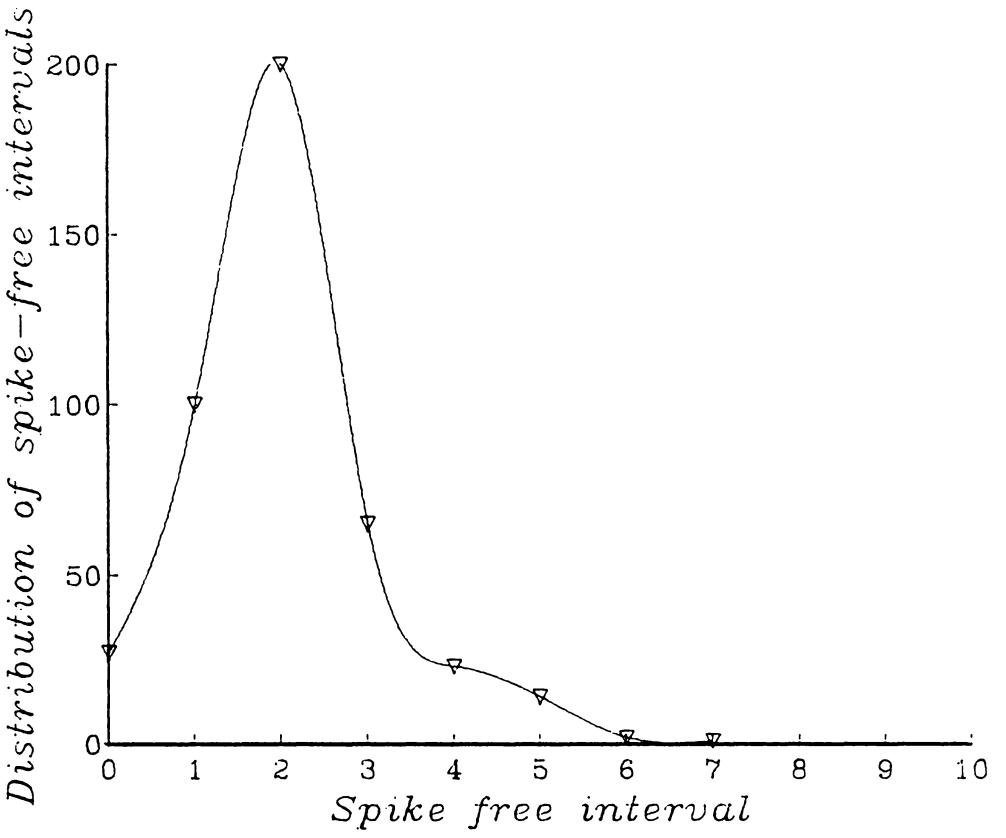

Figure 13: The distribution of spike-free intervals as a function of interval length. The x-axis shows the interval length in minutes, and the y-axis shows the number of spike-free intervals with a particular length. Note that the distribution is not Poisson. The curve shows a piecewise interpolated cubic spline function.

dividing the count rate by the interval. It was hoped that some distinct time evolution of the spike rate would emerge. See Figure 14 which shows the evolution of $\bar{\lambda}$ averaged over 10 minutes for one patient. (That is, $\bar{\lambda}$ is calculated by counting the number of spike events in ten minutes, and dividing by 600.)

Figure 15 shows the distribution of the spike rates as a function of spike rate. The spike rates are computed over 15 minute averaging intervals. The shape of the curve is reminiscent of the curves showing the distribution of seizure rates in the clinical data. Once again, one presumes that the curve reflects the way in which p varies, with higher spike rates implying that p is close to p_c.

5.6.4 Distributions of spike parameters

Distributions of the spike parameters (attack amplitude, decay amplitude, durations, etc.) were computed in the hope that some trend would emerge that could shed some light on the statistics of the EEG. These distributions are shown in Figures 16 through 19. Trends in the distributions of amplitude and duration, if indeed they do exist and are not artifacts, cannot be explained without more detailed theories of EEG than exist today.

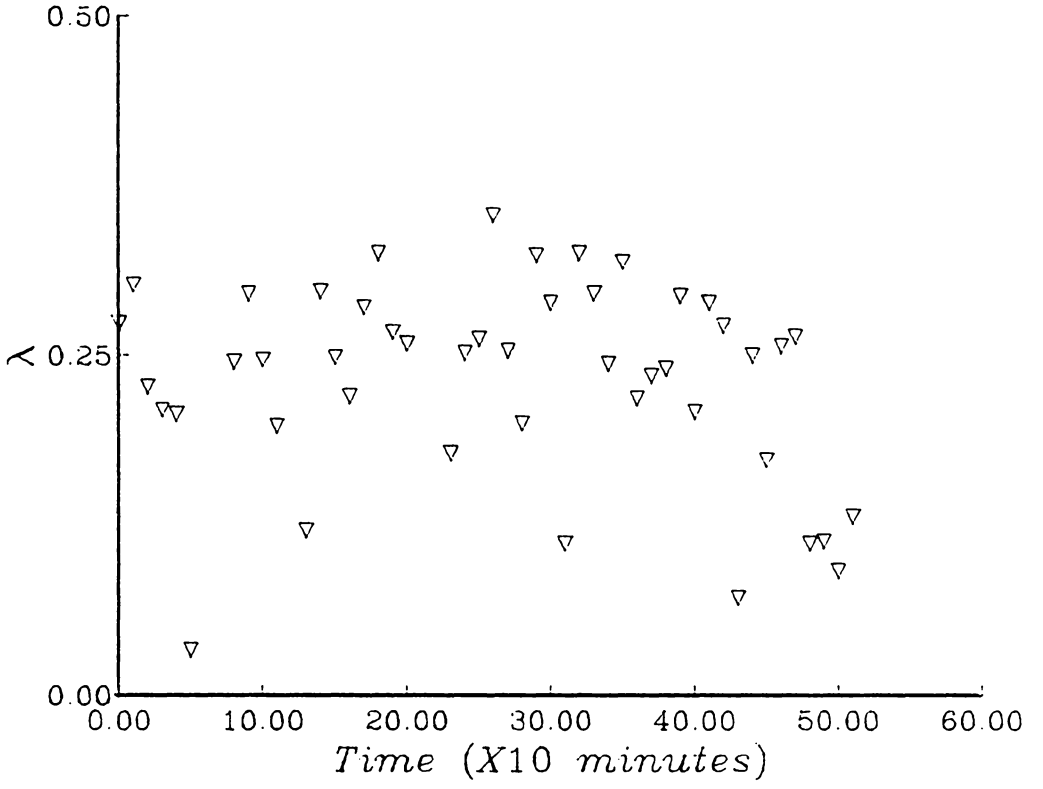

Figure 14: The time evolution of the average spike rate $\bar{\lambda}$ with a boxcar size of 10 minutes. The x-axis shows the evolution of time in units of minutes, and the y-axis shows the average spike rate.

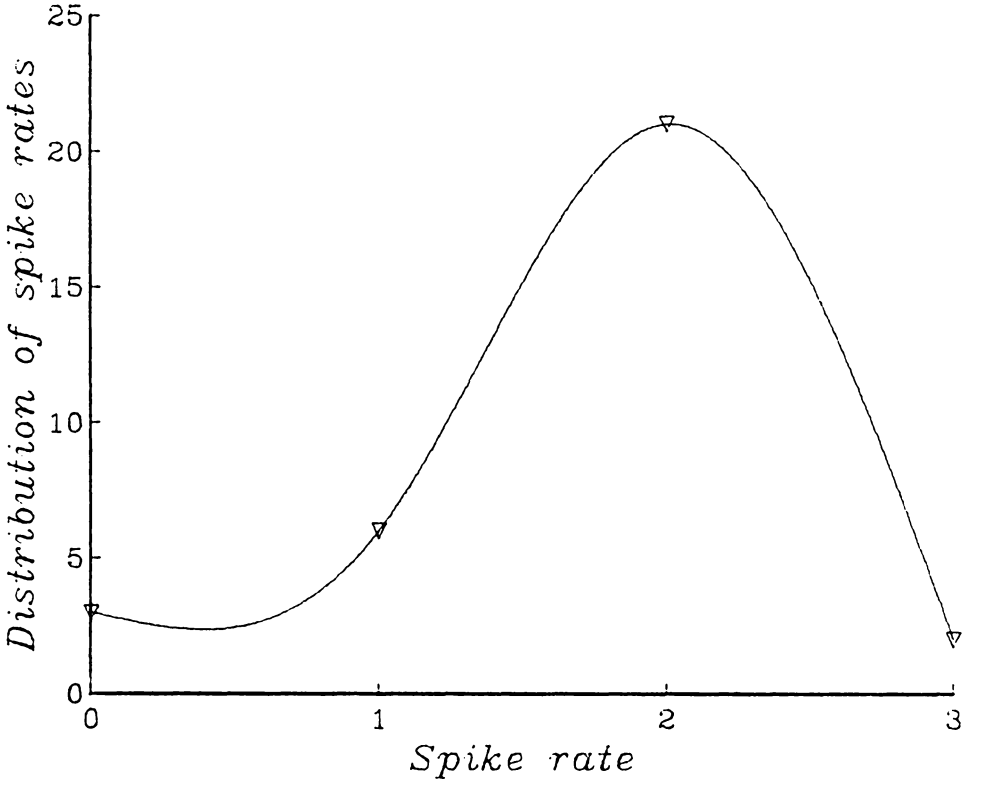

Figure 15: **The distribution of the average spike rate $\bar{\lambda}$ at a sample rate of 15 minutes.** The x-axis shows the spike rate observed in a 15 minute interval and the y-axis shows the number of such intervals in which a particular spike rate occurred.

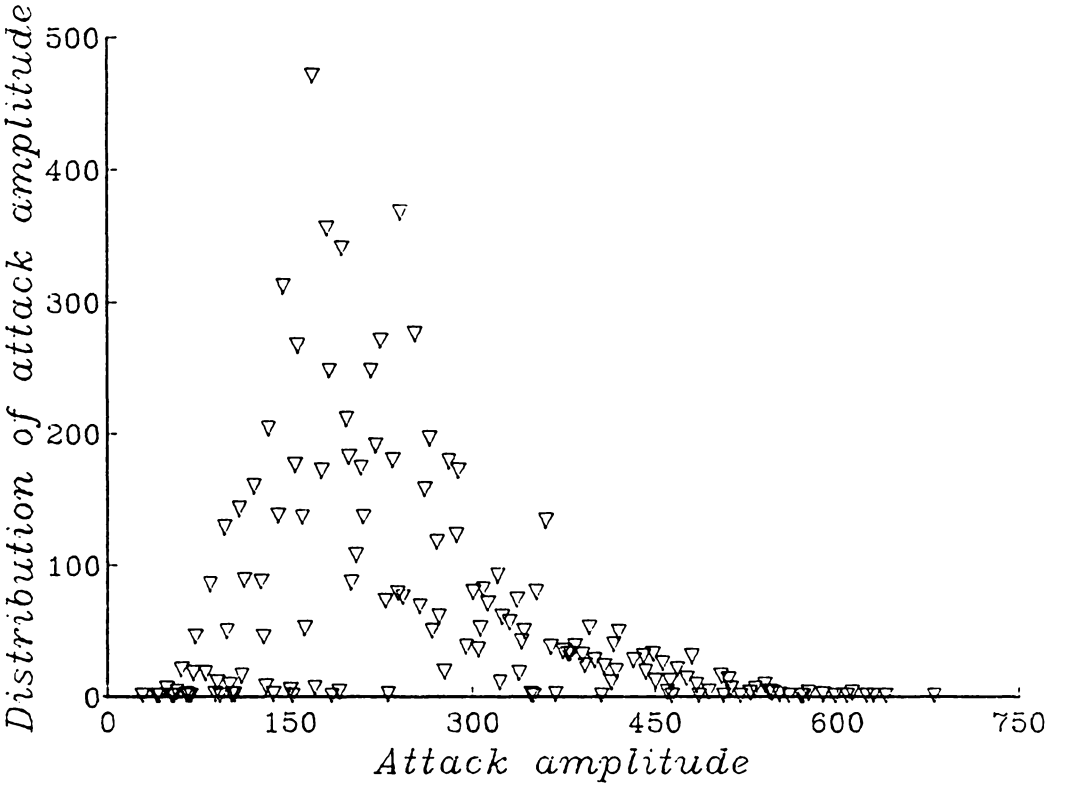

Figure 16: **The distributions of attack amplitude in the EEG.** The x-axis shows the attack amplitude and the y-axis shows the number of events with a particular attack amplitude.

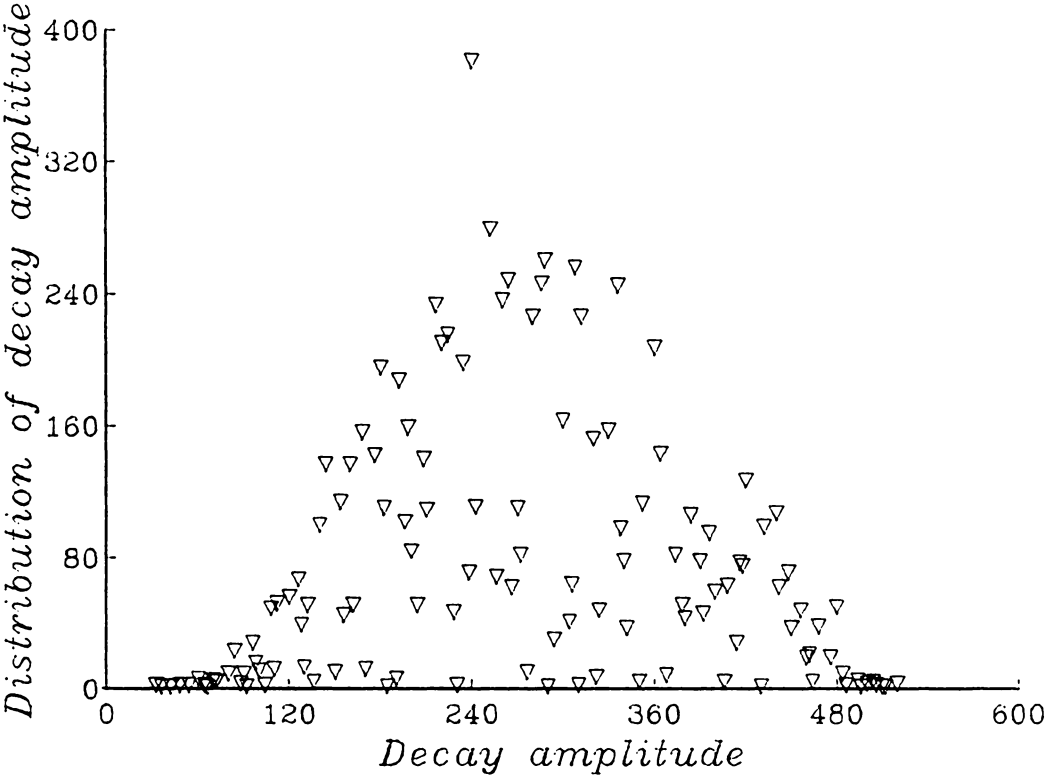

Figure 17: **The distributions of decay amplitude in the EEG.** The x-axis shows the decay amplitude and the y-axis shows the number of events with a particular decay amplitude.

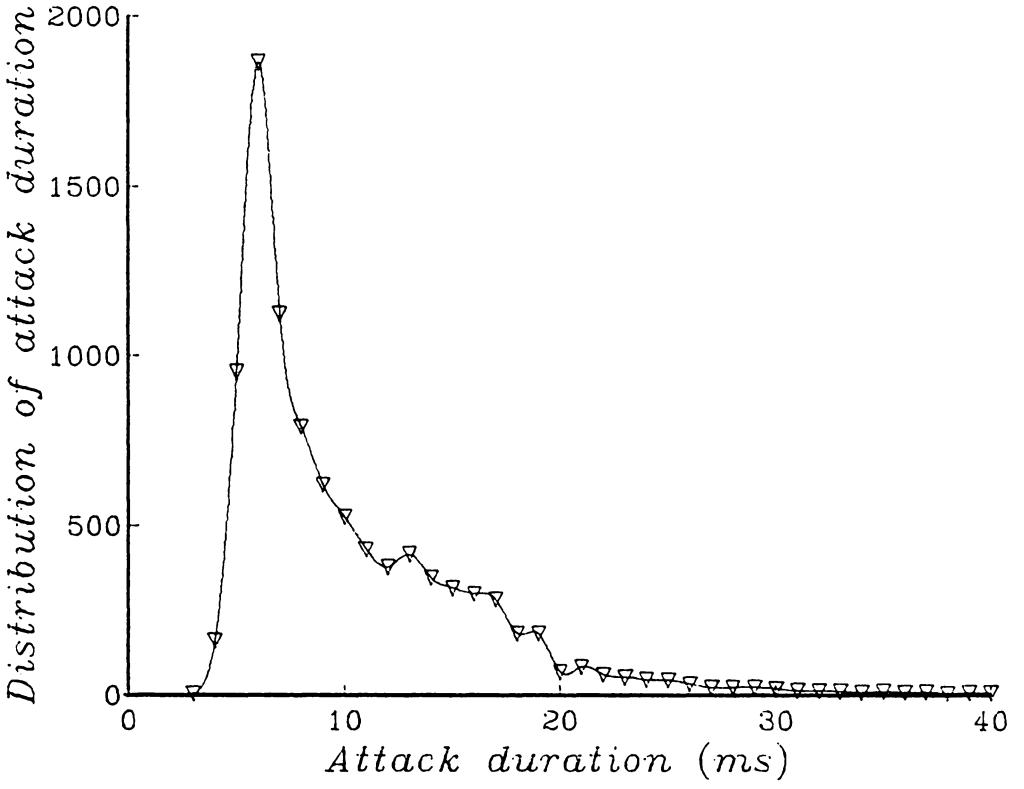

Figure 18: **The distributions of attack duration in the EEG.** The x-axis shows the attack duration and the y-axis shows the number of events with a particular attack duration.

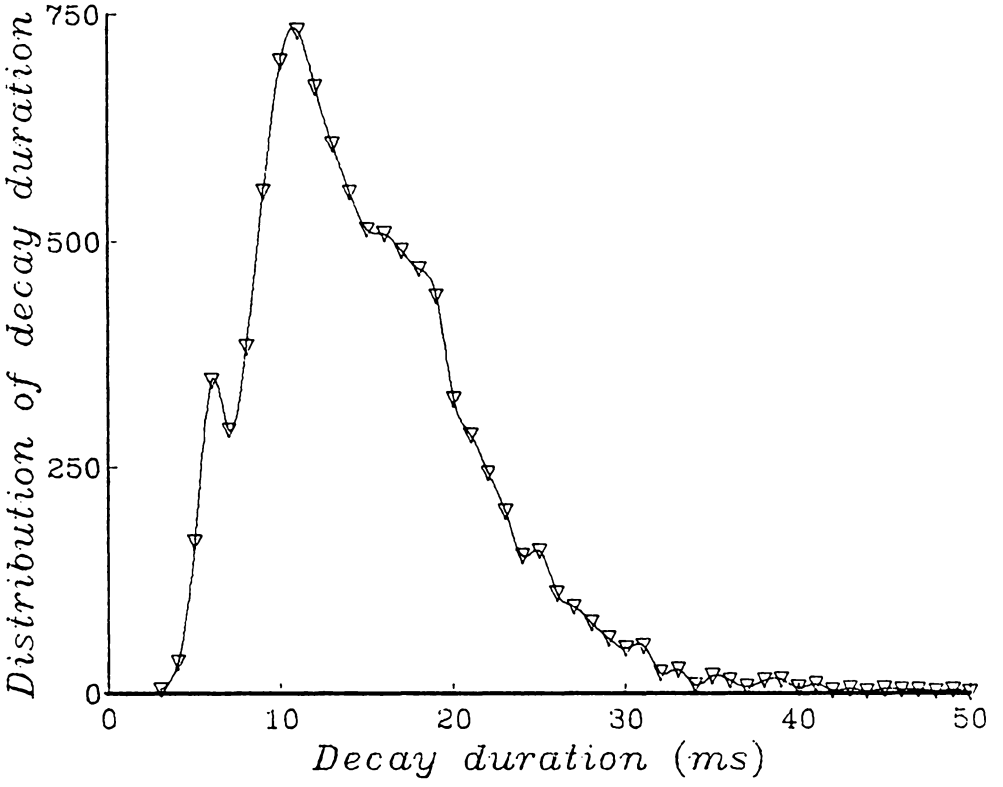

Figure 19: **The distributions of decay duration in the EEG.** The x-axis shows the decay duration and the y-axis shows the number of events with a particular decay duration.

Chapter 6

Monte-Carlo simulations

Wyler *et al.* [98,97] advance the hypothesis that there exist in the central nervous system certain types of neurons, which they call Group 1 neurons, which have the characteristic properties of high excitability and powerful recruiting capabilities. Such neurons, when excited, immediately cause a neighborhood of neurons to begin a sympathetic firing. This firing is sustained by the Group 1 neurons. Wyler *et al.* show that the frequency of seizures in epileptic monkeys is related to the concentration of these Group 1 neurons. It seems reasonable to assume that these neurons act as internal amplifiers to the runaway electrical oscillations that characterize a seizure. This chapter examines the effect of such excitatory sites on a bond percolating system.

A word on notation: this chapter makes use of two different lattice probabilities. The bond fraction, previously referred to as p, is here referred to as p_b.

6.1 Group 1 neurons and the percolation model

The existence of such neurons in the central nervous system affect the percolation model of the epilepsies by providing a mechanism which accounts for the higher bond fraction p_b of

epileptic patients. It has been pointed out earlier that even normal people can have seizures (though not strictly speaking *epileptic* seizures). This can occur if powerful environmental stimuli excite the brain: in the percolation model, these stimuli cause a large increase in p_b, forcing it above p_c.

Why then do epileptic patients suffer seizures in response to much lower stimulus levels? It is unlikely that p_c for such patients is lower—the critical bond fraction is a property of the lattice, and the brains of epileptic patients are presumably not very different in structure from those of normal people. The Group 1 neurons can provide an answer: if these neurons can be easily excited and recruit many other neurons into their excited state, they can serve to increase p_b artificially. Whereas normal people require strong external stimuli to exceed the threshold, epileptics have internal stimuli that achieve the same goal. The recurring seizures that characterize the epilepsies are a result of these abnormal neurons.

Wyler and Ward [98] lend credence to this model by showing that cortical resection on epileptic patients can stop seizures even though the entire epileptic focus is not removed. In a related study [97], they show that seizure frequency increases exponentially with Group 1 neuron concentration, and they claim that cortical resection works because it removes a sufficient number of these neurons that the seizure frequency drops to zero. Suppose that the occurrence of seizures were a manifestation of some property of the entire focus; then cortical resection would not work if the entire focus were not removed. This must mean that the occurrence of seizures is related to the size of or number of neurons in the focus.

6.2 A simulation of the effects of Group 1 neurons

6.2.1 Overview

To test the effects of such "recruiting offices" on the classical bond percolation model, a Monte-Carlo simulation of a percolating lattice was constructed and run. Classical bond

percolation simulations proceed by filling a lattice with bonds with the help of a random-number generator (RNG). Given a bond probability p_b, they run a RNG on the range from zero to one at each lattice site, and place a bond at that site if the RNG gives a value less than p_b.

This classical approach was modified to account for the presence of Group 1 neurons. Instead of filling the lattice with identical sites, the lattice is filled with a mixture of normal and Group 1 sites, using the RNG "die-casting" technique described above. Given a Group 1 site probability p_s, the lattice then contains approximately p_s/L^d Group 1 sites and $(1 - p_s)/L^d$ normal sites (here, L is the linear dimension and d the dimensionality of the lattice). When bonds are seeded, the algorithm examines the type of site it is about to seed. Normal sites are seeded with the classical random bond-seeding technique to simulate the random connections between normal neurons. Group 1 sites, on the other hand, are automatically assigned bonds to all nearest neighbors. This is a reasonable approximation to the spontaneous firing and recruiting capabilities of such neurons. The lattice was then examined for percolating clusters (that is, groups of connected sites extending from one side of the lattice to the opposite side).

6.2.2 Details of the simulation

Description of a run

The Monte-Carlo simulation was constructed to see if such a modified bond percolating system would account for the lowered critical threshold postulated above, and to see if it could replicate the relationship between Group 1 site concentration and seizure rate observed by Wyler *et al.* [97].

Each run accepted a fixed bond probability p_b and varied the Group 1 probability p_s over some given range, each time stepping p_s by some given amount. At each value of p_s, the

lattice was seeded with sites and bonds and examined for percolating clusters some number of times. After each lattice run, the simulation printed out p_b, p_s, and whether the lattice percolated or not.

The RNG's and their effect on the simulation

The random-number generator used in the simulation was of the classical linear congruential variety, using 48-bit integer arithmetic to compute 64-bit floating-point numbers [57]. It is particularly suited to Monte-Carlo simulations because it can be restarted at a given point in a particular sequence at any time. This allows one RNG to generate independent sequences of random numbers, and to restart the sequences at any time. Two independent streams of random numbers were maintained: one to seed the Group 1 sites, and the other to seed the bonds.

To determine the effect of Group 1 concentration on the percolating threshold, it is necessary to average over as many bond and Group 1 site configurations as possible (imagine a lattice that gets a row of Group 1 sites all lined up—such a lattice would always percolate because of the nearest-neighbor bond requirement, but is not very representative of lattices with that particular p_s). This is why the simulation was run several times for each value of p_s. The bond and site RNG's ran freely (that is, without being restarted) through all runs at a fixed p_s, allowing the lattice to be seeded with different configurations of bonds and Group 1 sites for each value of p_s.

On the other hand, when p_s is changed, the RNG's must be restarted to produce the same configurations of bonds and Group 1 sites. To properly simulate the effect of a larger p_s, the only thing that must change is the number of bonds and Group 1 sites. That is, if p_s changes from 0.1 to 0.2, all that must change is that approximately 10% more sites are Group 1 sites. The same sites that were marked Group 1 when p_s was 0.1 must be marked Group 1 when p_s is 0.2, so that the effects of different lattice configurations are overcome.

Thus, the RNG's were restarted to produce the same sequences of random numbers each time p_s was changed.

To summarize so far, a run at a fixed p_s averaged over the effects of several different lattice configurations. Each time p_s changed, the run averaged over the effects of the same varying lattice configurations as the previous value of p_s.

Finally, the simulation was run at several different RNG starting points. This averaged over as many different RNG sequences as possible. Of course, all these steps only simulate the effects at some particular p_b. The simulation was run several times in the above fashion with different values of p_b.

6.2.3 Results of the simulation

Because the simulation requires a great deal of computer power, it was run only on a square lattice with $L = 50$.

Lowering the critical threshold

The results are plotted in Figure 20. Here, the probability $R(p_s)$ of a spanning cluster appearing at a site probability p_s is shown averaged over the different values given by different initial starting points for the random-number generators. Note that for any $p_s > 0$, the system percolates well below the theoretical p_c for a square lattice (see Table 3).

Comparison with the Wyler study

Wyler *et al.* [97] postulated an exponential increase in the seizure frequency observed in monkeys as the Group 1 neuron concentration increased. Their data are shown in Figure 21 It is unlikely that their data do in fact fit an exponential curve. The seizure frequency must

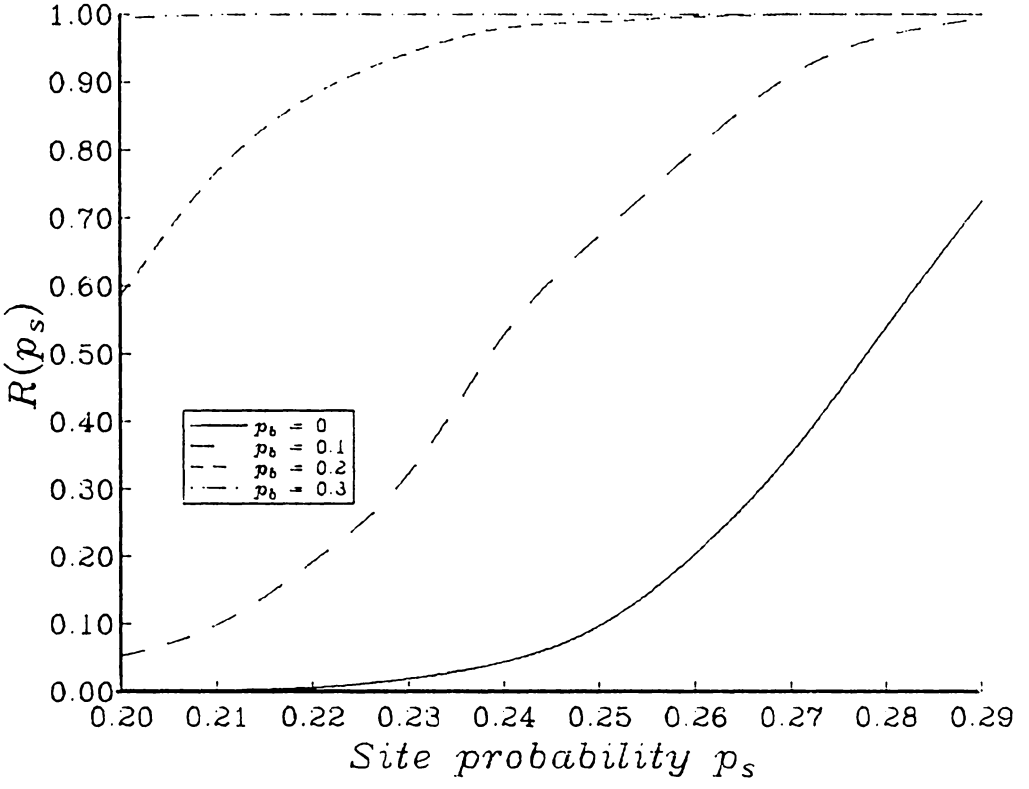

Figure 20: **The effect of Group 1 site concentration on a bond percolating system.** Each curve shows the probability of a percolating cluster appearing as the Group 1 site probability increases. Different curves show the effect of varying the bond fraction.

saturate as the Group 1 concentration increases—there are only so many periods over which a seizure frequency can be measured. This is borne out by their data: the last two points, at the highest Group 1 neuron concentration, begin to show the saturation of the seizure frequency.

The results of the simulation study represented in Figure 20 are plotted in the same style as that used by Wyler *at al.* in Figure 22, and shows the same form of increase. The ordinate in Figure 22 shows $\log(70R(p_s))$ because the simulation performed 70 runs at each value of p_s. This means the ordinate is showing the log of the number of spanning clusters observed at any given p_s, to bring it into closer correspondence with Figure 21.

This provides evidence for the percolation model. The simulation shows that the probability of a spanning cluster forming at a particular value of p_s is given by the curves in Figure 20. If this statement is recast into the language of this percolation model of the epilepsies, it says that the number of seizures (read "spanning clusters") in any unit of time (read "run of the Monte-Carlo simulator") obeys the curves of Figure 20. In fact, this curve is the so-called "erf" function,

$$\mathrm{erf}(x) = \frac{2}{\sqrt{\pi}} \int_0^x e^{-t^2}\, dt \tag{6.1}$$

also called "the area under a Gaussian." This follows from Monte-Carlo renormalization studies on $R(p)$ (see Equation 3.6), which have shown that [92]

$$\frac{dR}{dp} = \frac{1}{\sigma\sqrt{2\pi}} \exp\left[\frac{-(p - p_{\mathrm{av}})^2}{2\sigma^2}\right] \tag{6.2}$$

where p_{av} is the average probability at which a spanning cluster appears on a finite lattice. This Monte-Carlo simulation thus also shows that the modified bond percolating system behaves like a classical bond percolating system with a lower p_{av}.

The agreement with Wyler *et al.*'s data shows that the epileptic brain does have some correspondence with this modified finite bond percolation system.

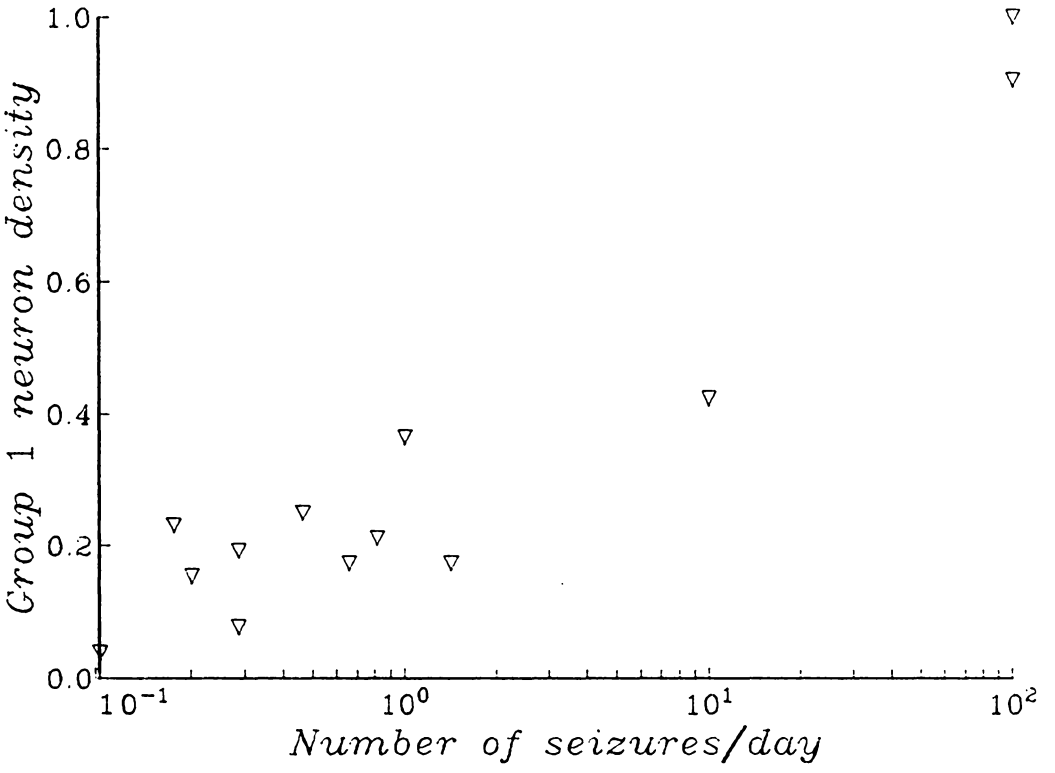

Figure 21: Results of the Wyler Group 1 neuron study. Their assumption was that the data lie on an exponential curve, but observe the last two points.

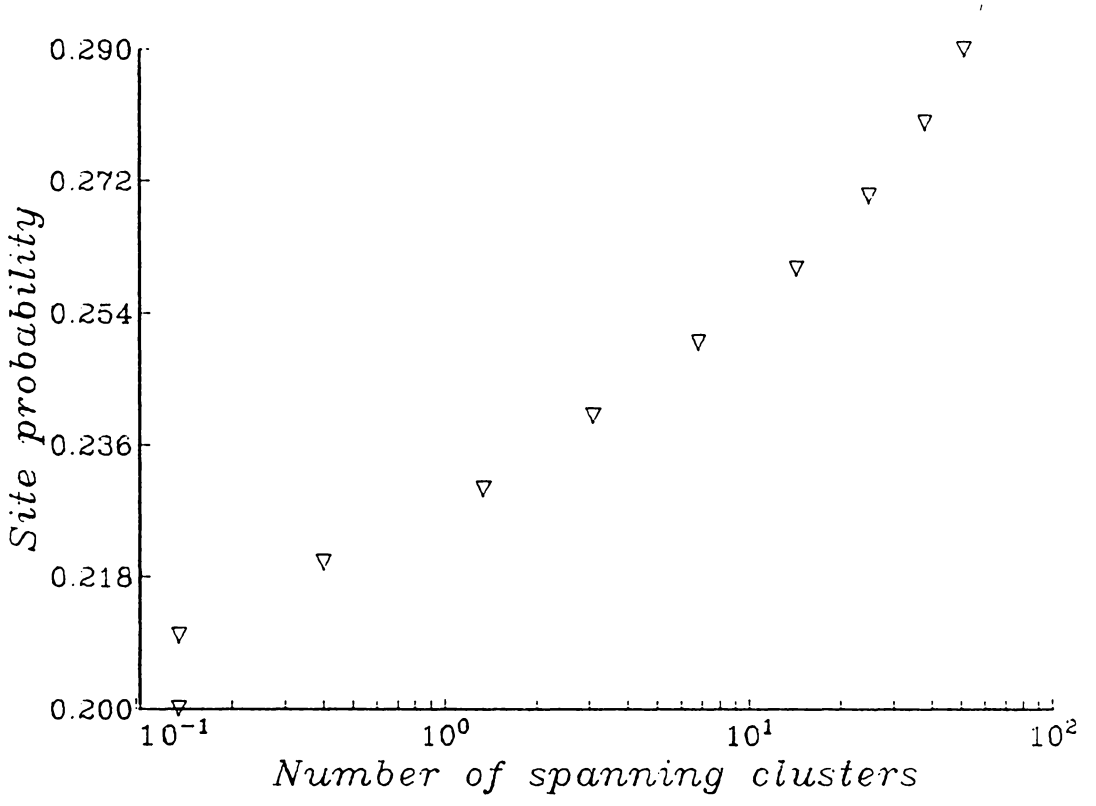

Figure 22: The results of the Monte-Carlo simulation after the style of Wyler *et al.* The abscissa is p_s, the ordinate is log number of spanning clusters detected—$\log(70R(p_s))$.

6.3 Simulation of daily seizure rates

A modified version of the Monte-Carlo simulator was run to examine the effects of various p_b's on the seizure rate of an epileptic patient. Such a simulation might help shed some light on the effects of AED's on the percolation system: AED's modify the shape of the seizure rate histograms as shown in Section 4.2.6, and the simulation may help explain the effects of the AED's on the various percolation parameters.

6.3.1 Overview of the daily seizure rate simulation

The simulations were run to observe the effects of different distributions of p_b on patient seizure rates. Assuming p_b varies in a Gaussian fashion (see Equation 3.10), the simulation sought to determine the effects of varying $\bar{p}_b$ and Δp_b. Presumably these are the quantities affected by AED's—consider the effect of phenobarbitol on a person's consciousness.

To accomplish this, the simulation generated 365 normally distributed random deviates with a given mean and variance, using the Box-Muller transformation [78]. Each deviate was taken as p_b for one day, using the generalization that diurnal variations in p_b are small enough to be averaged out this way. The Monte-Carlo simulation was then run 24 times for each day, using the p_b for that day and a fixed p_s, chosen at the start of the simulation (presumably, p_s is a fixed quantity for any given person). Each "hour" used different configurations of bonds (simulating the changing activity of the brain/lattice) but identical configurations of Group 1 neurons (representing the fact that Group 1 neurons do not move around in the brain/lattice).

Four such "years" were simulated, using the four combinations of $\bar{p}_b$ equal to 0.3 and 0.2, and Δp_b equal to 0.1 and 0.01.

6.3.2 Results of the seizure rate simulation

The results of the seizure rate simulations are shown in Figures 23 through 26. It is clear that altering $\bar{p}_b$ has an effect on the way that seizures are distributed. Consider Figures 23 and 26, which show the seizure rates at $\Delta p_b = 0.1$ for $\bar{p}_b = 0.3$ and $\bar{p}_b = 0.2$ respectively. There are many more seizure-free days in the second case. The effect of varying Δp_b, on the other hand, is to reduce the maximum number of seizures per day.

Seizure free intervals (in units of hours) are plotted for each of the cases in Figures 27 through 30. Again, the effects of varying the p_b distribution is clear. Note that the seizure free intervals are not Poisson distributed. This is because the interval over which seizure free intervals are computed (one hour) is equal to the interval over which a single seizure occurs. That is, the number of seizures per unit time (λ in Equation 4.2) varies widely (from zero to one). If the interval were increased to 1 day, the Poisson distribution would be more evident, but the parameters of the simulation were chosen to yield high daily seizure rates for analysis, and there are no runs of more than one seizure-free day in the data. Alternatively, consecutive pairs of seizure-free histogram bins may be combined, increasing the bin width to 2 hours. See Figure 31, which shows the same data as Figure 27, but with a bin width of 2 hours.

Perhaps this technique will allow doctors treating the epilepsies to target a particular type of treatment. It is a matter of some debate among such doctors what an effective treatment should accomplish: increase the maximum seizure-free interval, decrease the maximum number of seizures on any day, or maximize the number of seizure-free days [68]. Whatever treatment is judged most effective, administering drugs that vary the distribution of p_b can accomplish the treatment. In conjunction with the methods for estimating the effects of various AED's on this distribution (see Section 4.2.2), it may become possible to treat epileptic patients so that their lifestyles are returned to near normal.

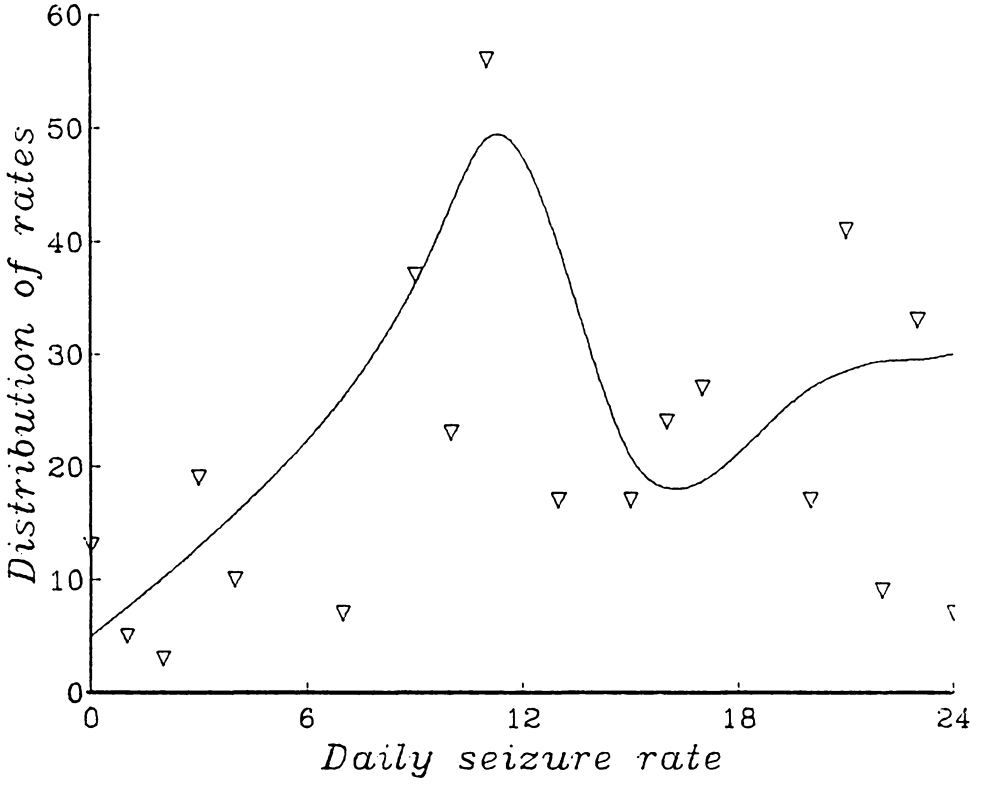

Figure 23: Daily seizure rate simulation with $\bar{p}_b = 0.3$ and $\Delta p_b = 0.1$. The abscissa shows the daily seizure rate, and the ordinate shows the number of days on which that particular seizure rate occurred.

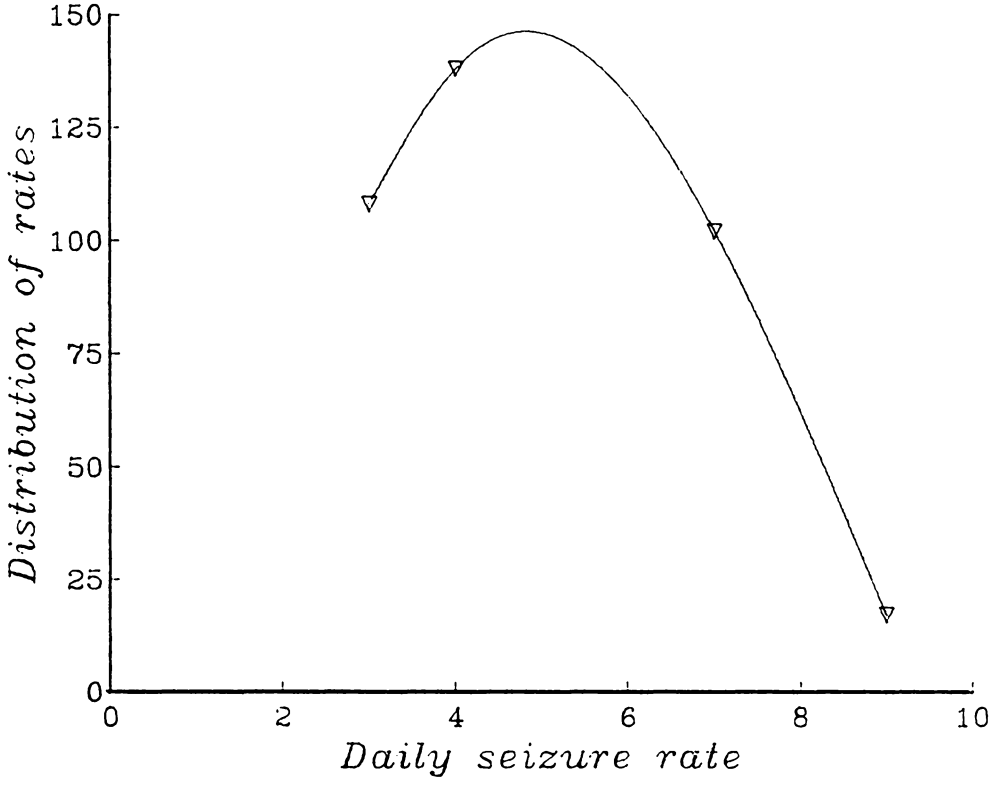

Figure 24: **Daily seizure rate simulation with $\bar{p}_b = 0.2$ and $\Delta p_b = 0.01$.** The abscissa shows the daily seizure rate, and the ordinate shows the number of days on which that particular seizure rate occurred.

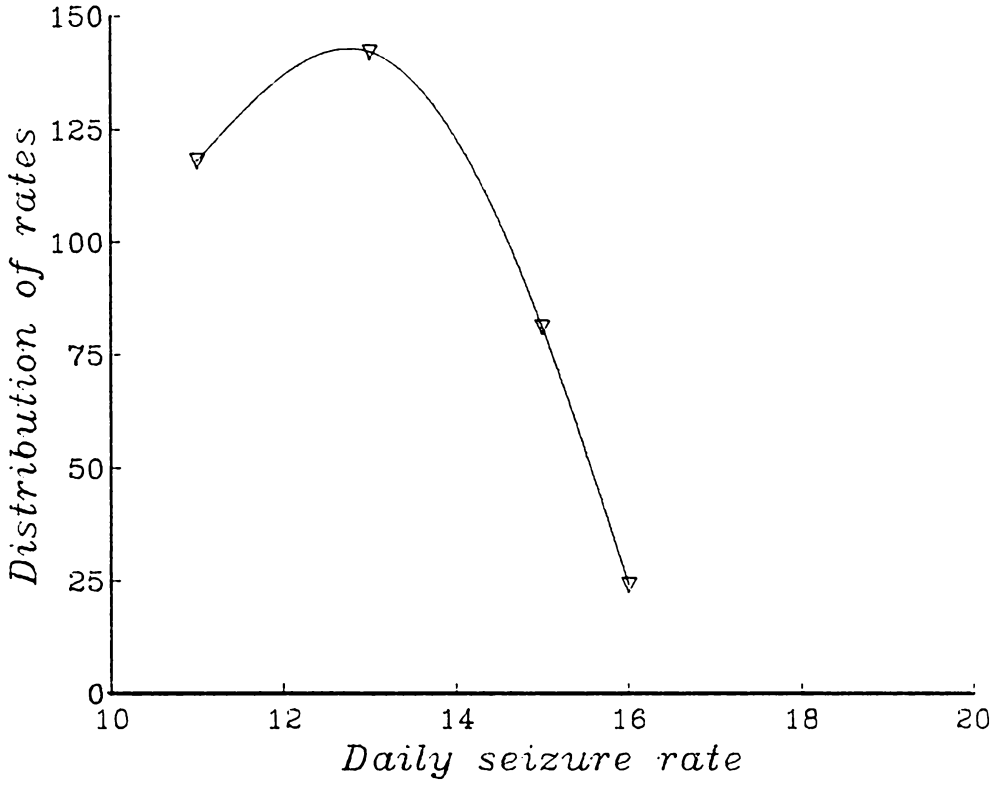

Figure 25: **Daily seizure rate simulation with $\bar{p}_b = 0.3$ and $\Delta p_b = 0.01$.** The abscissa shows the daily seizure rate, and the ordinate shows the number of days on which that particular seizure rate occurred.

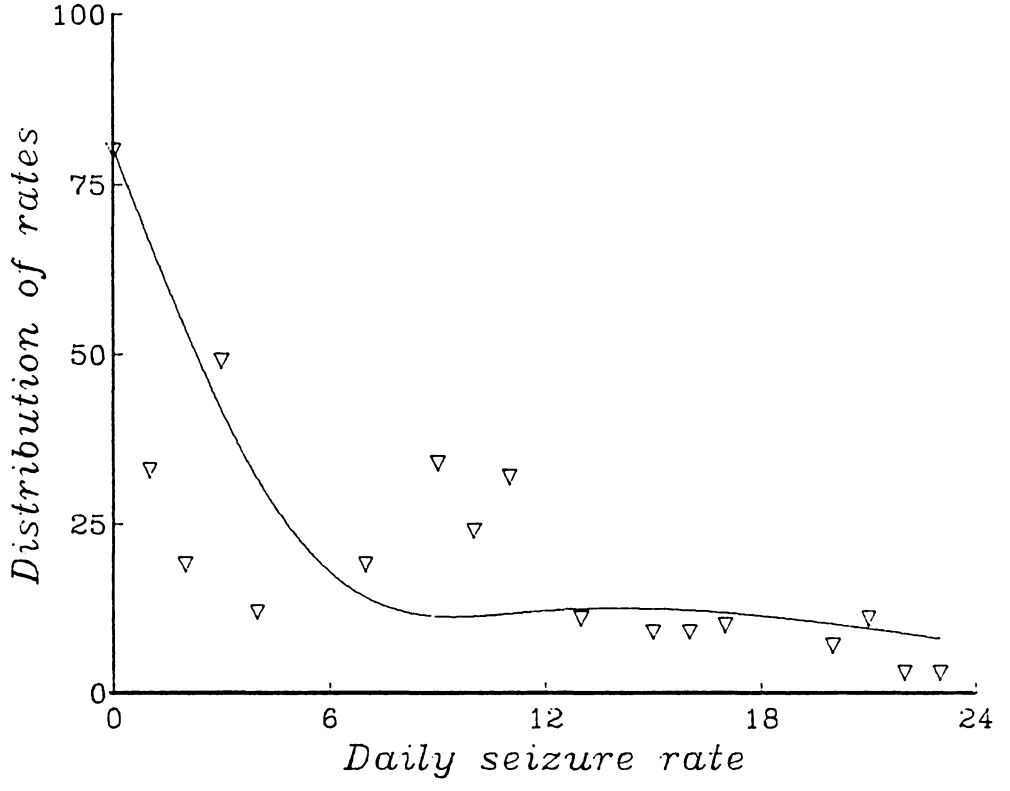

Figure 26: Daily seizure rate simulation with $\bar{p}_b = 0.2$ and $\Delta p_b = 0.1$. The abscissa shows the daily seizure rate, and the ordinate shows the number of days on which that particular seizure rate occurred.

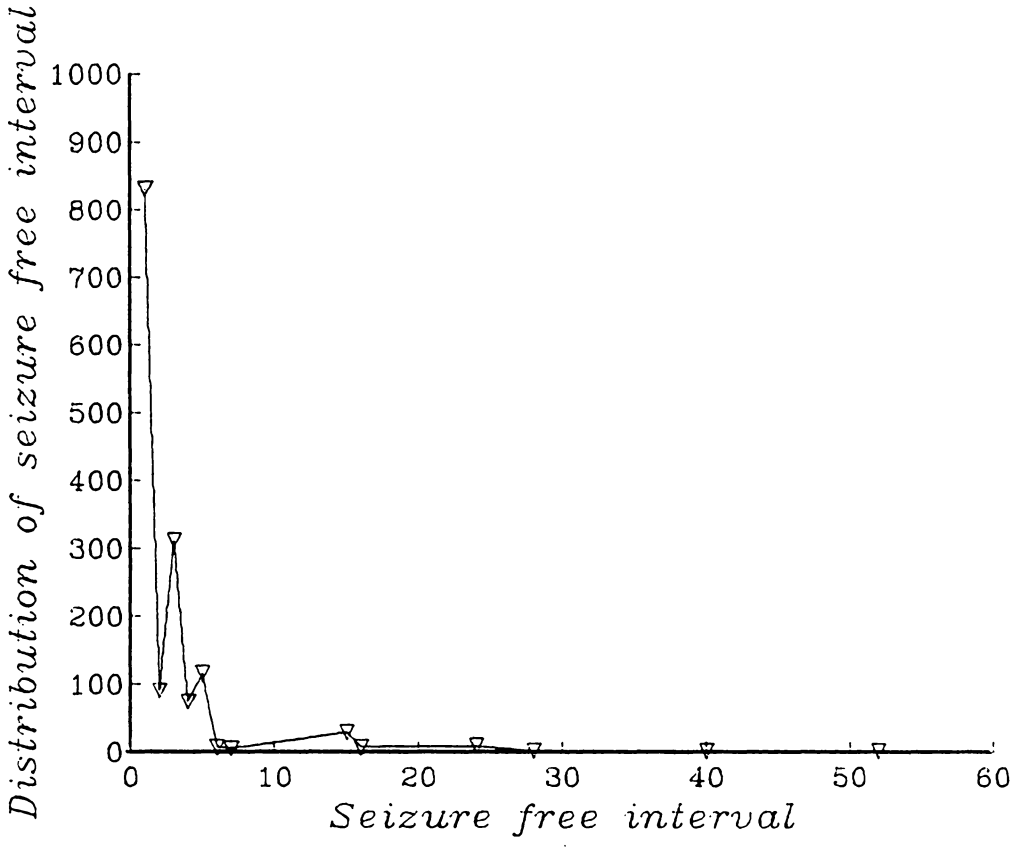

Figure 27: Seizure-free intervals with $\bar{p}_b = 0.3$ and $\Delta p_b = 0.1$. Intervals are in hours.

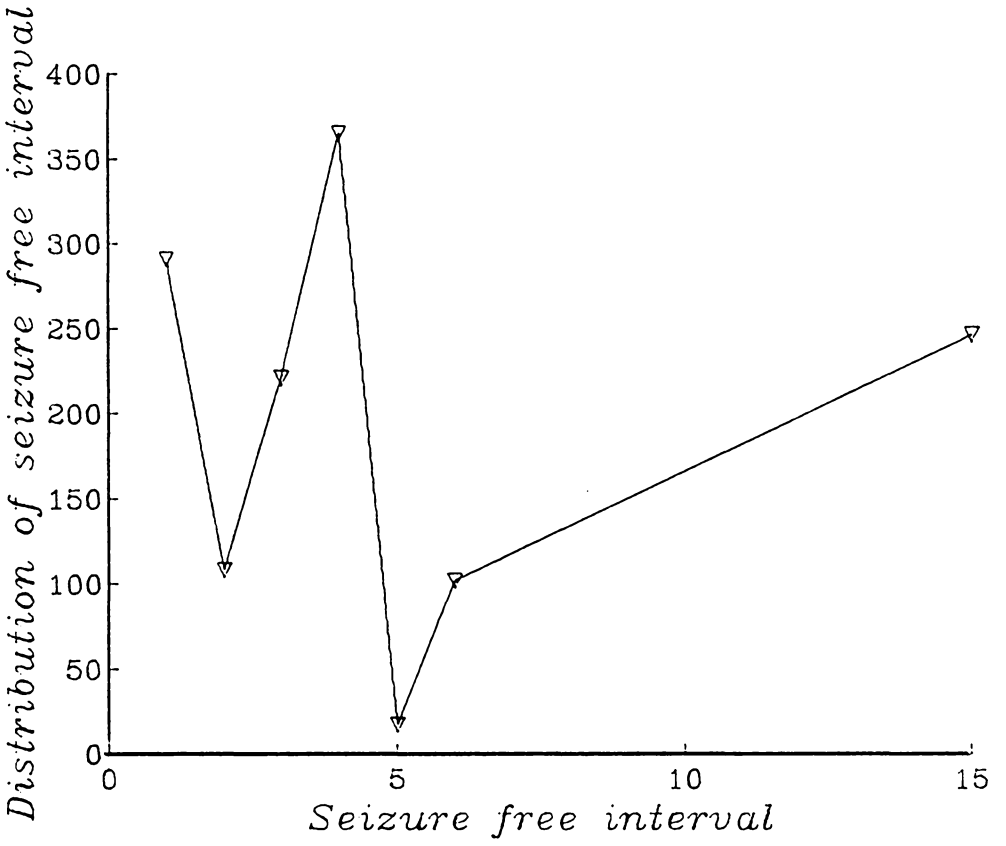

Figure 28: Seizure-free intervals with $\bar{p}_b = 0.2$ and $\Delta p_b = 0.01$. Intervals are in hours.

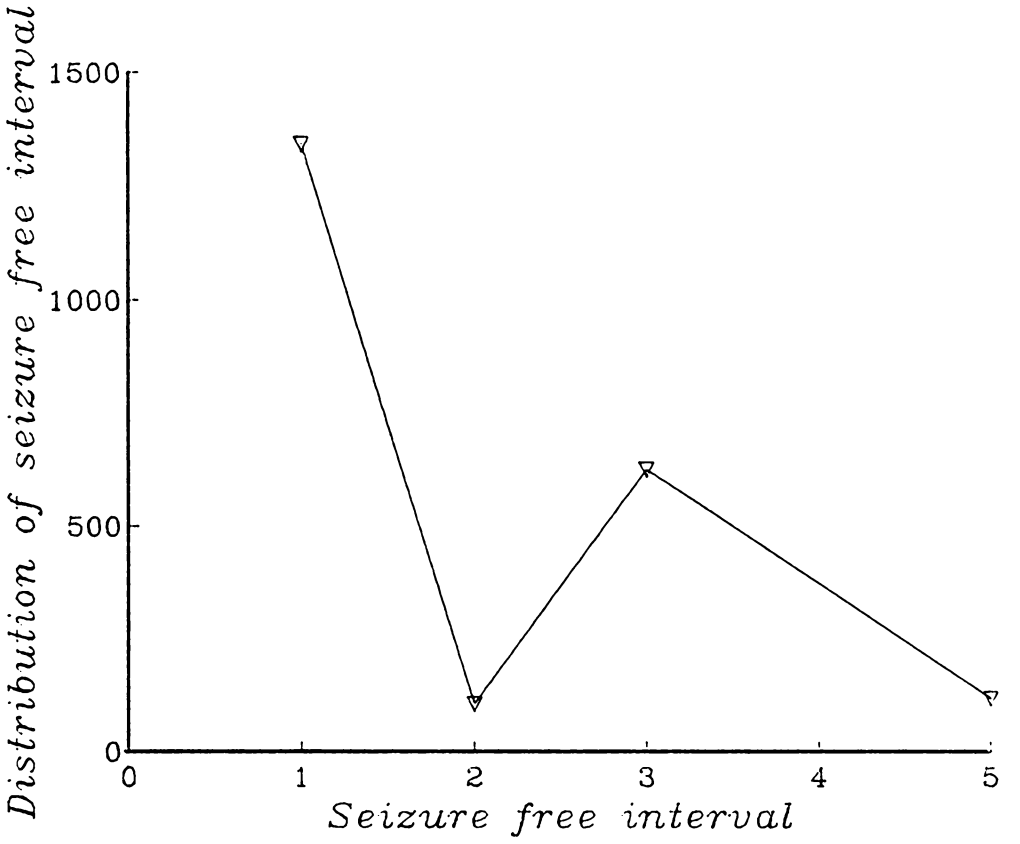

Figure 29: **Seizure-free intervals with $\bar{p}_b = 0.3$ and $\Delta p_b = 0.01$. Intervals are in hours.**

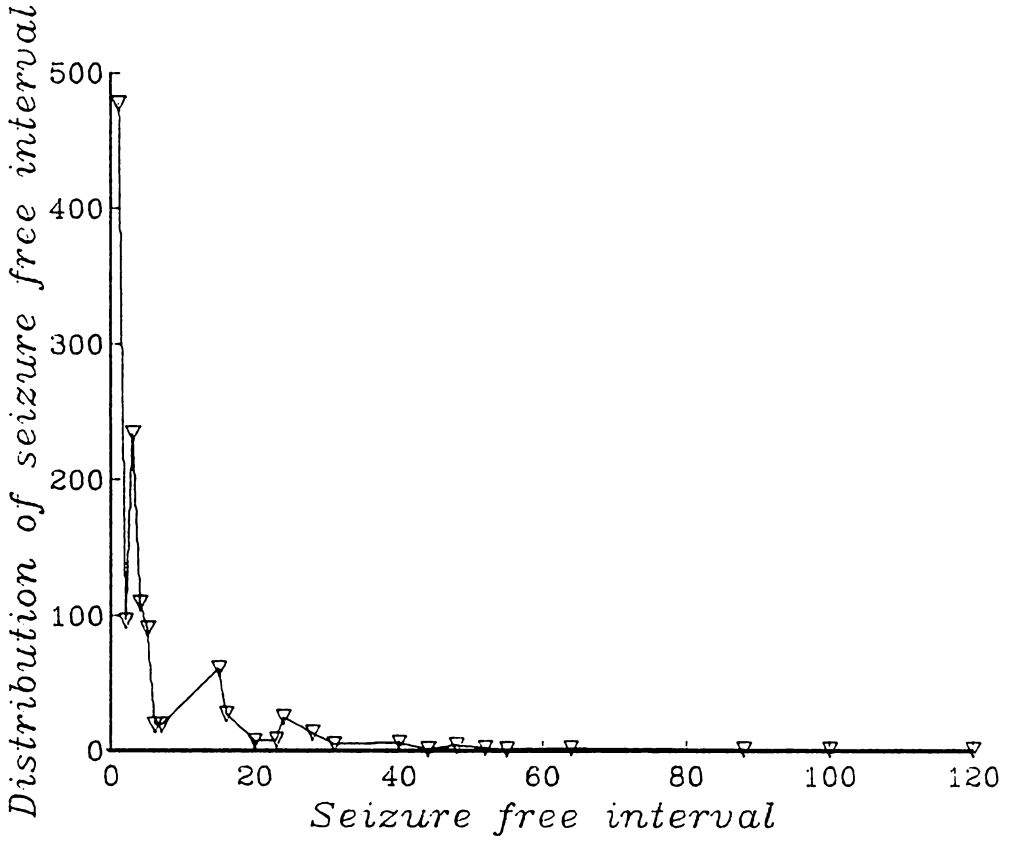

Figure 30: **Seizure-free intervals with $\bar{p}_b = 0.2$ and $\Delta p_b = 0.1$. Intervals are in hours.**

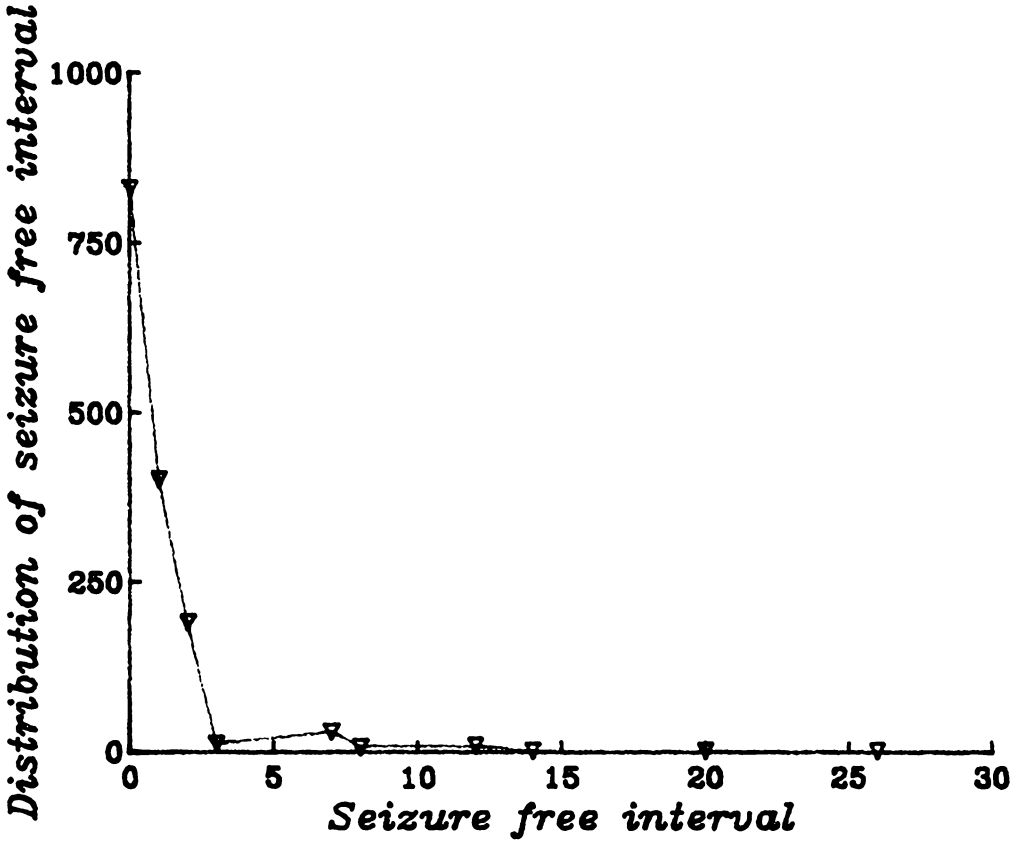

Figure 31: **Seizure-free intervals with $\bar{p}_b = 0.2$ and $\Delta p_b = 0.1$.** Intervals are in units of 2 hours.

Chapter 7

Conclusion

7.1 Conclusions of this study

Studies in the epilepsies have traditionally been severely handicapped by the complexity of the central nervous system. Many previous research attempts concentrated on specialized aspects of the epileptic brain: the errant behavior of epileptic neurons [8,98,97] or the cytochemistry of epileptic synapses [81] as examples. These studies have made valuable contributions to the understanding and treatment of the epilepsies. But they have done so by amassing a collection of facts. What is desperately needed is a model that can help to explain one facet of research in the epilepsies, *viz.*, their statistical behavior.

This research program started out by posing the hypothesis that the statistics of the epilepsies are those of a percolating system. It would be foolhardy to claim that the hypothesis has been proven to the extent that Darwin's original hypothesis of evolution has been proven, to use an example from the biological sciences. The data used in this study were of marginal quality at best, whereas Darwin had available the results of many years of first-hand observations of animals and plants throughout the world. But this study has shown that the statistical theory of percolation at least cannot be dismissed as a viable model for

the epileptic brain. This conclusion was by no means a predetermined one—this author for one was skeptical at the start of the program.

Gould [29] gives the following criteria for a reasonable model of a biological system:

1. It seems to account for what facts there are.
2. It is simple, rather than complex or contrived.
3. It avoids *ad hoc* invocation of external controls.
4. It is largely the product of direct deduction from an established principle.

Certainly the theory of percolation is simple and powerful. The model as described here is an internally sufficient theory which does not require any external controls: no unknown forces or actions are invoked. The following sections will recapitulate the reasons for believing why the proposed model accounts for what facts there are on the epilepsies.

7.1.1 The phenomenology of the epilepsies

The percolation model can explain the manner in which seizures begin at epileptic foci and then spread to recruit other regions of the brain. As the bond fraction p increases, the statistics of lattice interactions guarantee that more neurons in the brain become involved. Of course, this model cannot explain the mechanism by which p increases, but other research studies, such as those referred to above, have provided evidence for a model based on the depletion of inhibitors or the presence of pathologically misbehaving neurons.

There was no phenomenological property of seizures evident in the literature which directly contradicted some requirement of the percolation model. If, for example, a future research study shows that the transition from a non-seizing brain to a seizing brain does not involve an increase in the numbers of excited neurons, but rather their properties, then one would be

forced to conclude that the percolation model in its present form is not viable. Percolation theory is a theory of cluster sizes, not of cluster properties, although such a finding could be approached as a site percolation problem in which a site phenomenon identified as "neuron misbehavior" is used.

No such study was found in the published literature; on the contrary, research that addressed this problem tended to support the bond percolation hypothesis [1,81,98,97]. Studies on the so-called kindling model of the epilepsies have even come close to using the specific language of percolation theory. Consider this quote from Wasterlain *et al.*'s review paper on kindling theory [95]:

> Recent studies of chemical kindling favor the view that in this model, epilepsy is a property of neuronal networks that can take place in a structurally intact brain and does not depend on the presence of gross or microscopic brain damage... studies of seizure threshold suggest the need for a critical mass of neurons even on initial stimulation.

With a suitable change of vocabulary, this quote could have been taken from a review paper on percolation theory [99].

7.1.2 The estimates of β

The results of the estimates of the percolation exponent β in Section 4.2.4 are significant in their low standard deviation. This points to a confirmation of a percolation model. It seems reasonable to assert that the probability of deriving exponents for different people that are so close to each other simply by random chance is low. As pointed out in Section 4.2.4, the values are not close to the predicted values of theoretical calculations on three-dimensional percolation models in the nearest-neighbor universality class. However, there are several

explanations, also given in Section 4.2.4, ranging from the poor quality of the data to the possibility that this particular percolation problem might lie in a different universality class.

In fairness, it should be noted that one should not accuse the data of low quality when results do not agree with predictions, and then unreservedly accept favorable results from the same data. It may well be that the data are so poor that the closeness of the computed β's is meaningless.

7.1.3 The results of the Monte-Carlo simulations

The Monte-Carlo simulations of the correlated bond percolation model discussed in Chapter 6 show a good agreement with observations from this study and others. The results indicate that such a bond percolating system can account for the distribution of seizure rates as a function of pathologically misbehaving neurons as derived elsewhere [98,97]. By adjusting the parameters of the daily distribution of the bond fraction p, it can also duplicate the observed behavior of daily seizure rates from clinical data.

7.2 Suggestions for future research

This study was plagued by two recurring problems: the poor quality of the clinical data and the difficulty of drawing accurate conclusions from EEG data because of the lack of suitable models.

The first problem can be addressed by relying on automatic seizure detection and recording. The single worst aspect of the clinical data is the inability of patients to accurately maintain their own seizure calendars. If there were some mechanism for recording the EEG's of patients as they conduct normal lives, or at least for detecting a seizure and its duration, there would be a sufficient amount of high quality data to attempt a more accurate estimate of percolation exponents and other numerical values.

Just such a study has in fact been conducted by Holmes [34]. Several epileptic patients were monitored by closed circuit television and FM radiotelemetry, allowing physicians to make objective estimates of seizure duration and type. It would be useful to a further study of the percolation hypothesis if a clinic would replicate this study, extending it over a period of several months or even years. Of course, there would be the social problem of the invasion of the patients' privacy, but perhaps some solution to this could be worked out.

It is not so easy to find a solution to the problem of EEG models. The current theories of EEG are apparently unable to relate the parameters of epileptiform activity like spikes and slow waves to the size of the cluster of neurons involved in the activity. If such a theory could be derived, it would allow a crucial test to the percolation hypothesis: that the average cluster sizes scale in a power law as given in Equation 3.1. It would not be necessary to know the critical probability p_c to observe the power-law behavior. One could make the simplifying assumption that the spike rate is proportional to the bond fraction p, and then using a model relating spike parameters to cluster size, compute the cluster size as a function of the spike rate. The cluster size must be seen to increase sharply as the spike rate approaches some value.

A simple first approximation to such a law relating spike parameters to the cluster size could be made if there was a way to relate the spike parameters to the size of some current dipole that is theorized to be the source of the activity. The size of the dipole should offer some guide to the size of the brain area that is involved in the activity, and using values for the number density of neurons, one could derive a value for the number of neurons in the cluster. This would only be an approximation because it assumes that every neuron in the area is involved in the activity (recall that this is a *bond* percolation model, not a *site* percolation model), and that in fact the size of the equivalent dipole in some way measures the size of the seizing area.

Such an approximation is itself not easy to derive: consider that the simple first assumption that the amplitude of a spike relates to the size of the cluster is wrong because there is no

way of telling whether a small spike comes from a small dipole near the electrode or a large dipole far from the electrode. Perhaps the answer lies in attempting to "triangulate" the position of the dipole: if the same activity were measured in several electrodes at different times and at different amplitudes, one could work backwards to a position of the source inside the brain. The problem is that it is not always clear whether activity which shows up in several EEG channels can all be tied back to the same source. The dispersive properties of the medium through which the currents must travel on their way to the scalp electrodes are such that the waves are badly distorted by the time they arrive at the electrodes, by different amounts at different electrodes. Worse, there is no model of just what these dispersive properties are, so it is not possible to correct for them.

A solution to any one of these problems in the field of EEG research would be a significant advance in its own right, quite apart from any benefit that may be derived by tests of the model proposed in this work. An accurate model for explaining the EEG in terms of neural activity would greatly advance the use of the EEG in diagnosis and brain research.

Another problem is the distribution of spike-free intervals in the EEG as discovered in this study and by Binnie *et al.* [5]. This distribution appears to point towards a periodicity in the appearance of epileptiform activity in the brain. Why this is so is not clear—seizures, after all, do appear without periodicity, so why should the epileptiform activity appear periodically? And what is the significance of this period? Martins da Silva *et al.* [55] notice an inconsistent correlation between the Circadian rhythm and the frequency of seizures, and there are controversial theories that there exists in the brain some kind of pacemaker, perhaps in the thalamus [63]. One or the other study may have some bearing on the problem.

As pointed out earlier, in Section 3.1.5, percolation theory must of necessity be a "statics" theory, in that it can model the behavior of clusters in the lattice as p changes, but they cannot account for the dynamics of the changes. The physical theory of nucleation might be useful to explain the time evolution of the seizing cluster. Nucleation theory has been used to

explain dynamic situations such as order propagation in annealing and cloud formation, so there is hope that it might be fruitfully applied to an understanding of the order propagation inherent in the spread of seizing clusters. Empirical data exist for the dynamics of seizure spreading [1,26], and a model for seizure spreading based on nucleation theory capable of explaining these empirically observed data would be a powerful tool. For example, such a theory could conceivably be used by drug researchers to tailor the action of AED's so that the spread of seizures can be quickly arrested.

Perhaps a catalog of the unsolved problems facing research in the epilepsies is depressing. But as was stated at the beginning of this dissertation, if there is any benefit from the difficulty of the problems, it is that researchers from widely differing branches of science may be attracted to the field. Their combined expertise and ingenuity may finally lead to a complete understanding of the "divine illness" which has puzzled thinkers from the time of Plato and Hippocrates, and has afflicted people from the anonymous son of a man who approached Jesus in the crowd to Julius Caesar.

Bibliography

[1] K. Abraham and C. Ajmone-Marsan, "Patterns of cortical discharges and their relation to routine scalp electroencephalography," *Electroencephalography and Clinical Neurophysiology*, vol. 10, pp. 447–461, 1958.

[2] A. V. Aho, R. Sethi, and J. D. Ullmann, *Compilers: Principles, Techniques, and Tools.* Addison-Wesley, 1986.

[3] A. Autret, L. Auvert, F. Laffont, and P. Larmande, "Electroencephalographic spectral power and lateralized motor activities," *Electroencephalography and Clinical Neurophysiology*, vol. 60, pp. 228–236, 1985.

[4] H. Berger, "Das Elektrenkephalogramm des Menschen und seine Bedeutung für die Psychophysiologie," *Zeitschrift für Psychologie*, vol. 126, pp. 1–13, 1932.

[5] C. D. Binnie *et al.*, "Temporal characteristics of seizures and epileptoform discharges," *Electroencephalography and Clinical Neurophysiology*, vol. 58, pp. 498–505, 1984.

[6] J. Bockris and A. Reddy, *Modern Electrochemistry.* Vol. 2, Plenum Press, 1970.

[7] M. A. B. Brazier, "The electrical fields at the surface of the head during sleep," *Electroencephalography and Clinical Neurophysiology*, vol. 1, pp. 195–204, 1949.

[8] W. H. Calvin, "Normal repetitive firing and its pathophysiology," in *Epilepsy: A Window to Brain Mechanisms*, (J. S. Lockard and A. A. Ward, Jr., eds.), Raven Press, 1980.

[9] G. E. Chatrian, M. C. Petersen, and J. A. Lazarte, "The blocking of the Rolandic wicket rhythm and some central changes related to movement," *Electroencephalography and Clinical Neurophysiology*, vol. 11, pp. 497–510, 1960.

[10] J. P. Clerc *et al.*, "La percolation: Modèles, simulations analogiques et numériques. Chapitre 1: Introduction," *Annales de Physique (Paris)*, vol. 8, no. 1, pp. 7–23, 1983.

[11] J. P. Clerc *et al.*, "La percolation: Modèles, simulations analogiques et numériques. Chapitre 2: Simulations numériques," *Annales de Physique (Paris)*, vol. 8, no. 1, pp. 24–49, 1983.

[12] A. Coniglio, "Thermal phase transition of the dilute s-state Potts and n-vector models at the percolation threshold," *Physical Review Letters*, vol. 46, no. 4, pp. 250–253, 1981.

[13] B. N. Cuffin and D. Cohen, "Magnetic fields of a dipole in special volume conductor shapes," *IEEE Transactions on Biomedical Engineering*, vol. BME-24, no. 4, pp. 372–381, 1977.

[14] L. da Silva *et al.*, "Automatic detection and localization of epileptic foci," *Electroencephalography and Clinical Neurophysiology*, no. 13, pp. 1–13, 1977.

[15] D. D. Daly, "Use of the EEG for diagnosis and evaluation of epileptic seizures and nonepileptic episodic disorders," in *Current Practice of Clinical Electroencephalography*, (D. W. Klass and D. D. Daly, eds.), Raven Press, 1979.

[16] T. M. Darcey and P. D. Williamson, "Spatio-temporal EEG measures and their application to human intracranially recorded epileptic seizures," *Electroencephalography and Clinical Neurophysiology*, vol. 61, pp. 573–587, 1985.

[17] M. P. Deiber, M. H. Giard, and F. Mauguiere, "Separate generators with distinct orientations for N20 and P22 somatosensory evoked potentials to finger stimulation?," *Electroencephalography and Clinical Neurophysiology*, vol. 65, pp. 321–334, 1986.

[18] A. V. Delgado-Escueta, A. A. Ward, Jr., D. M. Woodbury, and R. J. Porter, "New wave of research in the epilepsies," in *Advances in Neurology, Vol 44*, (A. V. Delgado-Escueta, A. A. Ward, Jr., D. M. Woodbury, and R. J. Porter, eds.), Raven Press, 1986.

[19] C. Domb, "The percolation phase transition," in *Percolation Structures and Processes*, (G. Deutscher, R. Zallen, and J. Adler, eds.), Annals of the Israel Physical Society, Volume 5, Adam Hilger, 1983.

[20] R. Elul, "Randomness and synchrony in the generation of the electroencephalogram," in *Synchronization of EEG Activity in Epilepsies*, (H. Petsche and M. A. B. Brazier, eds.), Austrian Academy of Sciences, Springer-Verlag, 1972.

[21] C. M. Epstein and G. P. Brickley, "Interelectrode distance and amplitude of the scalp EEG," *Electroencephalography and Clinical Neurophysiology*, vol. 60, pp. 287–292, 1985.

[22] G. Garner. Private communication.

[23] C. D. Geisler and G. L. Gerstein, "The surface EEG in relation to its sources," *Electroencephalography and Clinical Neurophysiology*, vol. 13, pp. 927–934, 1961.

[24] W. R. Goff, T. Allison, and H. G. Vaughan, Jr., "The functional neuranatomy of event-related potentials," in *Event-Related Brain Potentials in Man*, (E. Callaway, P. Tueting, and S. H. Koslow, eds.), Academic Press, 1978.

[25] E. S. Goldensohn, "Neurophysiological substrates of EEG activity," in *Current Practice of Clinical Electroencephalography*, (D. W. Klass and D. D. Daly, eds.), Raven Press, 1979.

[26] E. S. Goldensohn and A. M. Salazar, "Temporal and spatial distribution of intracellular potentials during generation and spread of epileptogenic discharges," in *Advances in Neurology, Vol 44*, (A. V. Delgado-Escueta, A. A. Ward, Jr., D. M. Woodbury, and R. J. Porter, eds.), Raven Press, 1986.

[27] J. Gotman and P. Gloor, "Automatic recognition and quantification of interictal epileptic activity in the human scalp EEG," *Electroencephalography and Clinical Neurophysiology*, vol. 41, pp. 513–529, 1976.

[28] J. Gotman, J. R. Ives, and P. Gloor, "Automatic recognition of interictal epileptic activity in prolonged EEG recordings," *Electroencephalography and Clinical Neurophysiology*, vol. 46, pp. 510–520, 1979.

[29] S. J. Gould, *Ever Since Darwin: Reflections in Natural History.* Norton, 1977.

[30] G. S. Grest and M. H. Cohen, "Percolation and the glass transition," in *Percolation Structures and Processes*, (G. Deutscher, R. Zallen, and J. Adler, eds.), Annals of the Israel Physical Society, Volume 5, Adam Hilger, 1983.

[31] A. N. Guthkelch, D. Bursick, and R. J. Sclabassi, "The relationship of the latency of the visual P100 wave to gender and head size," *Electroencephalography and Clinical Neurophysiology*, vol. 68, pp. 219–222, 1987.

[32] J. M. Hammersley, "Origins of percolation theory," in *Percolation Structures and Processes*, (G. Deutscher, R. Zallen, and J. Adler, eds.), Annals of the Israel Physical Society, Volume 5, Adam Hilger, 1983.

[33] A. L. Hodgkin and A. F. Huxley, "Resting and action potentials in single nerve fibers," *Journal of Physiology*, vol. 104, p. 146, 1945.

[34] G. L. Holmes, "Partial complex seizures in children: An analysis of 69 seizures in 24 patients using EEG FM radiotelemetry and videotape recording," *Electroencephalography and Clinical Neurophysiology*, vol. 57, pp. 13–20, 1984.

[35] J. D. Jackson, *Classical Electrodynamics.* John Wiley, 2nd ed., 1975.

[36] D. L. Jewett, "The 3-channel Lissajous' trajectory of the auditory brain-stem response: (IX) Theoretical aspects," *Electroencephalography and Clinical Neurophysiology*, vol. 68, pp. 386–408, 1987.

[37] D. L. Jewett, W. H. Martin, Y. S. Siniger, and J. N. Gardi, "The 3-channel Lissajous' trajectory of the auditory brain-stem response: (I) Introduction and overview," *Electroencephalography and Clinical Neurophysiology*, vol. 68, pp. 323–326, 1987.

[38] B. Jouhier, C. Allain, B. Gauthier-Manuel, and E. Guyon, "The sol-gel transition," in *Percolation Structures and Processes*, (G. Deutscher, R. Zallen, and J. Adler, eds.), Annals of the Israel Physical Society, Volume 5, Adam Hilger, 1983.

[39] R. N. Kavanagh, T. M. Darcey, D. Lehmann, and D. H. Fender, "Evaluation of methods for three-dimensional localization of electrical sources in the human brain," *IEEE Transactions on Biomedical Engineering*, vol. BME-25, no. 5, pp. 421–429, 1978.

[40] P. Kellaway, "An orderly approach to visual analysis: The parameters of the normal EEG in adults and children," in *Current Practice of Clinical Electroencephalography*, (D. W. Klass and D. D. Daly, eds.), Raven Press, 1979.

[41] S. Kirkpatrick and R. H. Swendsen, "Statistical mechanics and disordered systems," *Communications of the ACM*, vol. 28, no. 4, pp. 363–373, 1985.

[42] K. A. Kooi, *Fundamentals of Electroencephalography*. Harper & Row, 1971.

[43] G. Kostopoulos and J. Gotman, "Computer assisted analysis of relations between single-unit activity and spontaneous EEG," *Electroencephalography and Clinical Neurophysiology*, vol. 57, pp. 69–82, 1984.

[44] M. A. Kraut, J. C. Arizzo, and H. G. Vaughan, Jr., "Intracortical generators of the flash VEP in monkeys," *Electroencephalography and Clinical Neurophysiology*, vol. 62, pp. 300–312, 1985.

[45] J. Larson and G. Lynch, "Induction of synaptic potentiation in hippocampus by patterned stimulation involves two events," *Science*, vol. 232, pp. 985–988, 1986.

[46] J. Larson, D. Wong, and G. Lynch, "Patterned stimulation at the theta frequency is optimal for the induction of hippocampal long-term potentiation," *Brain Research*, vol. 368, pp. 347–350, 1986.

[47] D. Lehmann, D. Brandeis, H. Ozaki, and I. Pal, "Human brain EEG fields: Micro-states and their functional significance," in *Computational Systems—Natural and Artificial*, (H. Haken, ed.), Springer-Verlag, 1987. Proceedings of the International Symposium on Synergetics at Schloss Elmau, Bavaria.

[48] L. S. Leung, "Spectral analysis of hippocampal EEG in the freely moving rat: Effects of centrally active drugs and relations to evoked potentials," *Electroencephalography and Clinical Neurophysiology*, vol. 60, pp. 65–77, 1985.

[49] D. F. Lindsley and J. E. Holmes, *Basic Human Neurophysiology*. Elsevier, 1984.

[50] F. Lopes da Silva and A. Van Rotterdam, "Biophysical aspects of EEG and MEG generation," in *Electroencephalography*, (E. Niedermeyer and F. Lopes da Silva, eds.), Urban and Schwarzenberg, 1982.

[51] M. D. Low, "Event-related potentials and their clinical applications," in *Current Practice of Clinical Electroencephalography*, (D. W. Klass and D. D. Daly, eds.), Raven Press, 1979.

[52] T. C. Lubensky and A. J. McKane, "Cluster size distribution above the percolation threshold," *Journal of Physics A*, vol. 14, pp. L157–L161, 1981.

[53] B. B. Mandelbrot, "An explicit fractal model of percolation clusters," in *Percolation Structures and Processes*, (G. Deutscher, R. Zallen, and J. Adler, eds.), Annals of the Israel Physical Society, Volume 5, Adam Hilger, 1983.

[54] B. B. Mandelbrot, *The Fractal Geometry of Nature*. Freeman, 1982.

[55] A. Martins da Silva *et al.*, "The Circadian distribution of interictal epileptoform EEG activity," *Electroencephalography and Clinical Neurophysiology*, vol. 58, pp. 1–13, 1984.

[56] Microport Systems, *UNIX System V/AT Runtime System Manual.*

[57] Microport Systems, *UNIX System V/AT Software Development System Manual.*

[58] A. R. Moller, P. J. Jannetta, and J. E. Burgess, "Neural generators of the somatosensory evoked potentials: Recording from the cuneate nucleus in man and monkeys," *Electroencephalography and Clinical Neurophysiology*, vol. 65, pp. 241–248, 1986.

[59] C. Nicholson, "Theoretical analysis of field potentials in anisotropic ensembles of neuronal elements," *IEEE Transactions on Biomedical Engineering*, vol. BME-20, no. 4, pp. 278–288, 1973.

[60] E. Niedermeyer, "Abnormal EEG patterns (epileptic and paroxysmal)," in *Electroencephalography*, (E. Niedermeyer and F. Lopes da Silva, eds.), Urban and Schwarzenberg, 1982.

[61] E. Niedermeyer, "Epileptic seizure disorders," in *Electroencephalography*, (E. Niedermeyer and F. Lopes da Silva, eds.), Urban and Schwarzenberg, 1982.

[62] E. Niedermeyer, "The normal EEG of the waking adult," in *Electroencephalography*, (E. Niedermeyer and F. Lopes da Silva, eds.), Urban and Schwarzenberg, 1982.

[63] P. L. Nunez, *Electric Fields of the Brain: The Neurophysics of EEG.* Oxford University Press, 1981.

[64] M. R. Nuwer, "Frequency analysis and topographic mapping of EEG and evoked potentials in epilepsy," *Electroencephalography and Clinical Neurophysiology*, vol. 69, pp. 118–126, 1988.

[65] R. W. Olsen, J. K. Wamsley, R. J. Lee, and P. Lomax, "Benzodiazepine/barbiturate/GABA receptor-chloride ionophore complex in a genetic model for generalized epilepsy," in *Advances in Neurology, Vol 44*, (A. V. Delgado-Escueta, A. A. Ward, Jr., D. M. Woodbury, and R. J. Porter, eds.), Raven Press, 1986.

[66] L. Ott, *An Introduction to Statistical Methods and Data Analysis.* Duxbury Press, 1977.

[67] G. Palm, *Neural Assemblies: An Alternative Approach to Artificial Intelligence.* Springer-Verlag, 1982.

[68] J. K. Penry. Private communication.

[69] J. K. Penry, *Diagnosis and Management of Epilepsy: Monotherapy of Primary Generalized Seizures.* Published by the Biomedical Information Corporation and distributed by Abbott Laboratories, 1986.

[70] J. K. Penry, ed., *Epilepsy: Diagnosis, Management, Quality of Life*, ch. 1, pp. 1–3. Raven Press, 1986. Summary of material presented at the 1985 symposium on the epilepsies at the Bowman-Gray School of Medicine.

[71] J. K. Penry, ed., *Epilepsy: Diagnosis, Management, Quality of Life*, ch. 2, pp. 4–7. Raven Press, 1986. Summary of material presented at the 1985 symposium on the epilepsies at the Bowman-Gray School of Medicine.

[72] J. K. Penry, ed., *Epilepsy: Diagnosis, Management, Quality of Life*, ch. 4, pp. 14–21. Raven Press, 1986. Summary of material presented at the 1985 symposium on the epilepsies at the Bowman-Gray School of Medicine.

[73] J. Pernier, F. Perrin, and O. Bertrand, "Scalp current density fields: Concept and properties," *Electroencephalography and Clinical Neurophysiology*, vol. 69, pp. 385–389, 1988.

[74] F. Perrin, O. Bertrand, and J. Pernier, "Scalp current density mapping: Value and estimation from potential data," *IEEE Transactions on Biomedical Engineering*, vol. BME-34, no. 4, pp. 283–288, 1987.

[75] J. Persson, "Comments on estimations and tests of EEG amplitude distributions," *Electroencephalography and Clinical Neurophysiology*, vol. 37, pp. 309–313, 1974.

[76] G. Pfurtscheller and R. Cooper, "Frequency dependence of the transmission of the EEG from cortex to scalp," *Electroencephalography and Clinical Neurophysiology*, vol. 38, pp. 93–96, 1975.

[77] R. Pike and H. E. Stanley, "Order propagation near the percolation threshold," *Journal of Physics A*, vol. 14, pp. L169–L177, 1981.

[78] W. H. Press, B. P. Flannery, S. A. Teukolsky, and W. T. Vetterling, *Numerical Recipes: The Art of Scientific Programming.* Cambridge University Press, 1986.

[79] E. L. Reilly, "EEG recording and operation of the apparatus," in *Electroencephalography*, (E. Niedermeyer and F. Lopes da Silva, eds.), Urban and Schwarzenberg, 1982.

[80] P. J. Reynolds, H. E. Stanley, and W. Klein, "?," *Physical Review B*, vol. 21, pp. 1223–?, 1980.

[81] E. Roberts, "Failure of GABAergic inhibition: A key to local and global seizures," in *Advances in Neurology, Vol 44*, (A. V. Delgado-Escueta, A. A. Ward, Jr., D. M. Woodbury, and R. J. Porter, eds.), Raven Press, 1986.

[82] G. F. Rossi, G. Colicchio, and P. Pola, "Interictal epileptic activity during sleep: A stereo-EEG study in patients with partial epilepsy," *Electroencephalography and Clinical Neurophysiology*, vol. 58, pp. 97–106, 1984.

[83] B. Saltzberg, W. D. Burton, Jr., J. S. Barlow, and N. R. Burch, "Moments of the power spectral density estimated from samples of the autocorrelation function (a robust procedure for monitoring changes in the statistical properties of lengthy non-stationary time series such as the EEG)," *Electroencephalography and Clinical Neurophysiology*, vol. 61, pp. 89–93, 1985.

[84] M. Scherg and D. von Cramon, "Evoked dipole source potentials of the human auditory cortex," *Electroencephalography and Clinical Neurophysiology*, vol. 65, pp. 344–360, 1986.

[85] M. Scherg and D. von Cramon, "A new interpretation of the generators of BAEP waves I–V: Results of a spatio-temporal dipole model," *Electroencephalography and Clinical Neurophysiology*, vol. 62, pp. 290–299, 1985.

[86] L. S. Schulman and P. E. Seiden, "Propagating stochastic star formation and galactic structure," in *Percolation Structures and Processes*, (G. Deutscher, R. Zallen, and J. Adler, eds.), Annals of the Israel Physical Society, Volume 5, Adam Hilger, 1983.

[87] P. A. Schwartzkroin, "Ionic and synaptic determinants of burst generation," in *Epilepsy: A Window to Brain Mechanisms*, (J. S. Lockard and A. A. Ward, Jr., eds.), Raven Press, 1980.

[88] R. Sedgewick, *Algorithms*. Addison-Wesley, 1983.

[89] D. Shah, "The 3-channel Lissajous' trajectory of the auditory brain-stem response: (X) Proof that a rotating dipole generates planar data sequences," *Electroencephalography and Clinical Neurophysiology*, vol. 68, pp. 409–411, 1987.

[90] F. W. Sharbrough, "Nonspecific abnormal EEG patterns," in *Electroencephalography*, (E. Niedermeyer and F. Lopes da Silva, eds.), Urban and Schwarzenberg, 1982.

[91] H. E. Stanley and A. Coniglio, "Fractal structure of the incipient infinite cluster in percolation," in *Percolation Structures and Processes*, (G. Deutscher, R. Zallen, and J. Adler, eds.), Annals of the Israel Physical Society, Volume 5, Adam Hilger, 1983.

[92] D. Stauffer, *Introduction to Percolation Theory*. Taylor and Francis, 1985.

[93] M. Steriade, "Interneuronal epileptic discharges related to spike-and-wave cortical seizures in behaving monkeys," *Electroencephalography and Clinical Neurophysiology*, vol. 37, pp. 247–263, 1974.

[94] M. A. Tribe and M. R. Eraut, *Nerves and Muscle. Basic Biology Course*, Cambridge University Press, 1977.

[95] C. G. Wasterlain, D. B. Farber, and M. D. Fairchild, "Synaptic mechanisms in the kindled epileptic focus: A speculative synthesis," in *Advances in Neurology, Vol 44*, (A. V. Delgado-Escueta, A. A. Ward, Jr., D. M. Woodbury, and R. J. Porter, eds.), Raven Press, 1986.

[96] J. P. Wikswo, Jr. and B. J. Roth, "Magnetic determination of the spatial extent of a single cortical current source: A theoretical analysis," *Electroencephalography and Clinical Neurophysiology*, vol. 69, pp. 266–276, 1988.

[97] A. R. Wyler, K. J. Burchiel, and A. A. Ward, Jr., "Chronic epileptic foci in monkeys: Correlation between seizure frequency and proportion of pacemaker epileptic neurons," *Epilepsia*, vol. 19, pp. 475–483, 1978.

[98] A. R. Wyler and A. A. Ward, Jr., "Epileptic neurons," in *Epilepsy: A Window to Brain Mechanisms*, (J. S. Lockard and A. A. Ward, Jr., eds.), Raven Press, 1980.

[99] R. Zallen, "Percolation: A model for all seasons," in *Percolation Structures and Processes*, (G. Deutscher, R. Zallen, and J. Adler, eds.), Annals of the Israel Physical Society, Volume 5, Adam Hilger, 1983.

Appendix A

The clinical data

As mentioned in Chapter 4, this Appendix shows the data from ten representative patients who participated in the epilepsies treatment program at the Bowman Gray School of Medicine.

The figures are divided into five groups of ten:

1. Figures 32 through 41 show the distribution of seizures by time of day. Note that there seem to be few seizures at night. This is an artifact of the way the data were recorded: patients do not know if they have had a seizure during sleep.

2. Figures 42 through 51 show the distribution of seizures by day of the week. There seems to be little or no correlation.

3. Figures 52 through 61 show the distribution of seizures by seizure duration. The theory for this distribution is derived in Section 4.2.3. Note that the y-axes of these graphs are logarithmic.

4. Figures 62 through 71 show the distribution of seizure-free intervals by length of seizure-free interval. Most of these graphs display an overall Poisson-type distribution.

Note that the y-axes of these graphs are logarithmic; the straight lines running through the data are expected exponential fits to the data.

5. Figures 72 through 81 show distributions of daily seizure rates as a function of the seizure rate. These are a measure of the probability that the bond fraction p exceeds the percolation threshold p_c. If $\bar{R}$ is the daily seizure rate, then using the model that p varies with a Gaussian distribution with average $\bar{p}$ and standard deviation Δp,

$$\bar{R} \sim 1 - \int_0^{p_c} \exp\left(\frac{p - p_c}{\Delta p}\right)^2 dp \qquad \text{(A.1)}$$

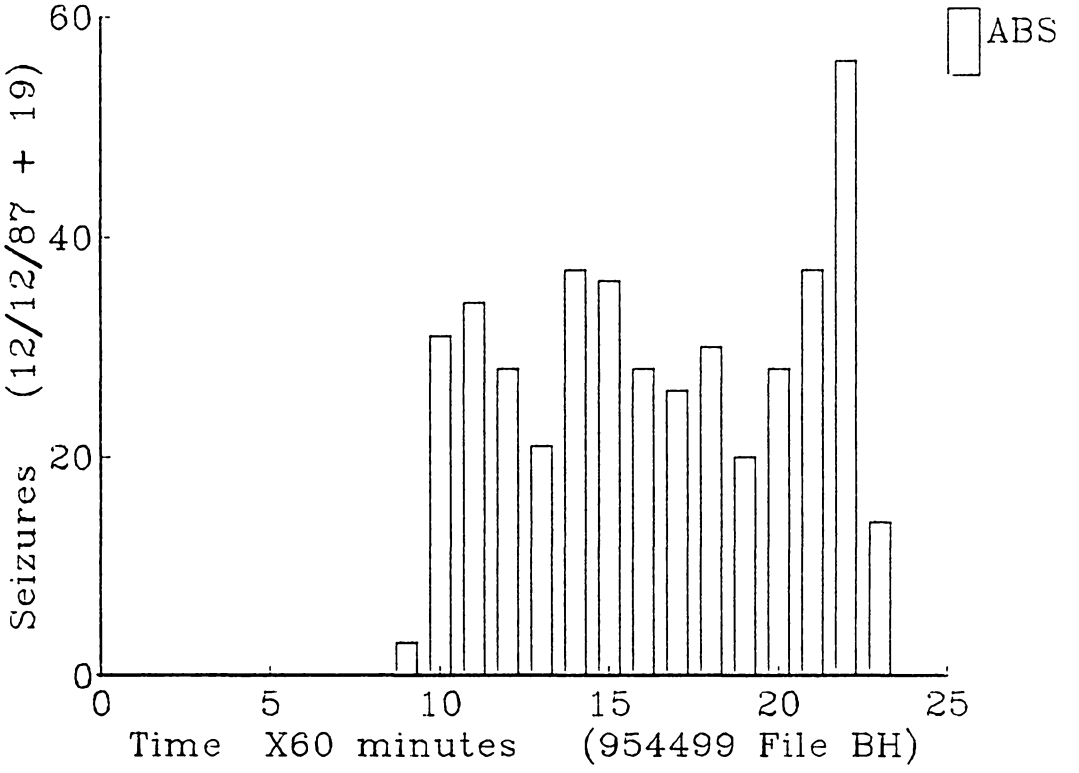

Figure 32: Distribution of seizures as a function of the time of the day for patient BH. The x-axis shows the hour of the day, and the y-axis is the total number of seizures that occurred during that hour.

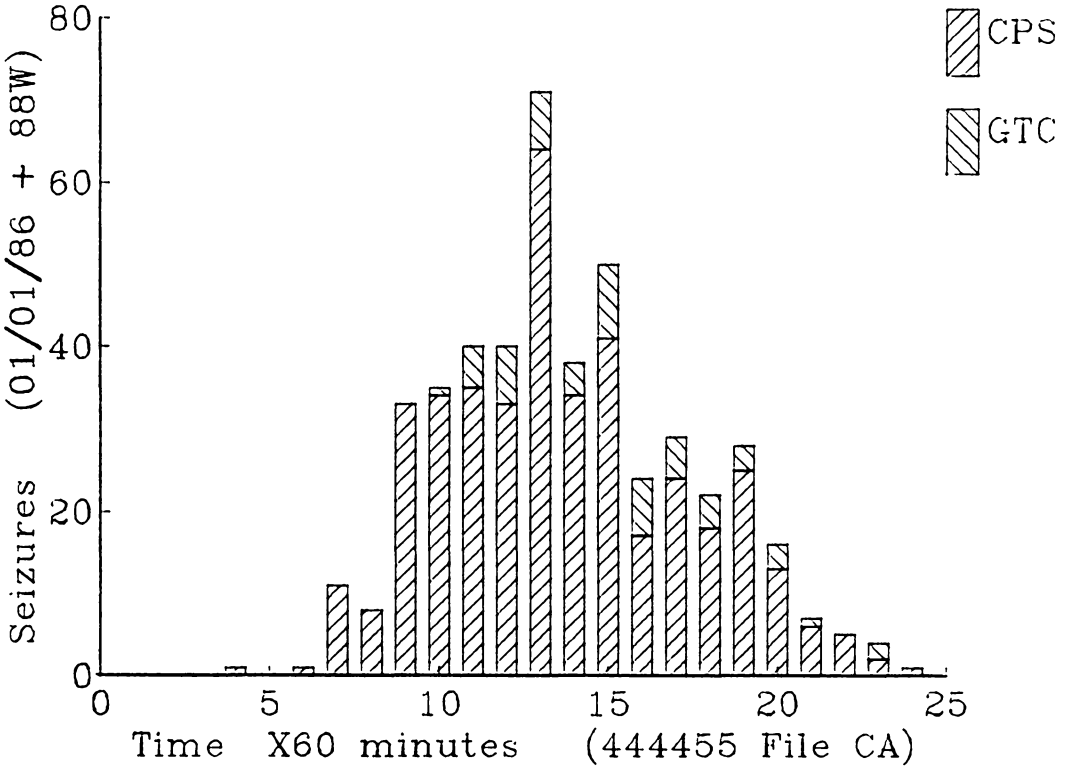

Figure 33: Distribution of seizures as a function of the time of the day for patient CA. The x-axis shows the hour of the day, and the y-axis is the total number of seizures that occurred during that hour.

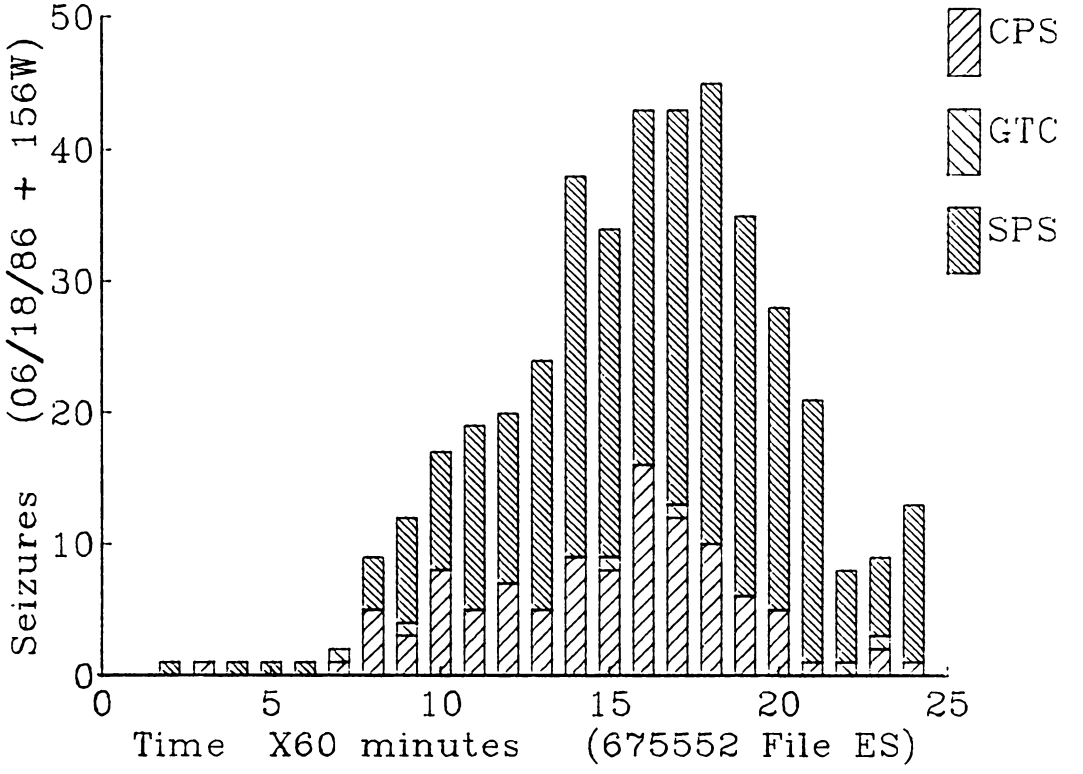

Figure 34: Distribution of seizures as a function of the time of the day for patient ES. The x-axis shows the hour of the day, and the y-axis is the total number of seizures that occurred during that hour.

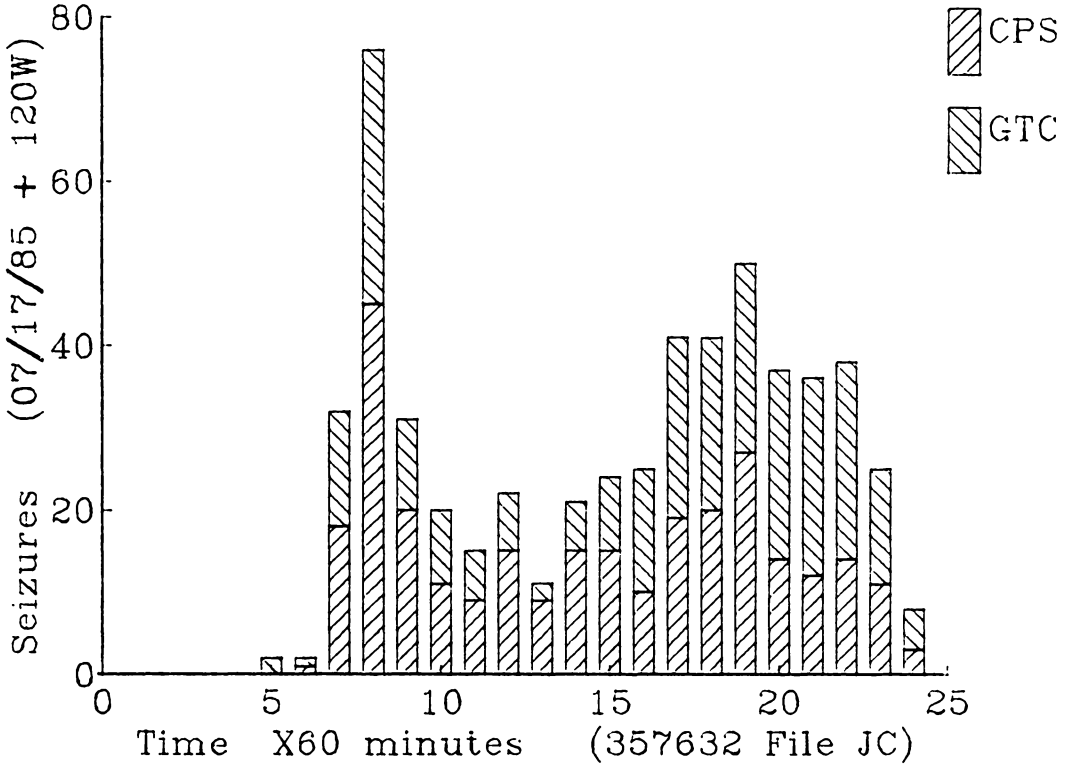

Figure 35: **Distribution of seizures as a function of the time of the day for patient JC.** The x-axis shows the hour of the day, and the y-axis is the total number of seizures that occurred during that hour.

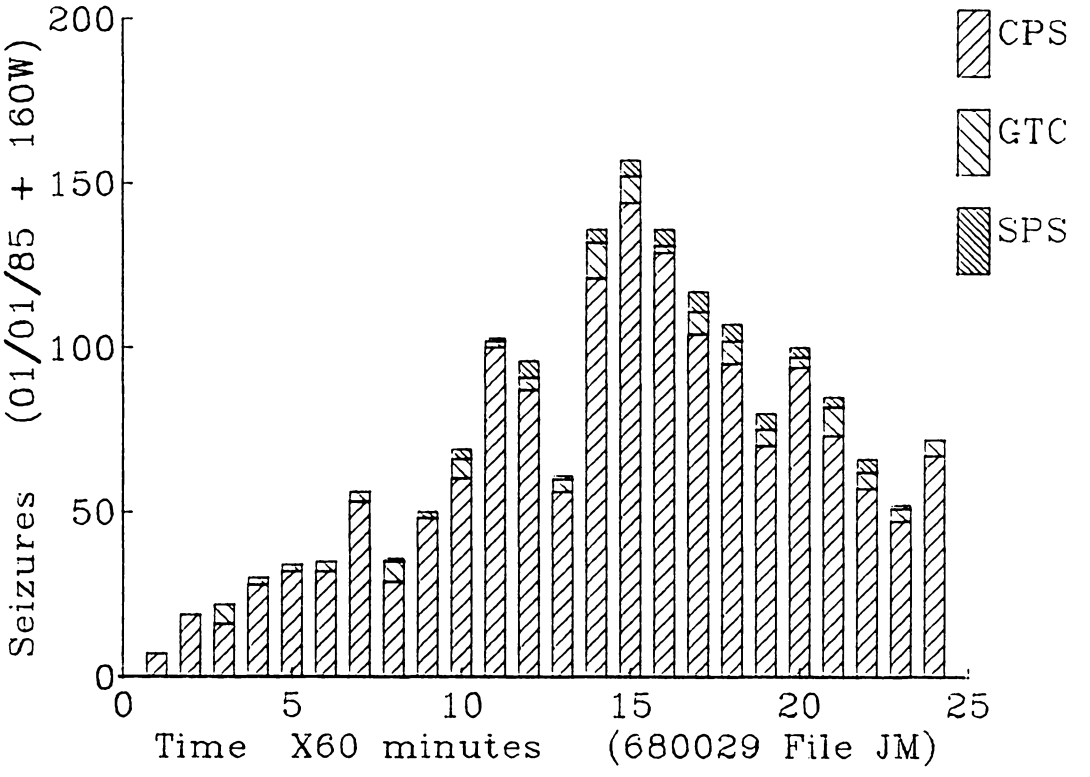

Figure 36: Distribution of seizures as a function of the time of the day for patient JM. The x-axis shows the hour of the day, and the y-axis is the total number of seizures that occurred during that hour.

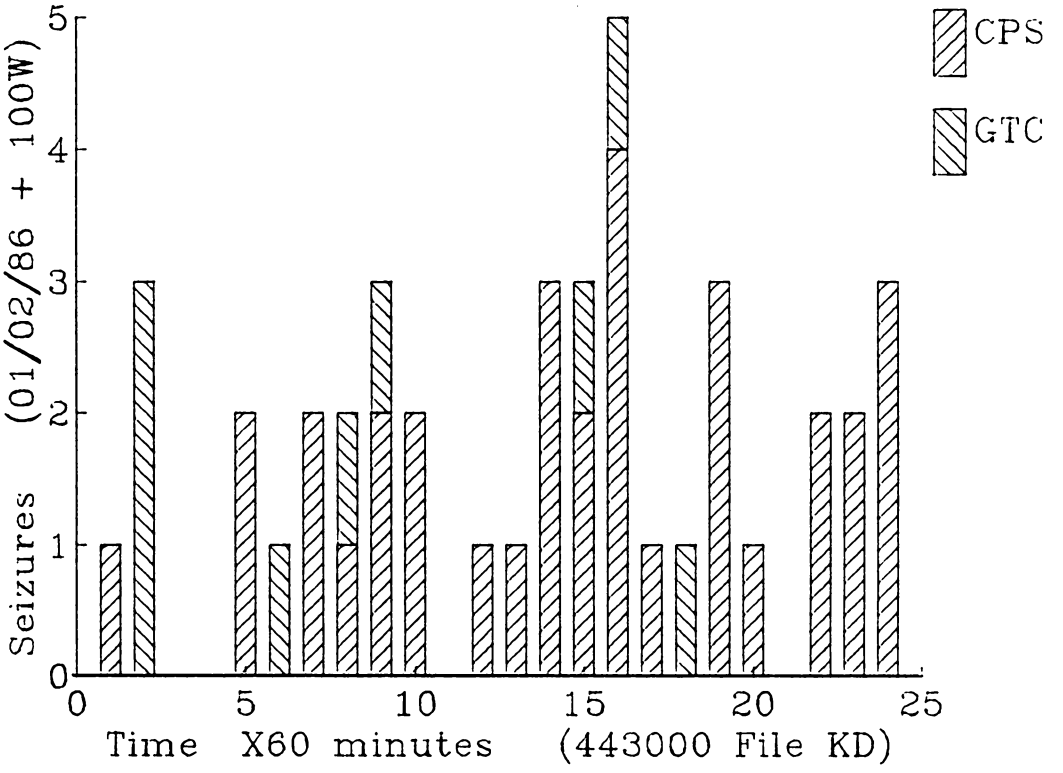

Figure 37: Distribution of seizures as a function of the time of the day for patient KD. The x-axis shows the hour of the day, and the y-axis is the total number of seizures that occurred during that hour.

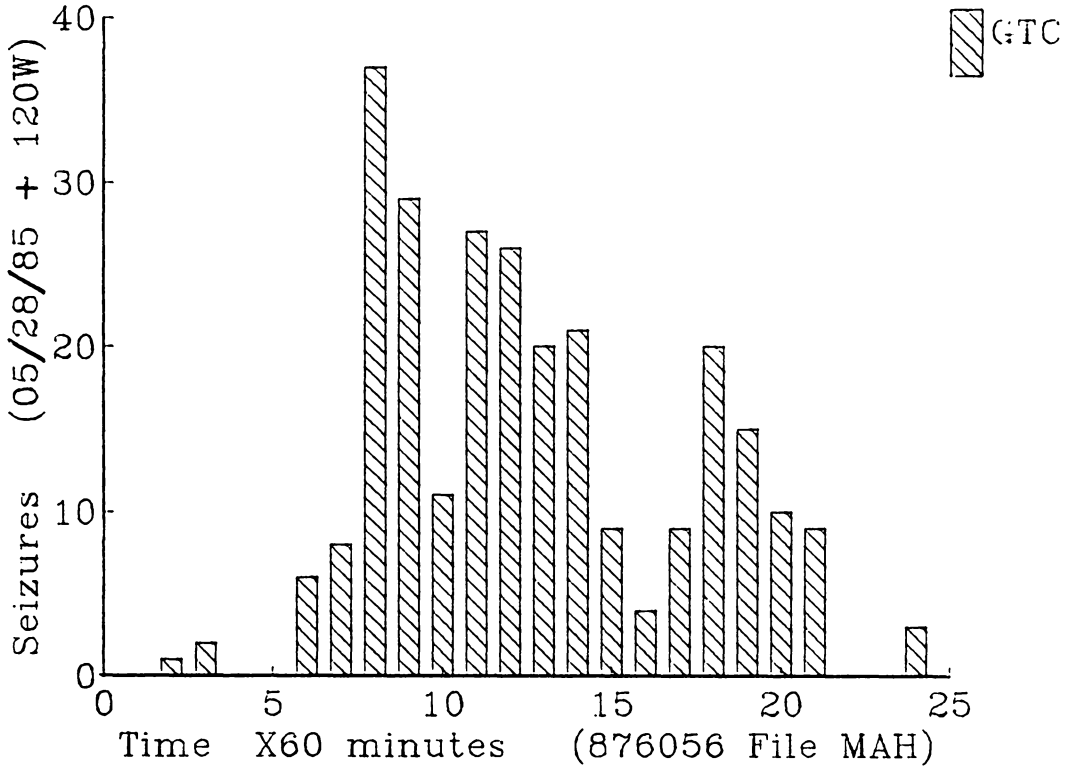

Figure 38: **Distribution of seizures as a function of the time of the day for patient MAH.** The x-axis shows the hour of the day, and the y-axis is the total number of seizures that occurred during that hour.

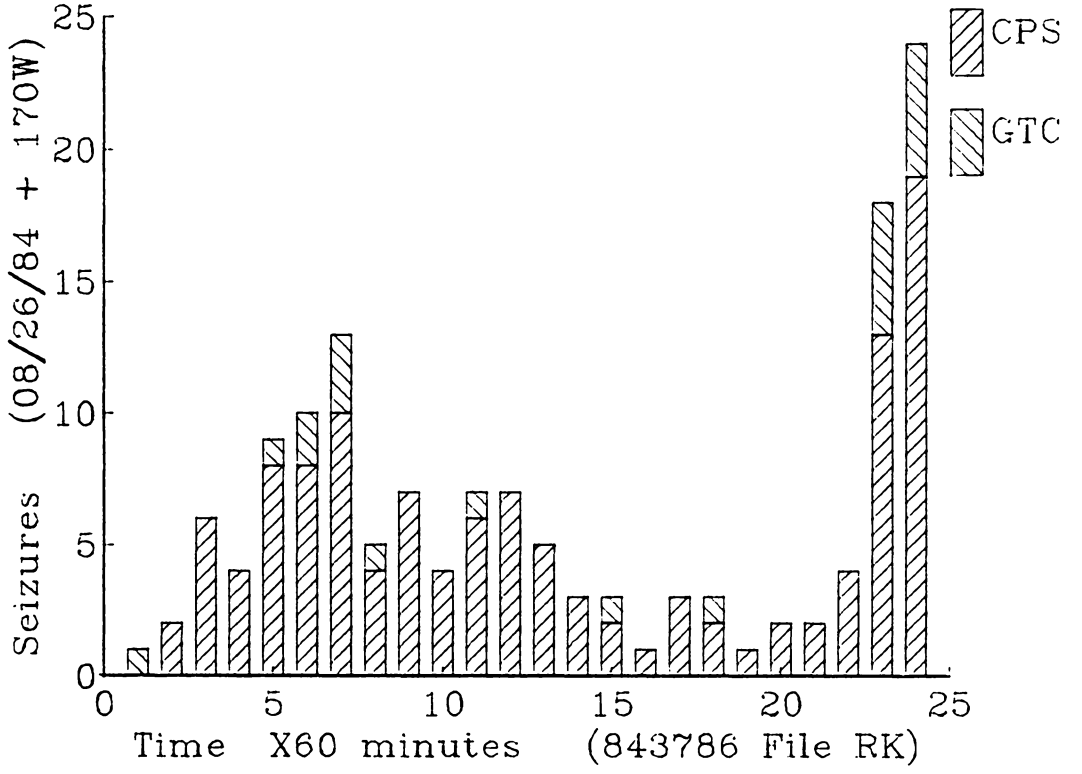

Figure 39: **Distribution of seizures as a function of the time of the day for patient RK.** The x-axis shows the hour of the day, and the y-axis is the total number of seizures that occurred during that hour.

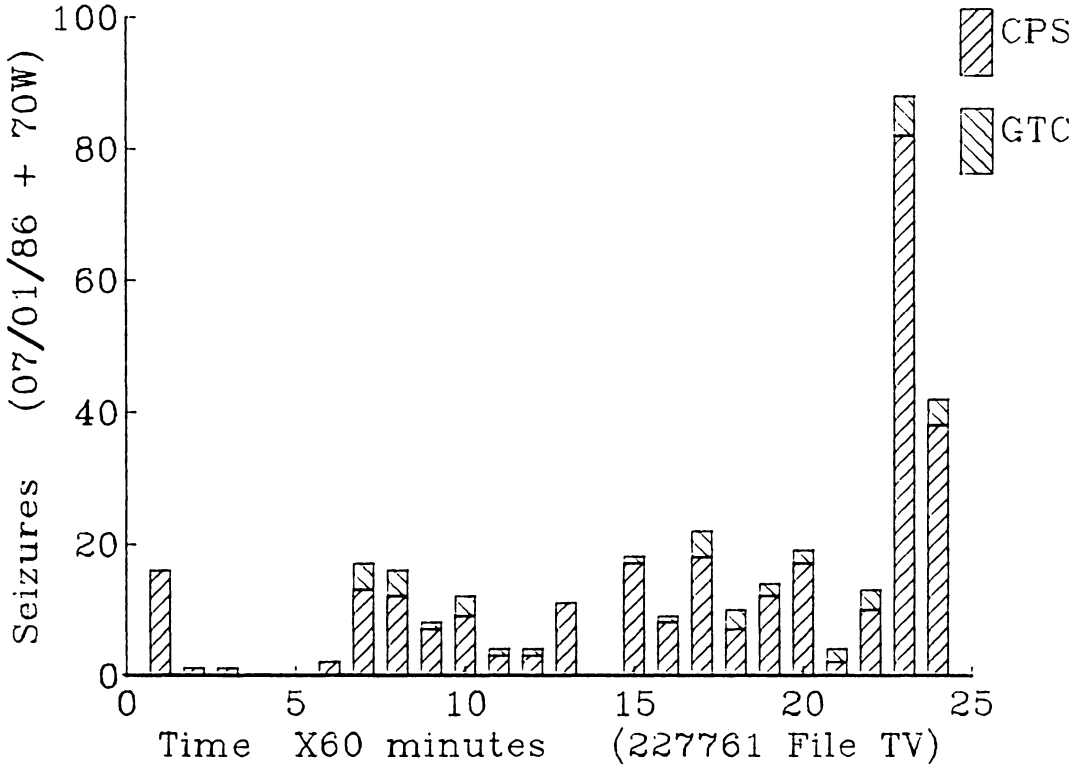

Figure 40: **Distribution of seizures as a function of the time of the day for patient TV.** The x-axis shows the hour of the day, and the y-axis is the total number of seizures that occurred during that hour.

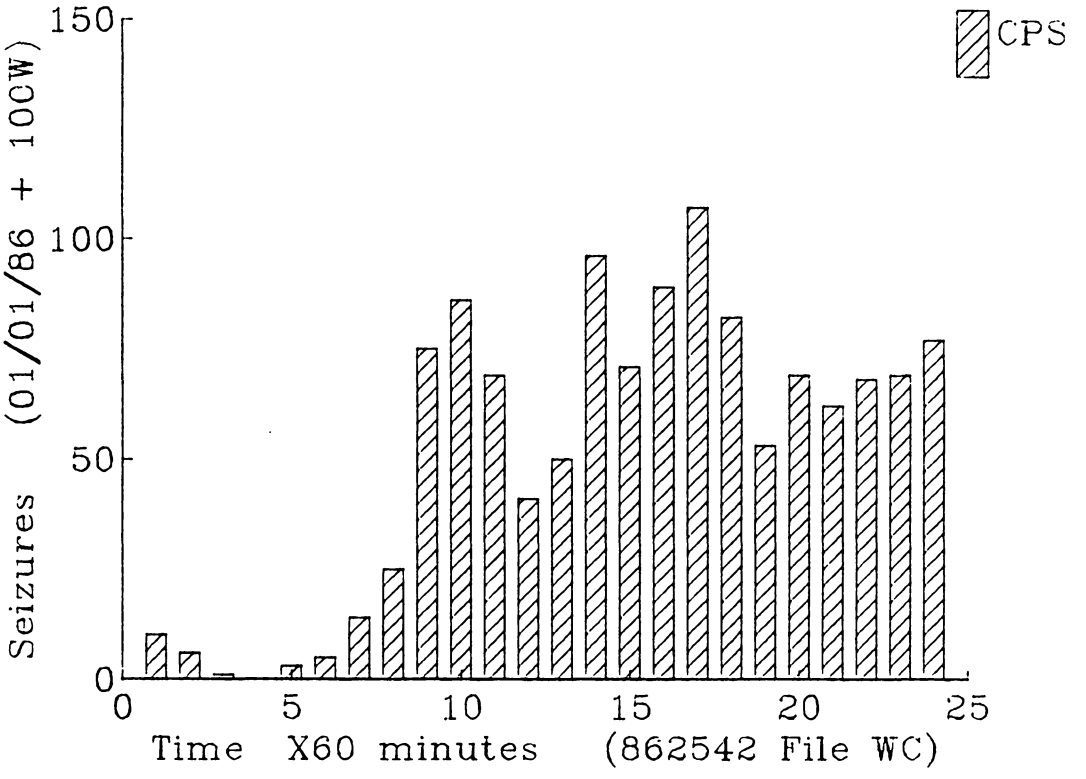

Figure 41: **Distribution of seizures as a function of the time of the day for patient WC.** The x-axis shows the hour of the day, and the y-axis is the total number of seizures that occurred during that hour.

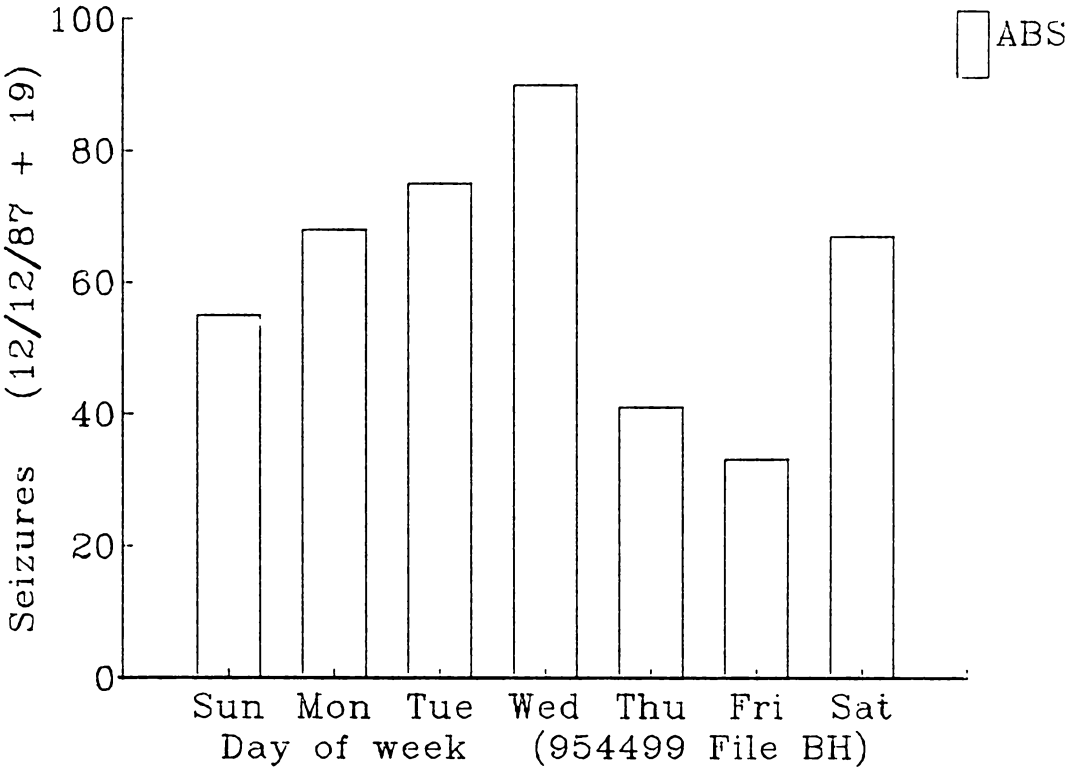

Figure 42: **Distribution of seizures as a function of the day of the week for patient BH.** The x-axis shows the day of the week, and the y-axis shows the total number of seizures that occurred on that day of the week.

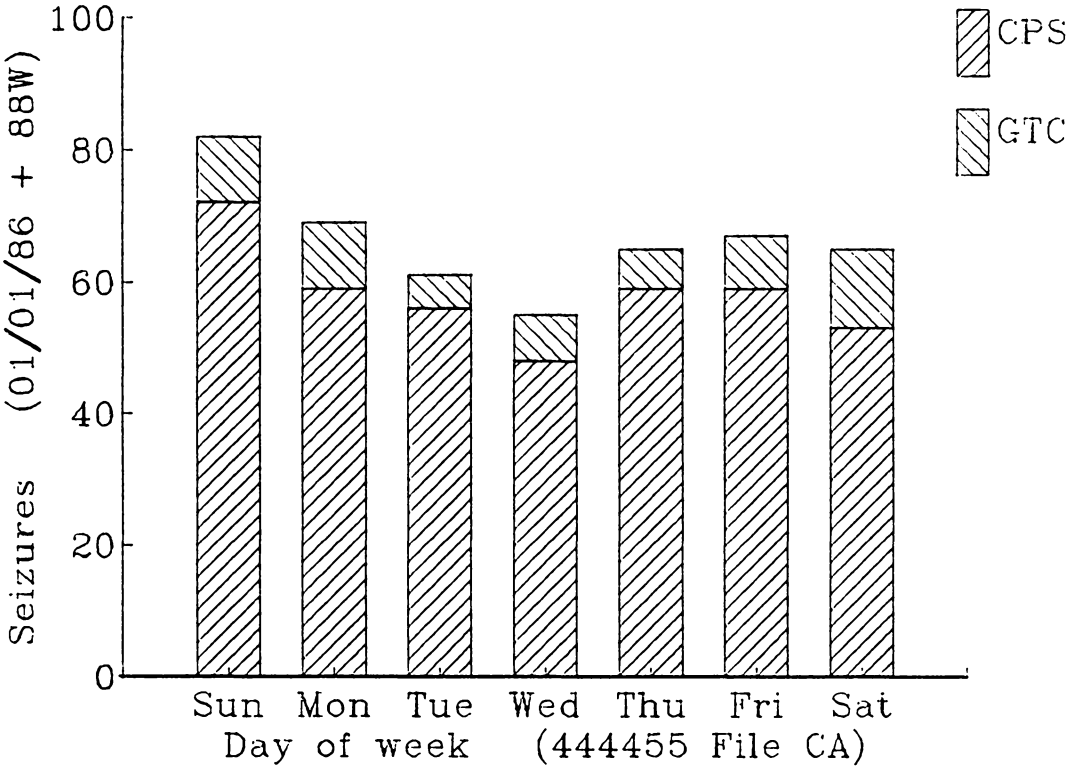

Figure 43: **Distribution of seizures as a function of the day of the week for patient CA.** The x-axis shows the day of the week, and the y-axis shows the total number of seizures that occurred on that day of the week.

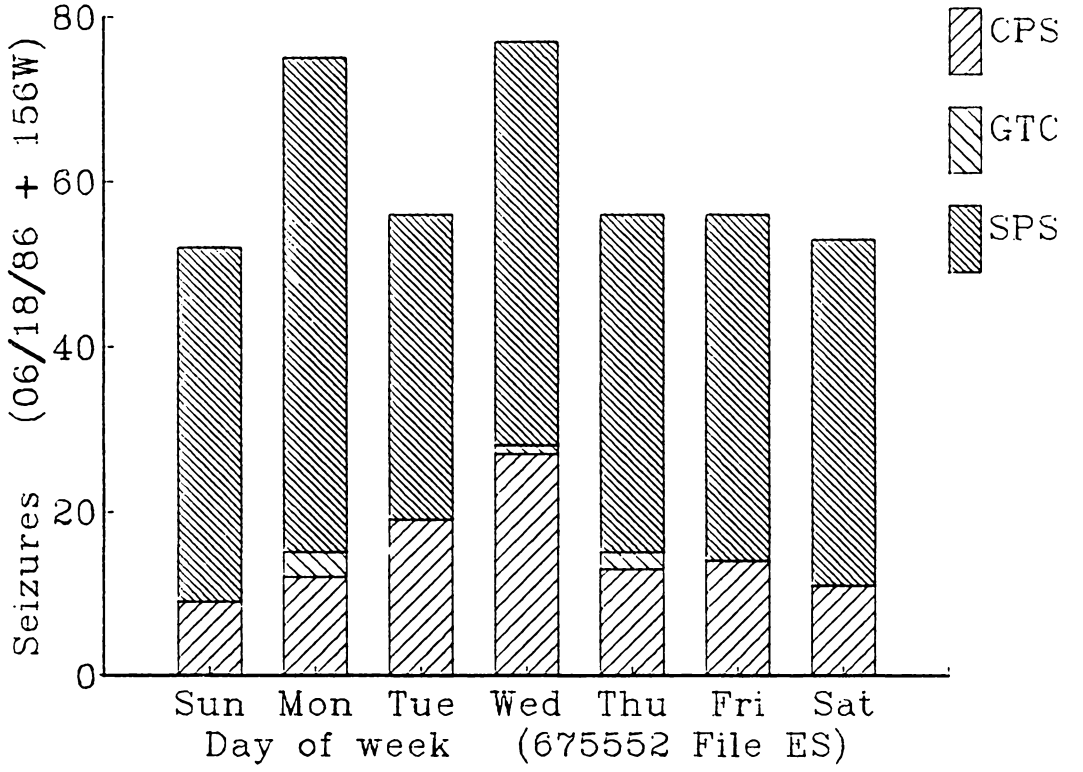

Figure 44: **Distribution of seizures as a function of the day of the week for patient ES.** The x-axis shows the day of the week, and the y-axis shows the total number of seizures that occurred on that day of the week.

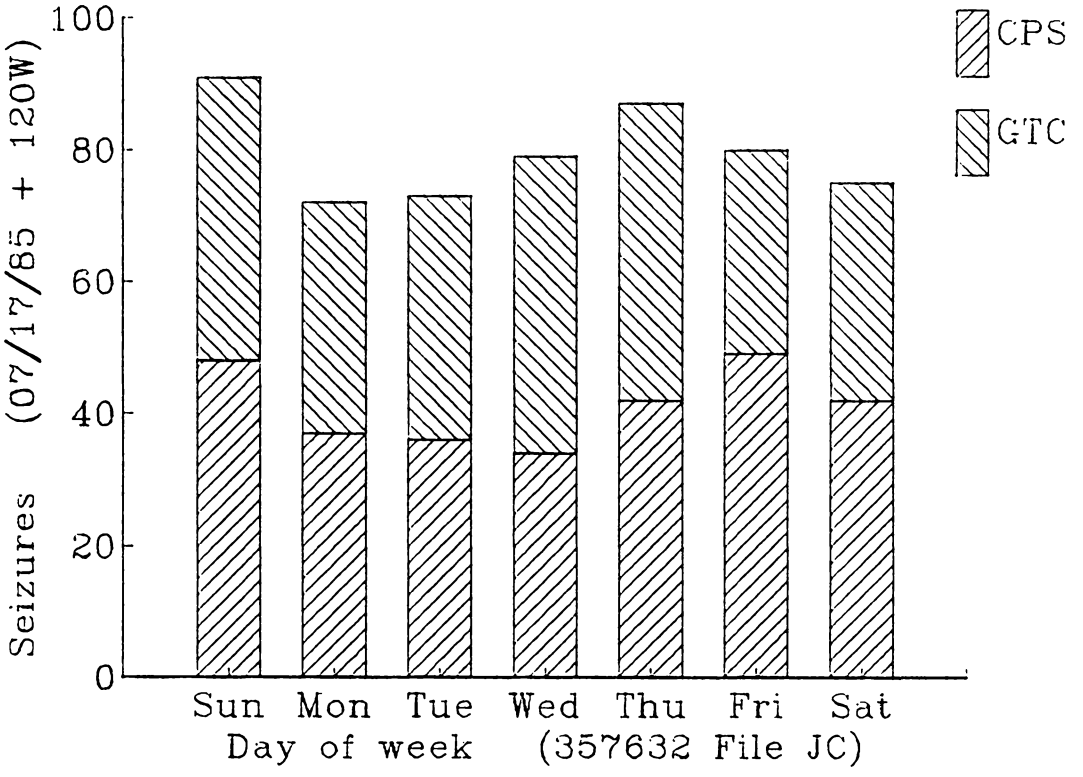

Figure 45: **Distribution of seizures as a function of the day of the week for patient JC.** The x-axis shows the day of the week, and the y-axis shows the total number of seizures that occurred on that day of the week.

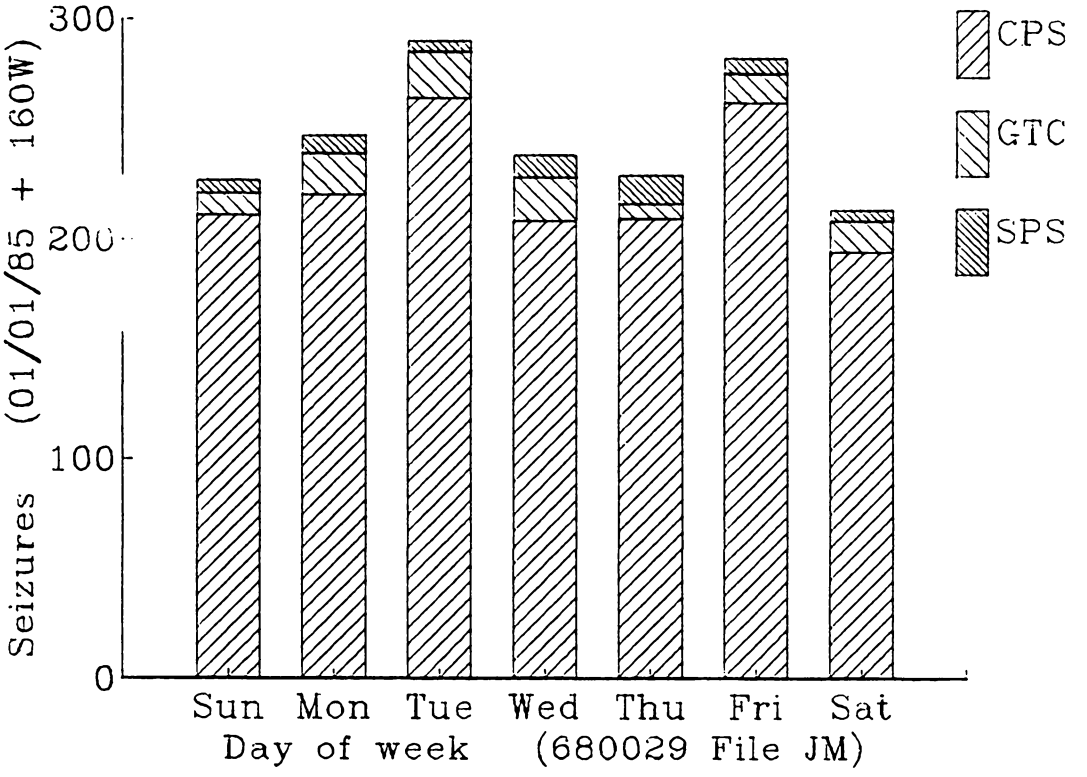

Figure 46: **Distribution of seizures as a function of the day of the week for patient JM.** The x-axis shows the day of the week, and the y-axis shows the total number of seizures that occurred on that day of the week.

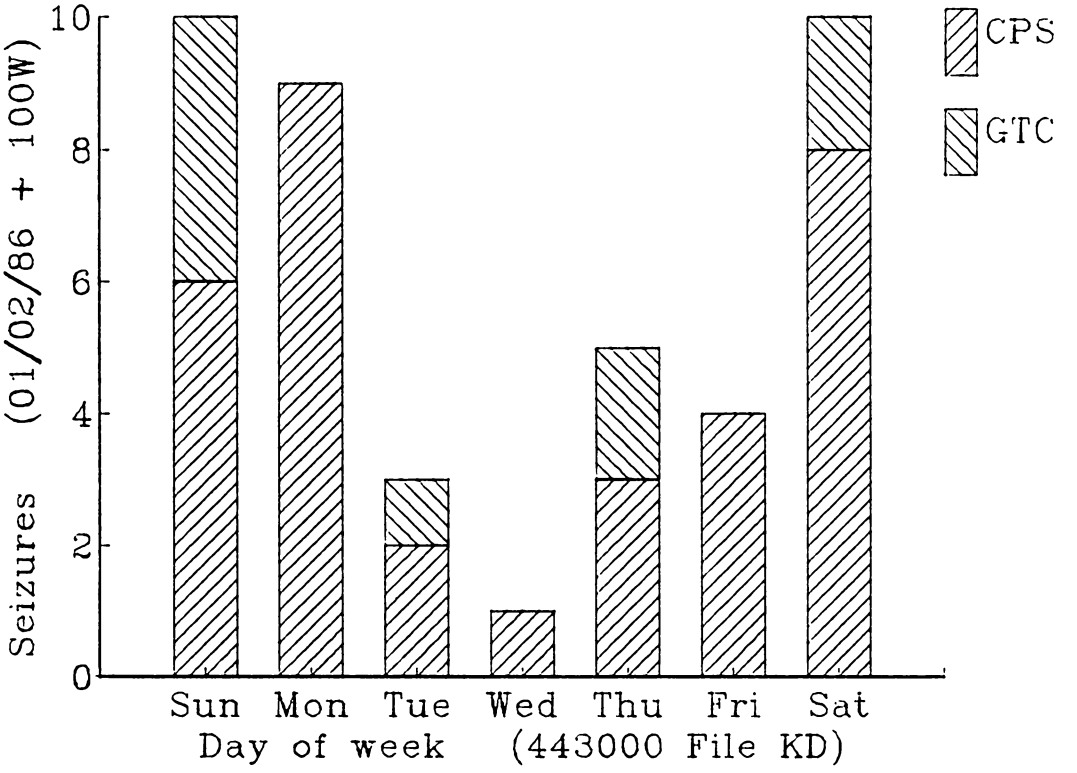

Figure 47: Distribution of seizures as a function of the day of the week for patient KD. The x-axis shows the day of the week, and the y-axis shows the total number of seizures that occurred on that day of the week.

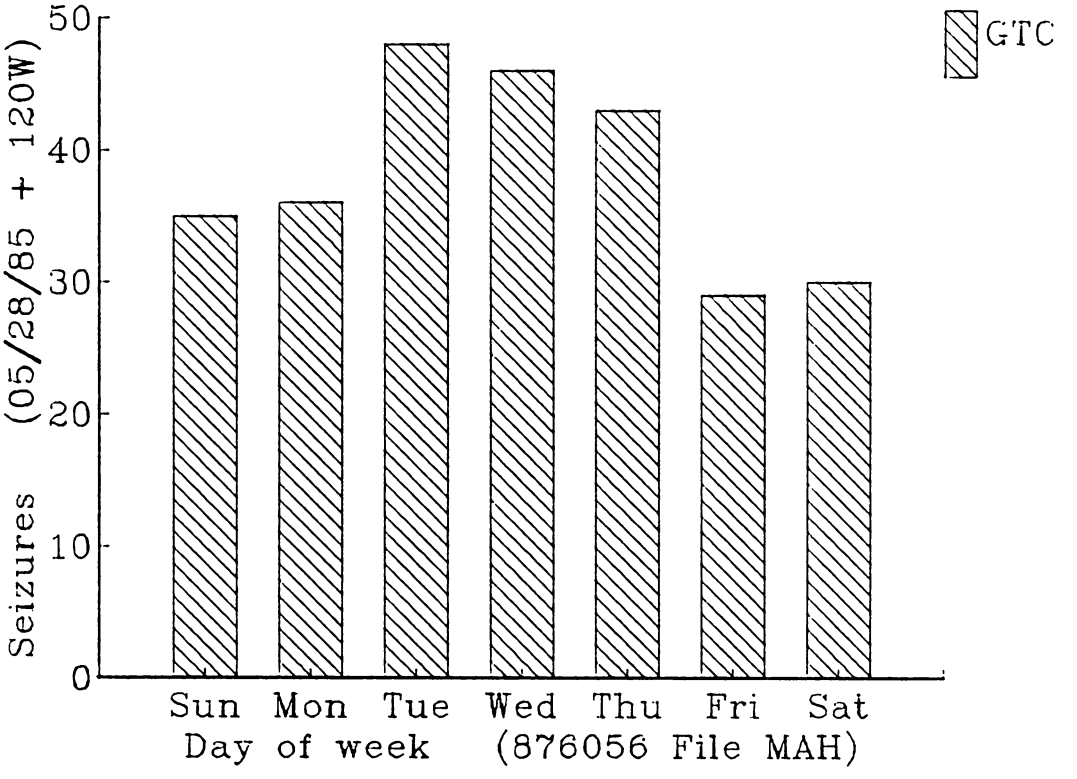

Figure 48: **Distribution of seizures as a function of the day of the week for patient MAH.** The x-axis shows the day of the week, and the y-axis shows the total number of seizures that occurred on that day of the week.

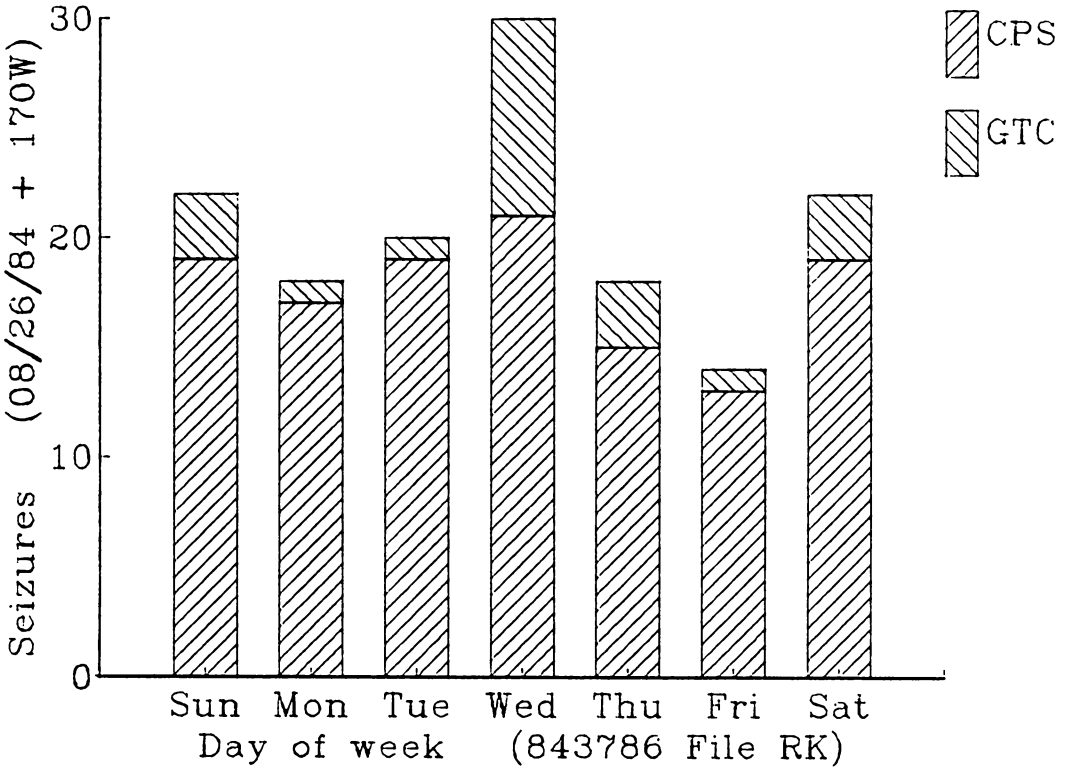

Figure 49: **Distribution of seizures as a function of the day of the week for patient RK.** The x-axis shows the day of the week, and the y-axis shows the total number of seizures that occurred on that day of the week.

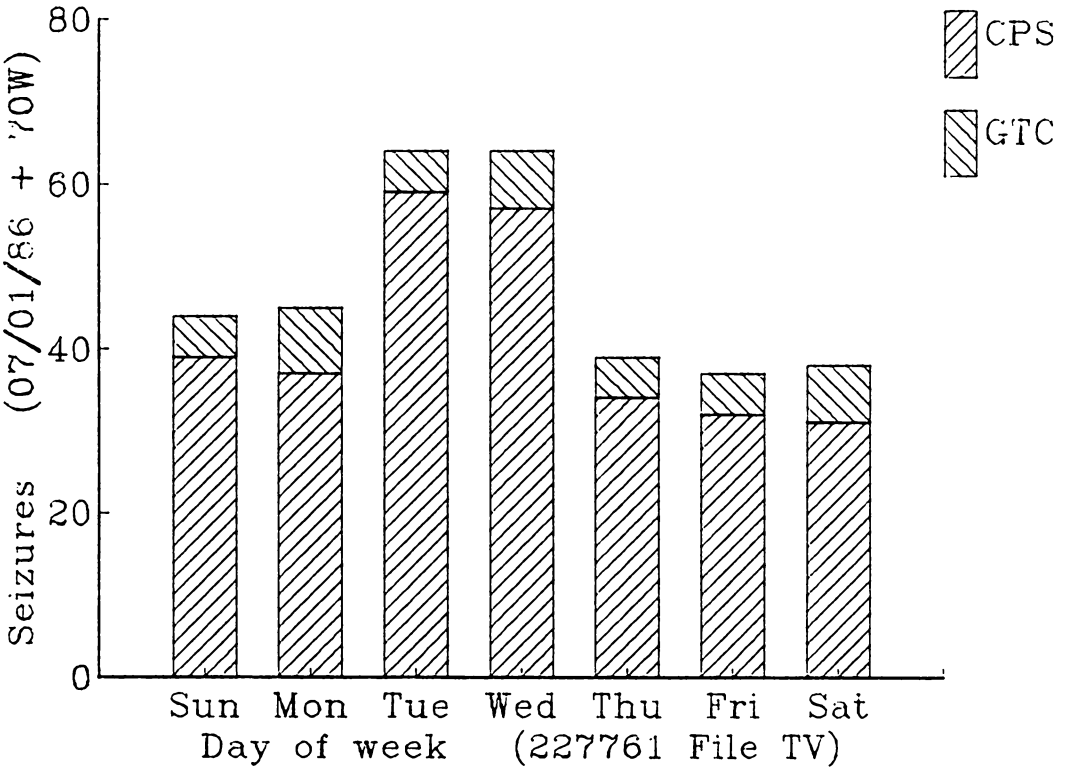

Figure 50: **Distribution of seizures as a function of the day of the week for patient TV.** The x-axis shows the day of the week, and the y-axis shows the total number of seizures that occurred on that day of the week.

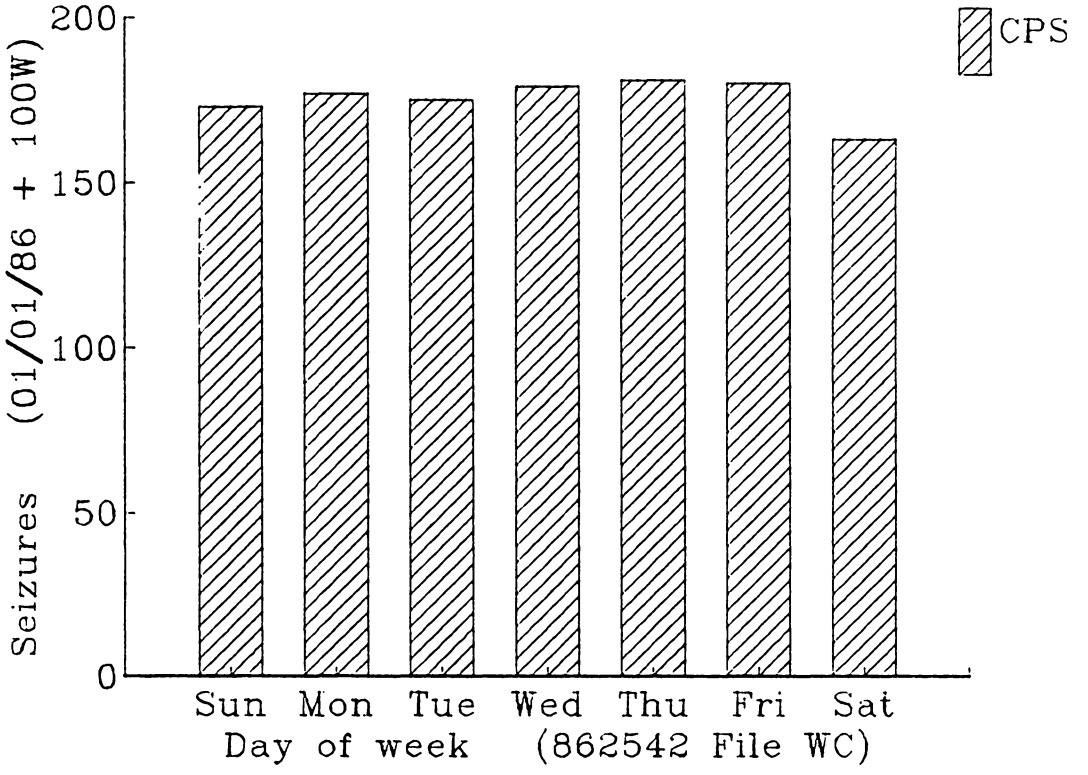

Figure 51: **Distribution of seizures as a function of the day of the week for patient WC.** The x-axis shows the day of the week, and the y-axis shows the total number of seizures that occurred on that day of the week.

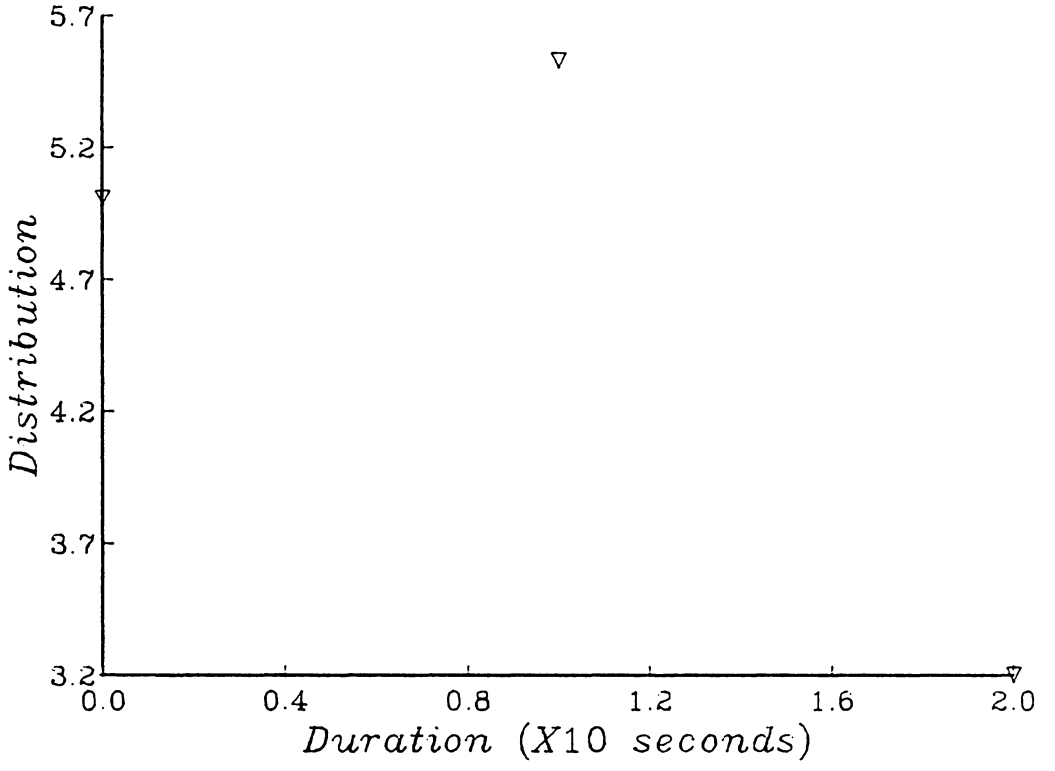

Figure 52: **Distribution of seizures as a function of seizure duration for patient BH.** The x-axis shows the duration of the seizure in seconds, and the y axis shows the log of the total number of seizures with that duration.

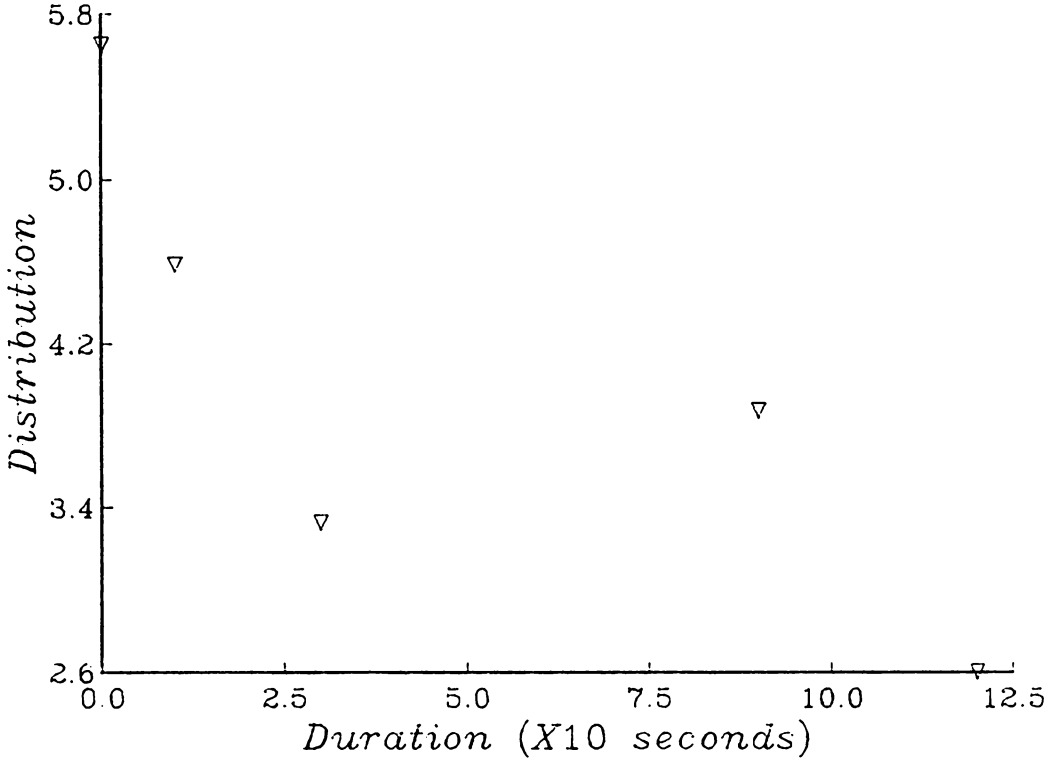

Figure 53: **Distribution of seizures as a function of seizure duration for patient CA.** The x-axis shows the duration of the seizure in seconds, and the y axis shows the log of the total number of seizures with that duration.

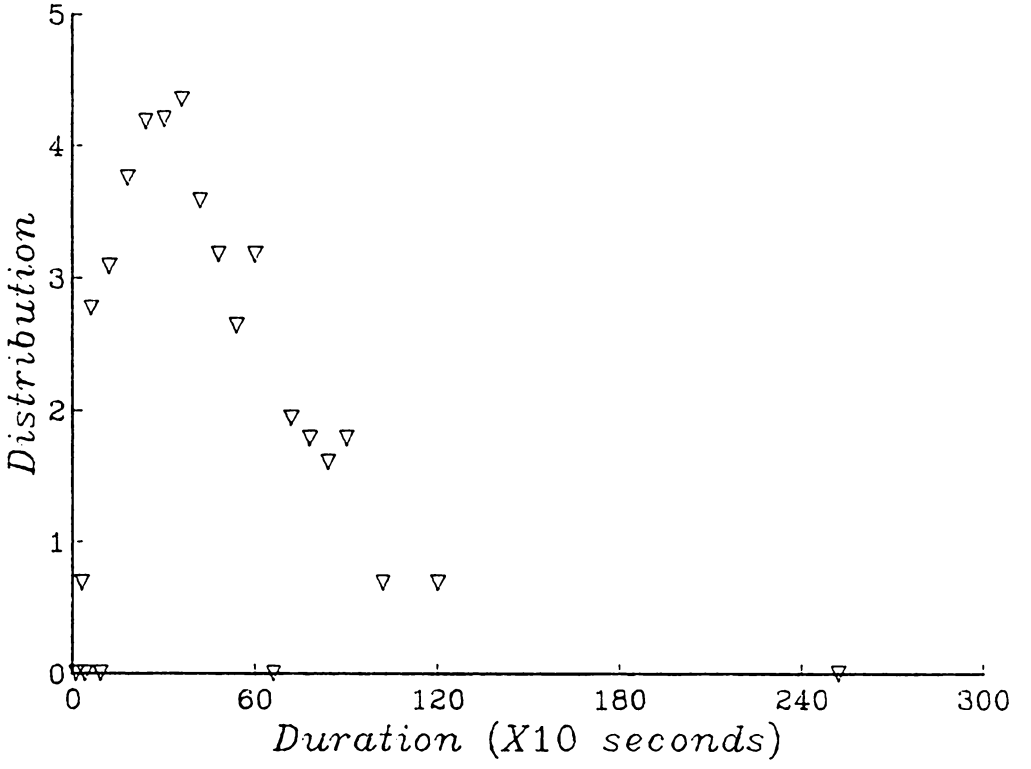

Figure 54: **Distribution of seizures as a function of seizure duration for patient ES.** The x-axis shows the duration of the seizure in seconds, and the y axis shows the log of the total number of seizures with that duration.

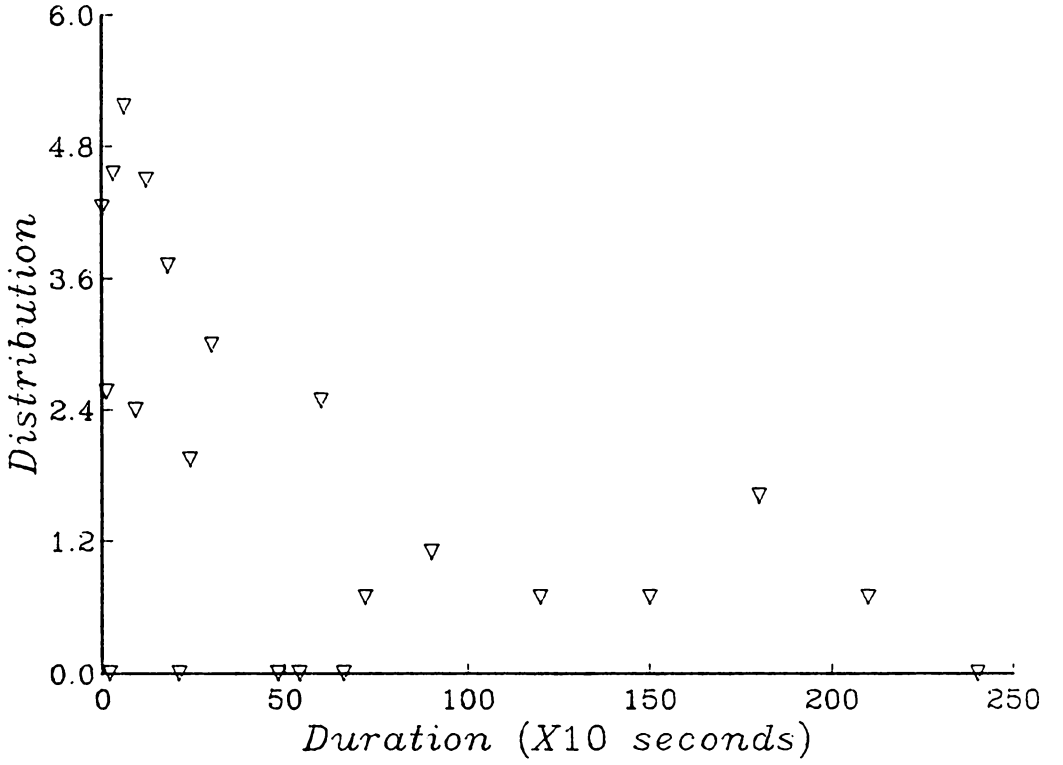

Figure 55: **Distribution of seizures as a function of seizure duration for patient JC.** The x-axis shows the duration of the seizure in seconds, and the y axis shows the log of the total number of seizures with that duration.

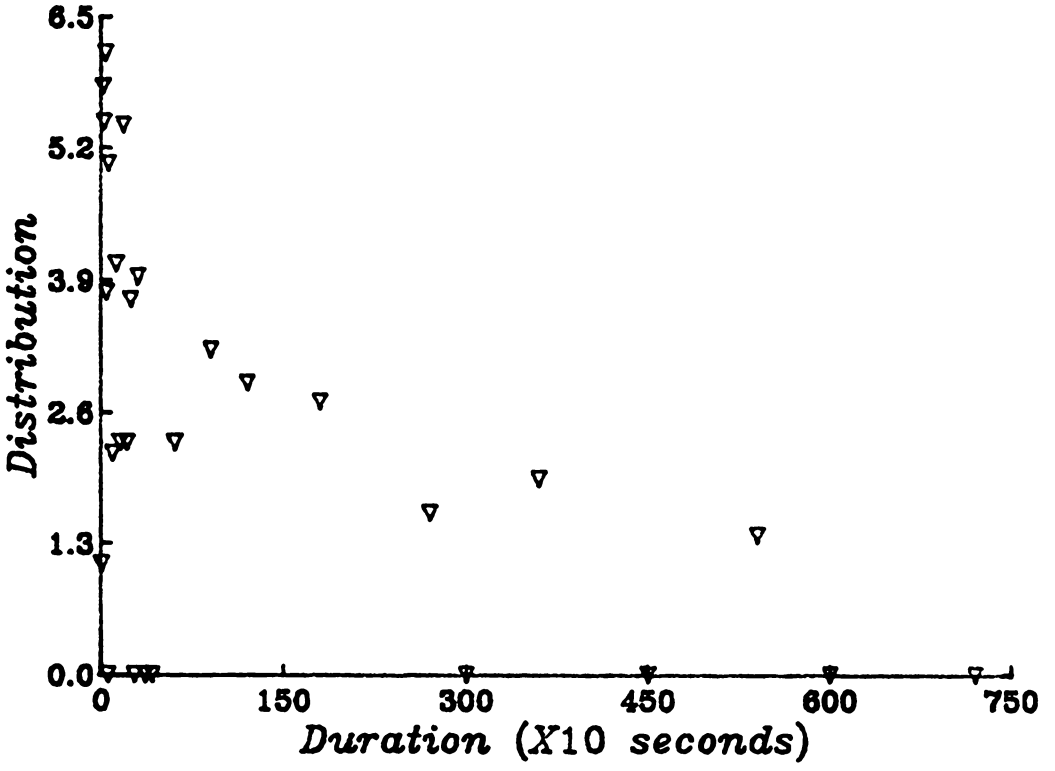

Figure 56: **Distribution of seizures as a function of seizure duration for patient JM.** The x-axis shows the duration of the seizure in seconds, and the y axis shows the log of the total number of seizures with that duration.

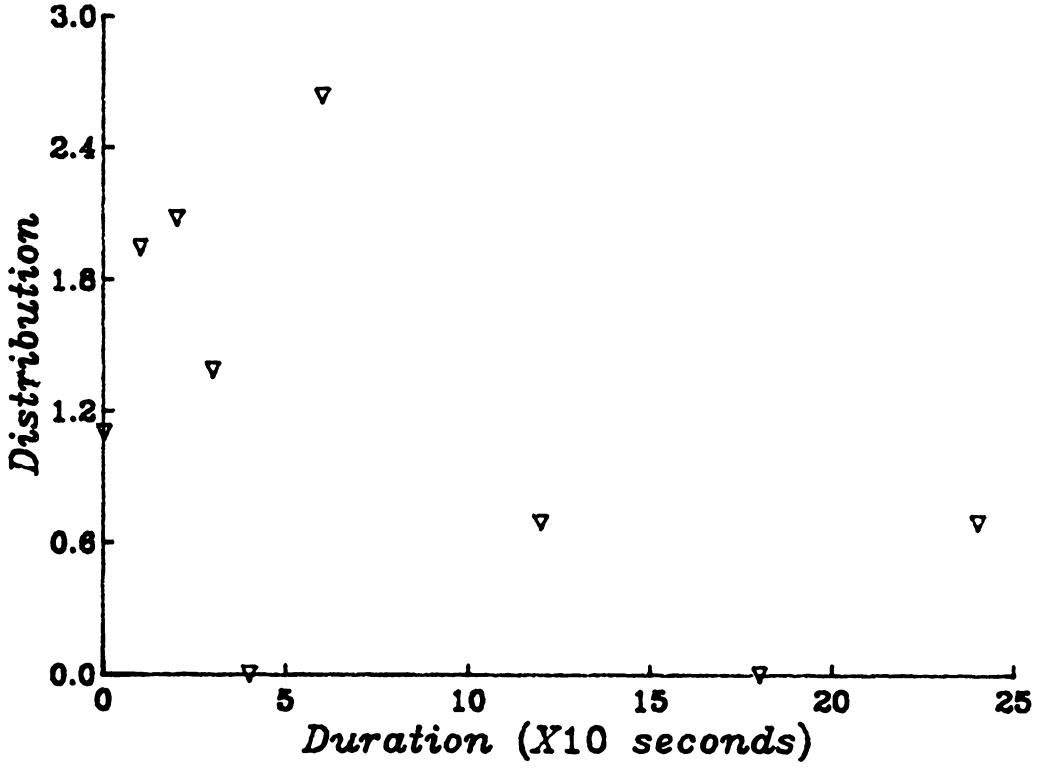

Figure 57: **Distribution of seizures as a function of seizure duration for patient KD.** The x-axis shows the duration of the seizure in seconds, and the y axis shows the log of the total number of seizures with that duration.

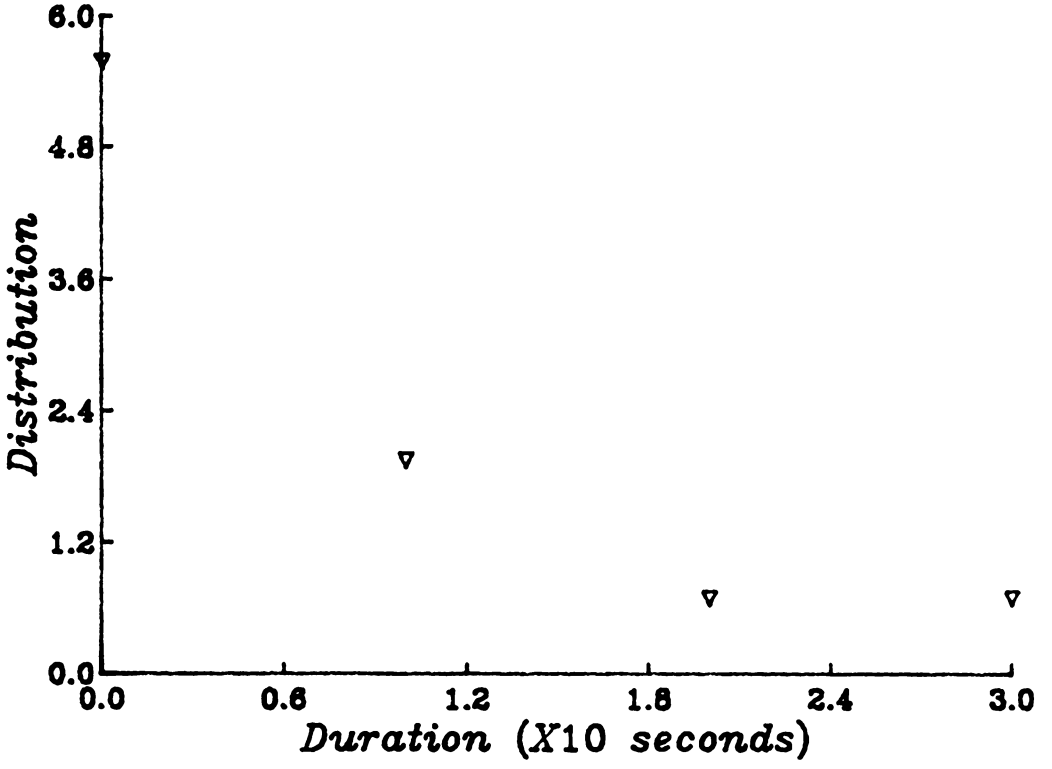

Figure 58: **Distribution of seizures as a function of seizure duration for patient MAH.** The x-axis shows the duration of the seizure in seconds, and the y axis shows the log of the total number of seizures with that duration.

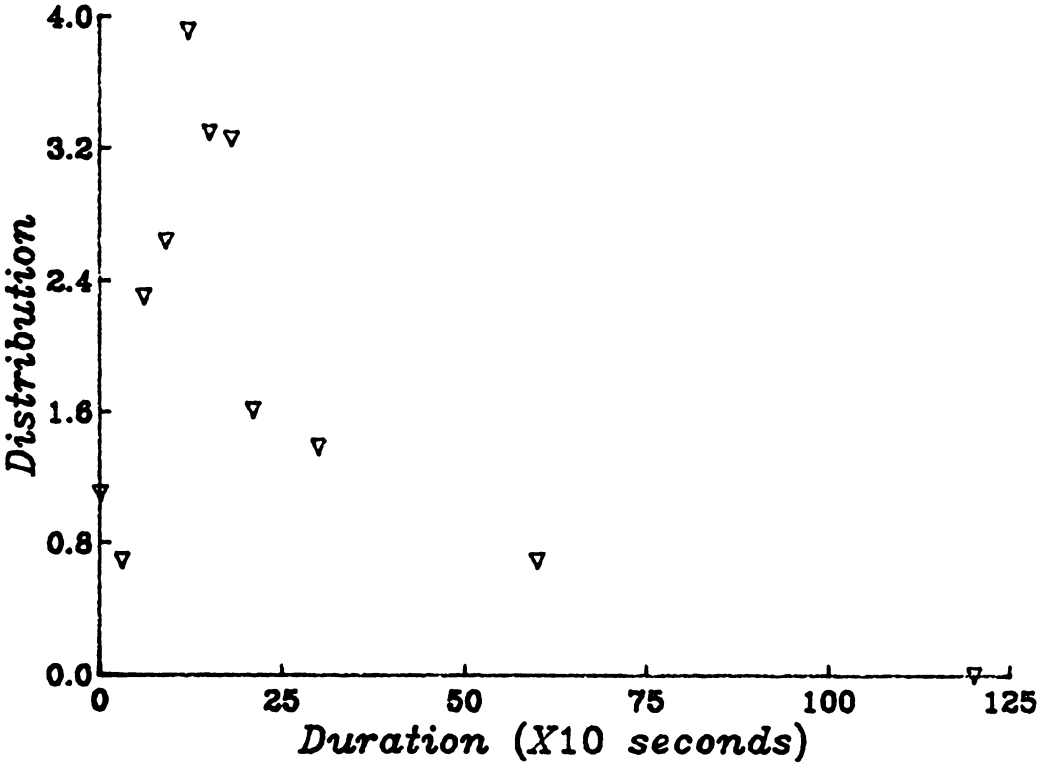

Figure 59: **Distribution of seizures as a function of seizure duration for patient RK.** The x-axis shows the duration of the seizure in seconds, and the y axis shows the log of the total number of seizures with that duration.

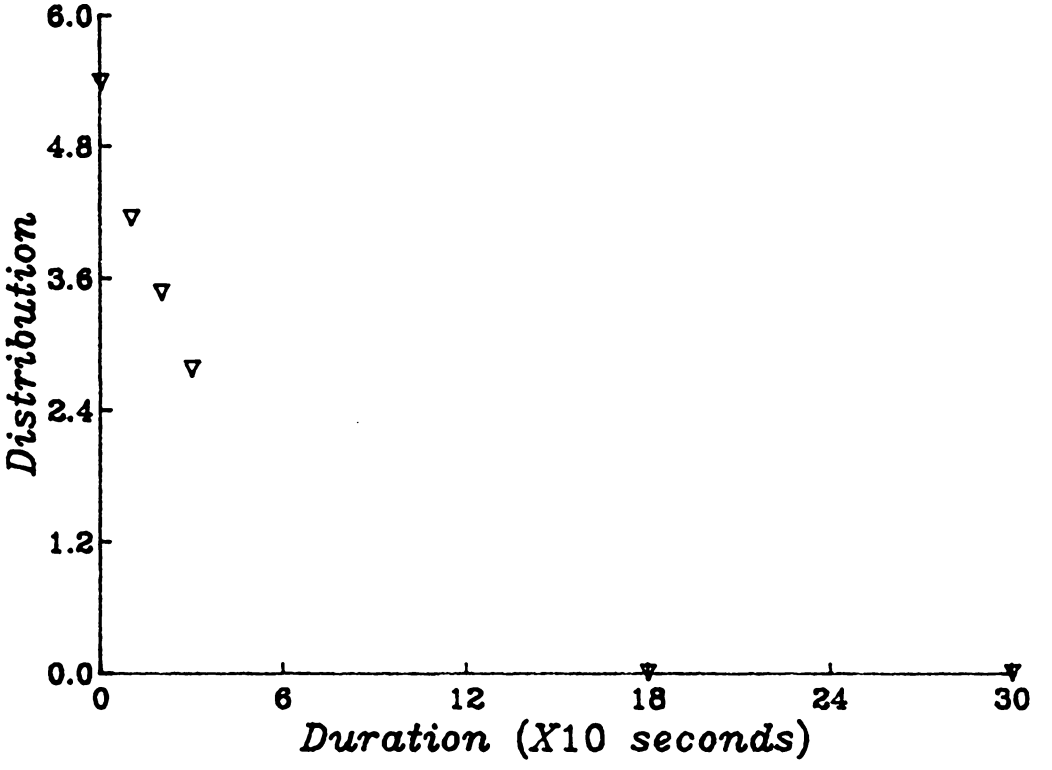

Figure 60: **Distribution of seizures as a function of seizure duration for patient TV.** The x-axis shows the duration of the seizure in seconds, and the y axis shows the log of the total number of seizures with that duration.

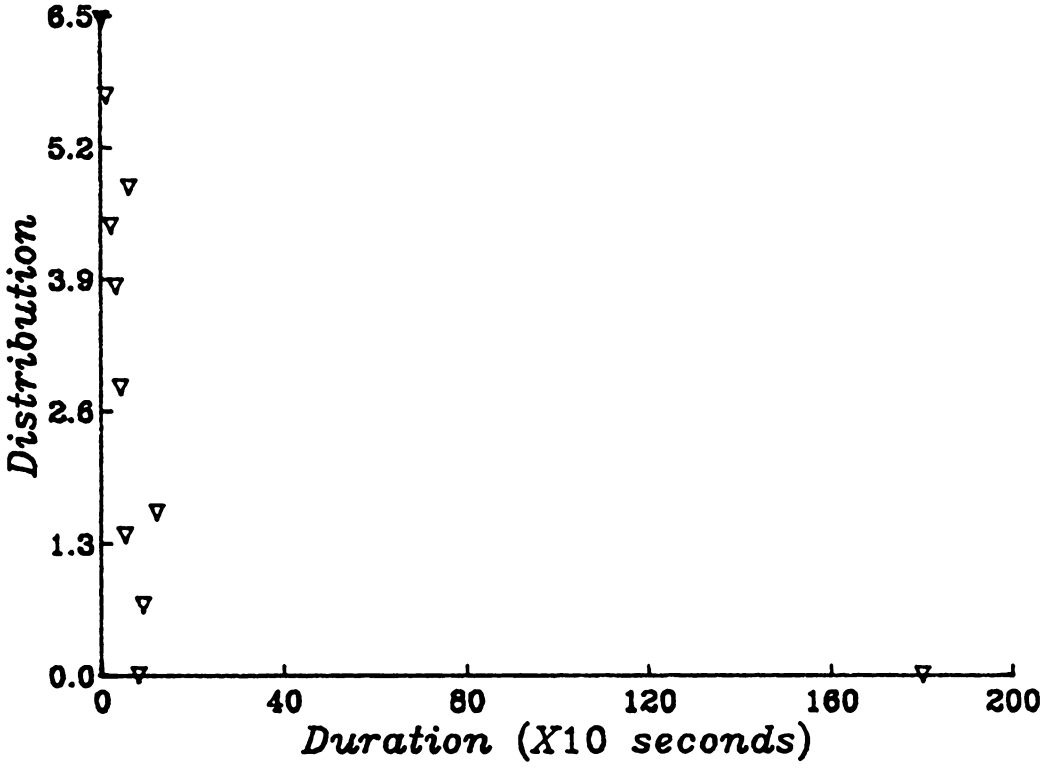

Figure 61: **Distribution of seizures as a function of seizure duration for patient WC.** The x-axis shows the duration of the seizure in seconds, and the y axis shows the log of the total number of seizures with that duration.

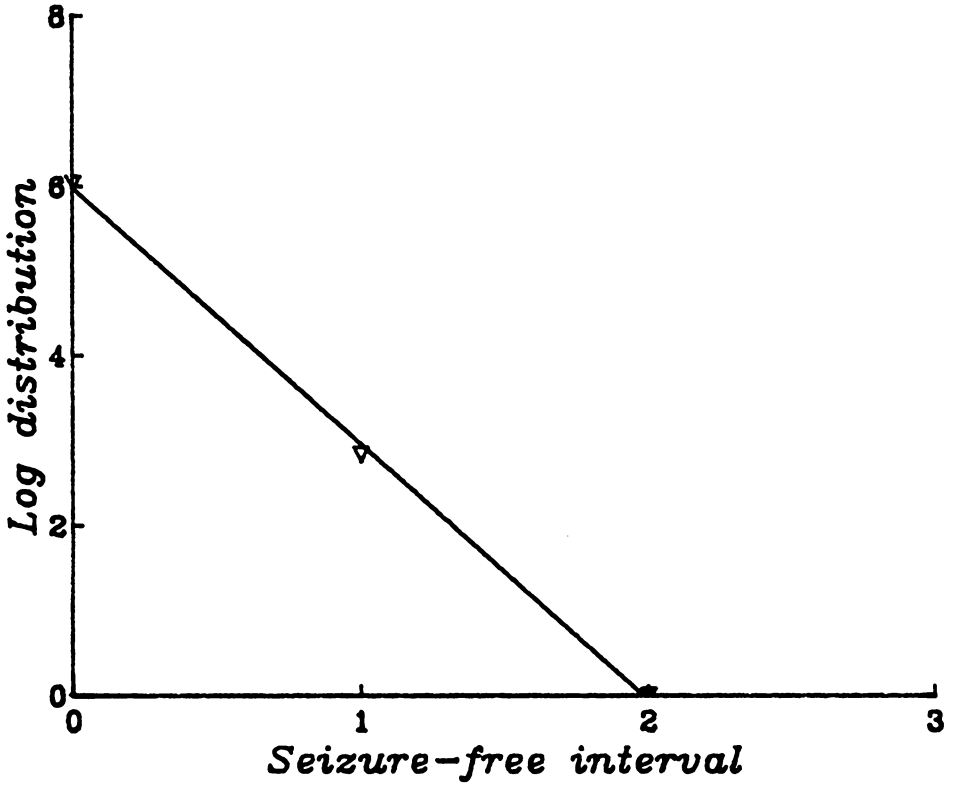

Figure 62: **Distribution of seizure-free intervals as a function of interval length for patient BH.** The x-axis shows the length of the seizure-free interval in days, and the y-axis shows the log of the number of seizure-free intervals of that length.

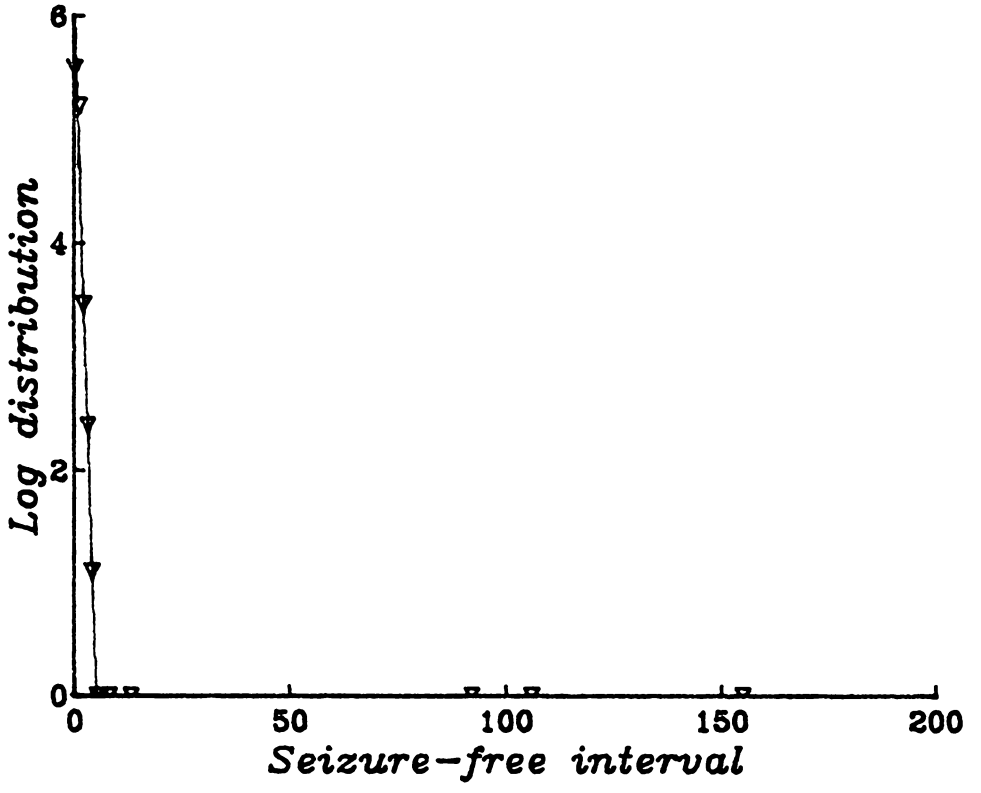

Figure 63: **Distribution of seizure-free intervals as a function of interval length for patient CA.** The x-axis shows the length of the seizure-free interval in days, and the y-axis shows the log of the number of seizure-free intervals of that length.

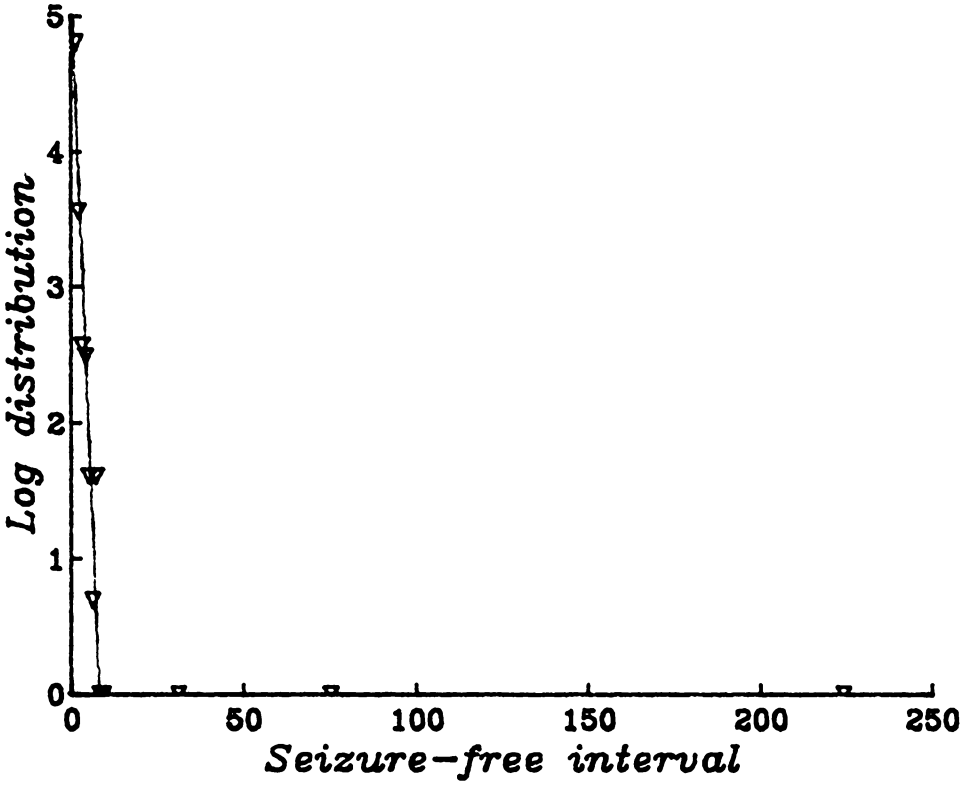

Figure 64: **Distribution of seizure-free intervals as a function of interval length for patient ES.** The x-axis shows the length of the seizure-free interval in days, and the y-axis shows the log of the number of seizure-free intervals of that length.

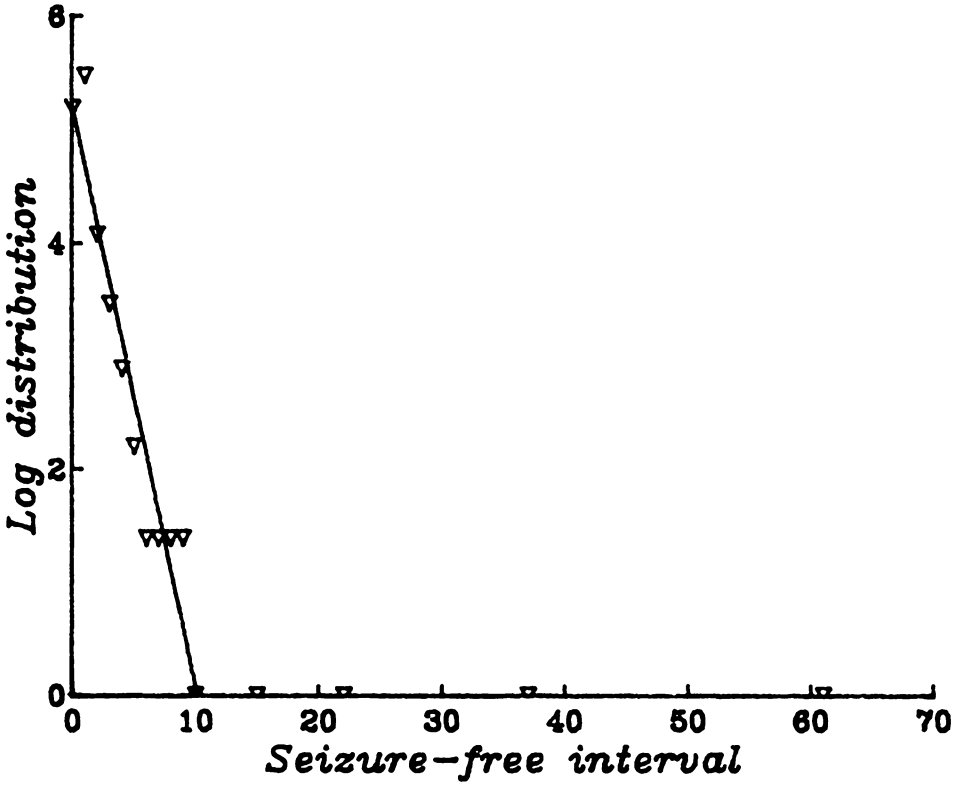

Figure 65: **Distribution of seizure-free intervals as a function of interval length for patient JC.** The x-axis shows the length of the seizure-free interval in days, and the y-axis shows the log of the number of seizure-free intervals of that length.

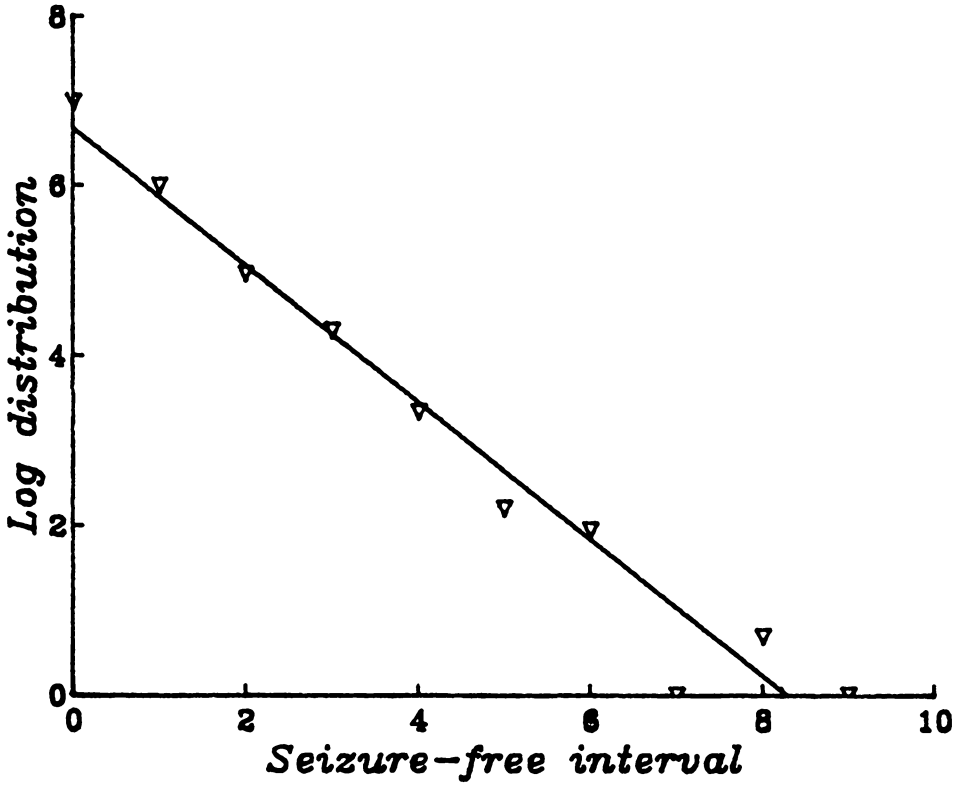

Figure 66: **Distribution of seizure-free intervals as a function of interval length for patient JM.** The x-axis shows the length of the seizure-free interval in days, and the y-axis shows the log of the number of seizure-free intervals of that length.

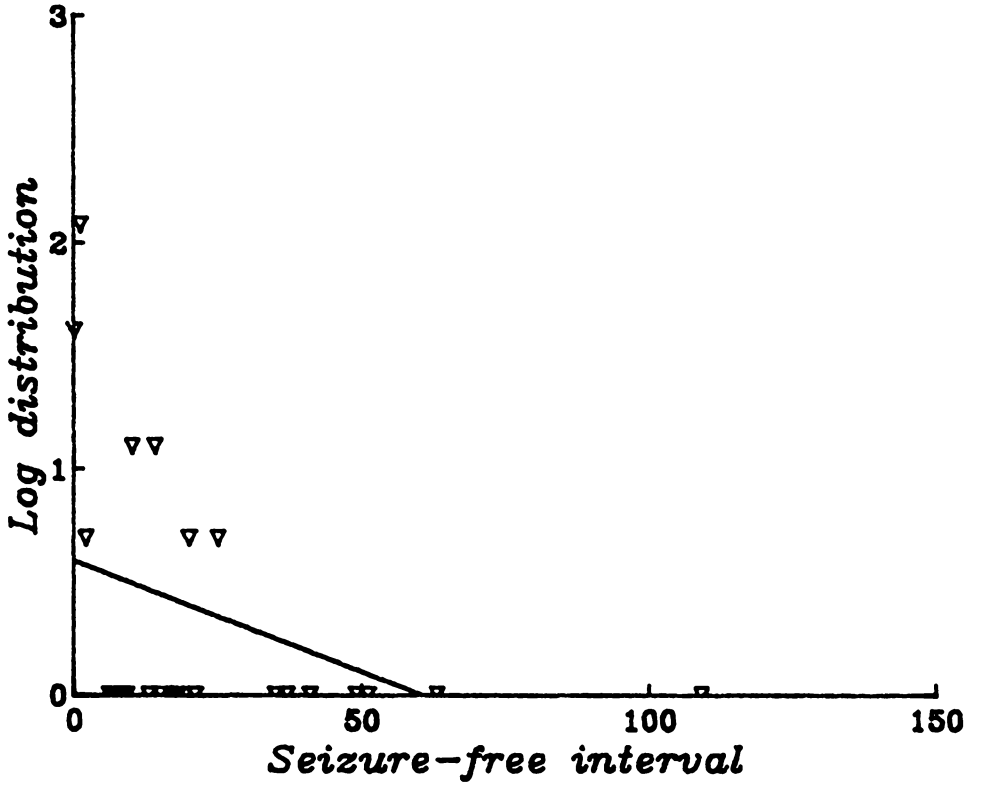

Figure 67: **Distribution of seizure-free intervals as a function of interval length for patient KD.** The x-axis shows the length of the seizure-free interval in days, and the y-axis shows the log of the number of seizure-free intervals of that length.

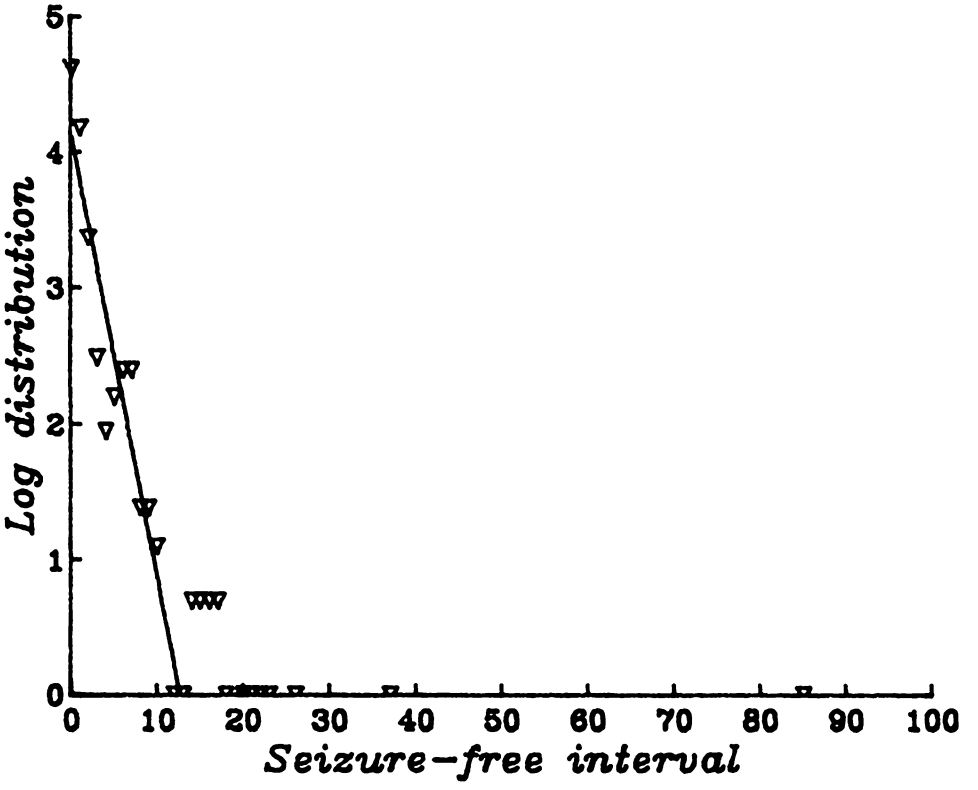

Figure 68: **Distribution of seizure-free intervals as a function of interval length for patient MAH.** The x-axis shows the length of the seizure-free interval in days, and the y-axis shows the log of the number of seizure-free intervals of that length.

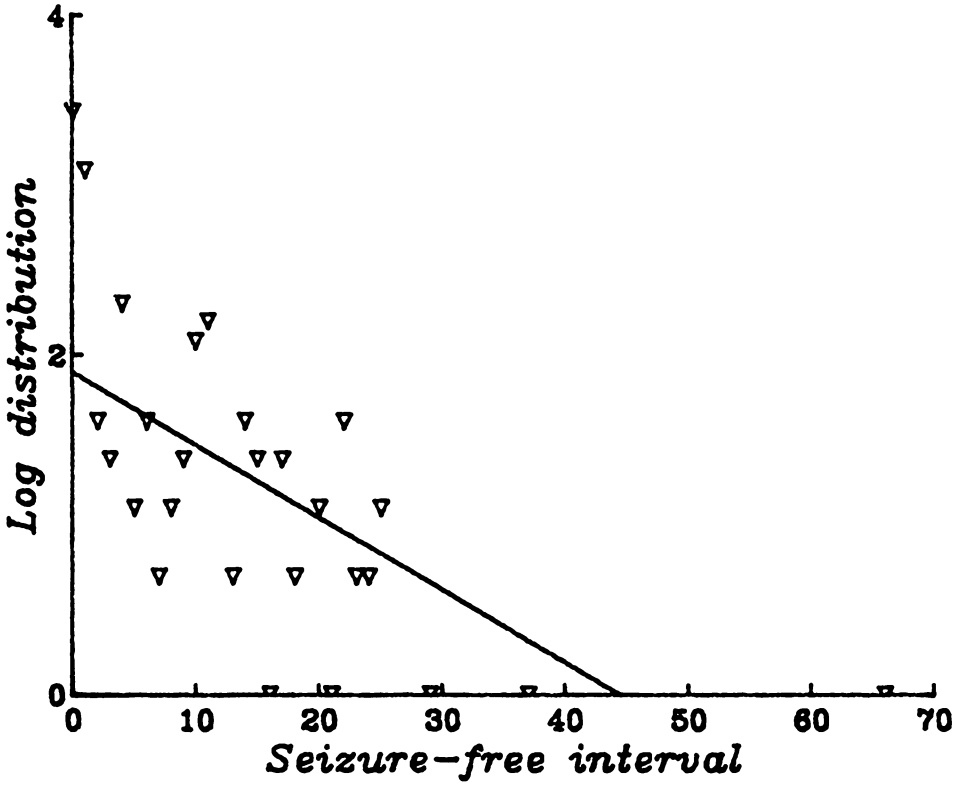

Figure 69: **Distribution of seizure-free intervals as a function of interval length for patient RK.** The x-axis shows the length of the seizure-free interval in days, and the y-axis shows the log of the number of seizure-free intervals of that length.

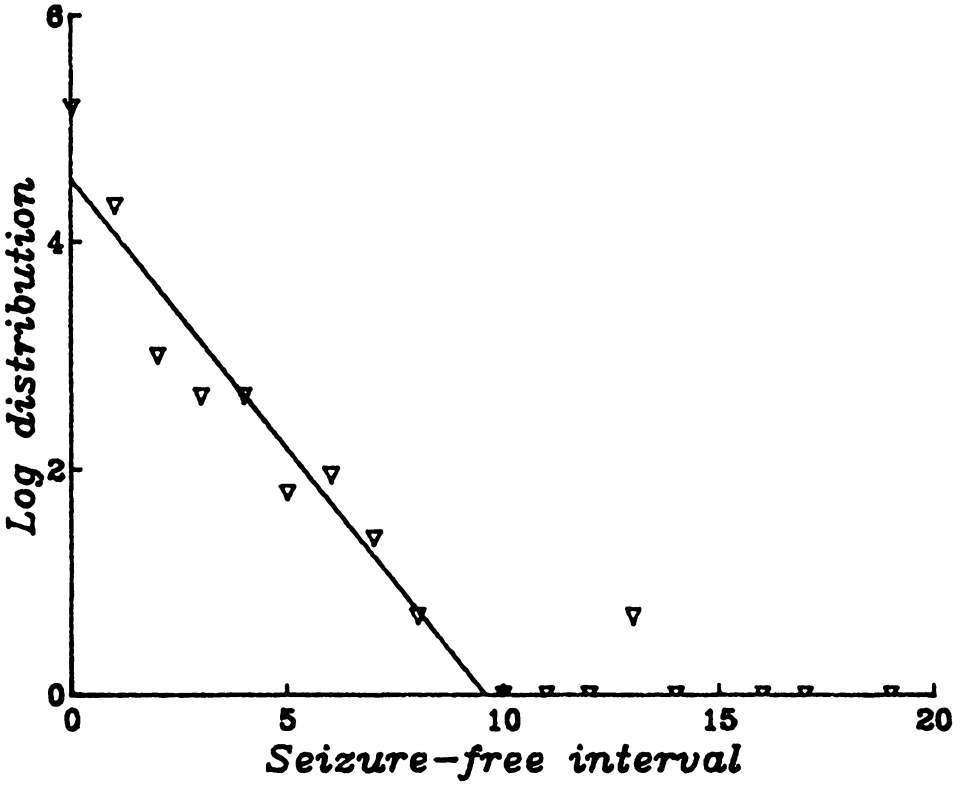

Figure 70: **Distribution of seizure-free intervals as a function of interval length for patient TV.** The x-axis shows the length of the seizure-free interval in days, and the y-axis shows the log of the number of seizure-free intervals of that length.

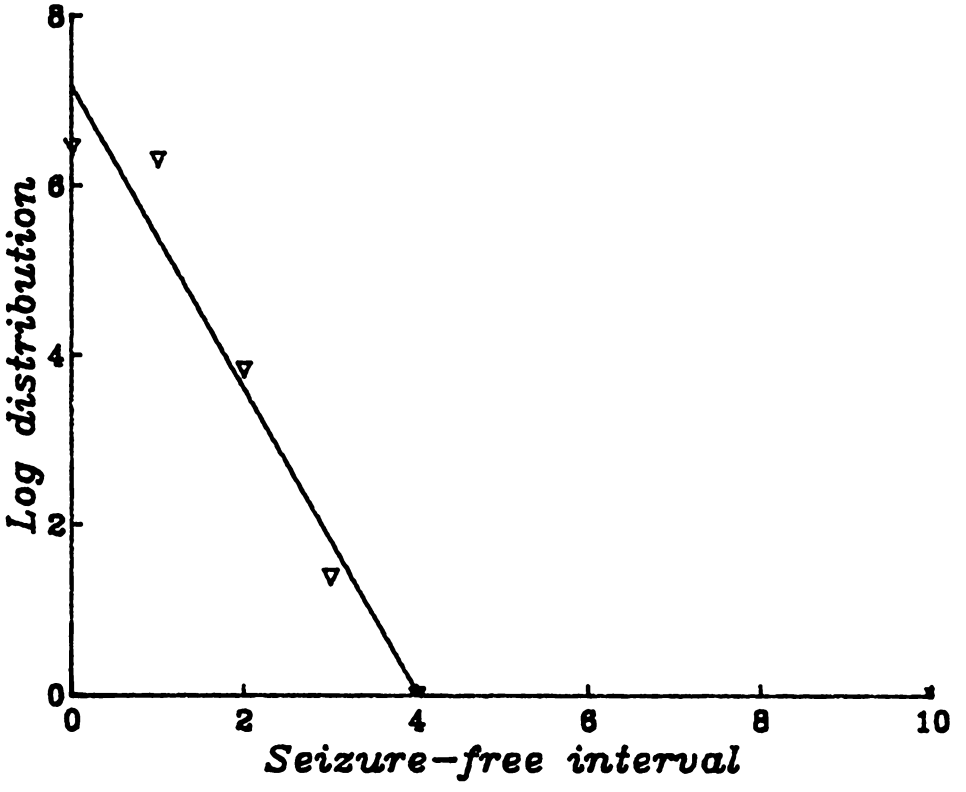

Figure 71: **Distribution of seizure-free intervals as a function of interval length for patient WC.** The x-axis shows the length of the seizure-free interval in days, and the y-axis shows the log of the number of seizure-free intervals of that length.

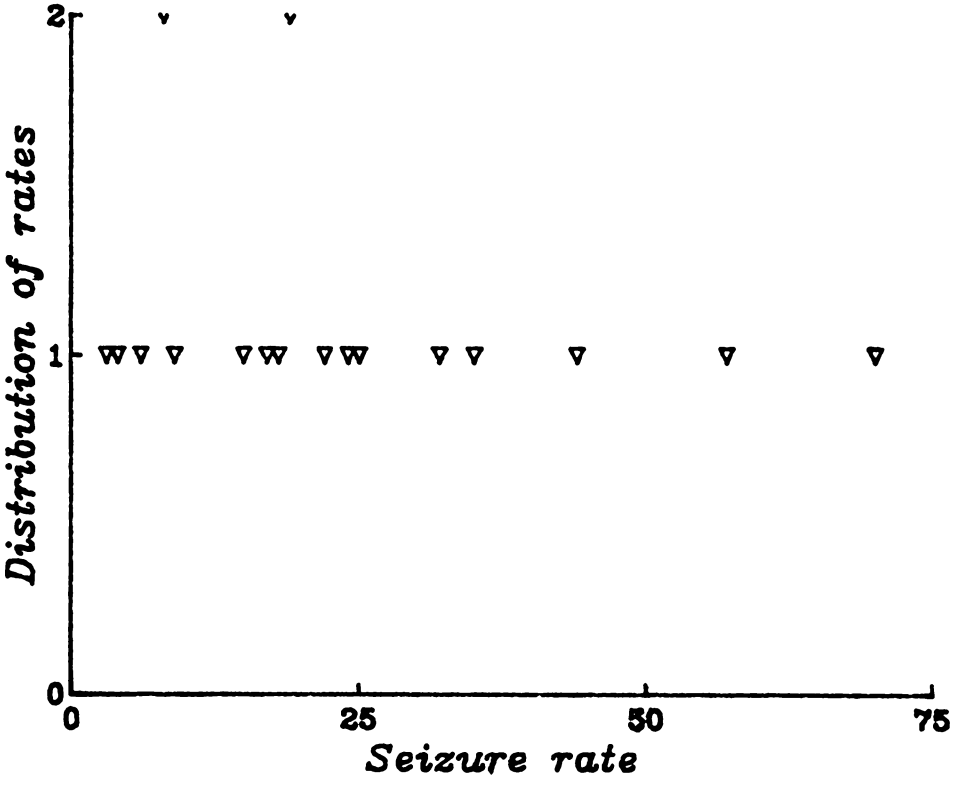

Figure 72: **Distribution of daily seizure rates as a function of seizure rate for patient BH.** The x-axis shows the daily seizure rate, and the y-axis shows the number of days on which a particular seizure rate occurred.

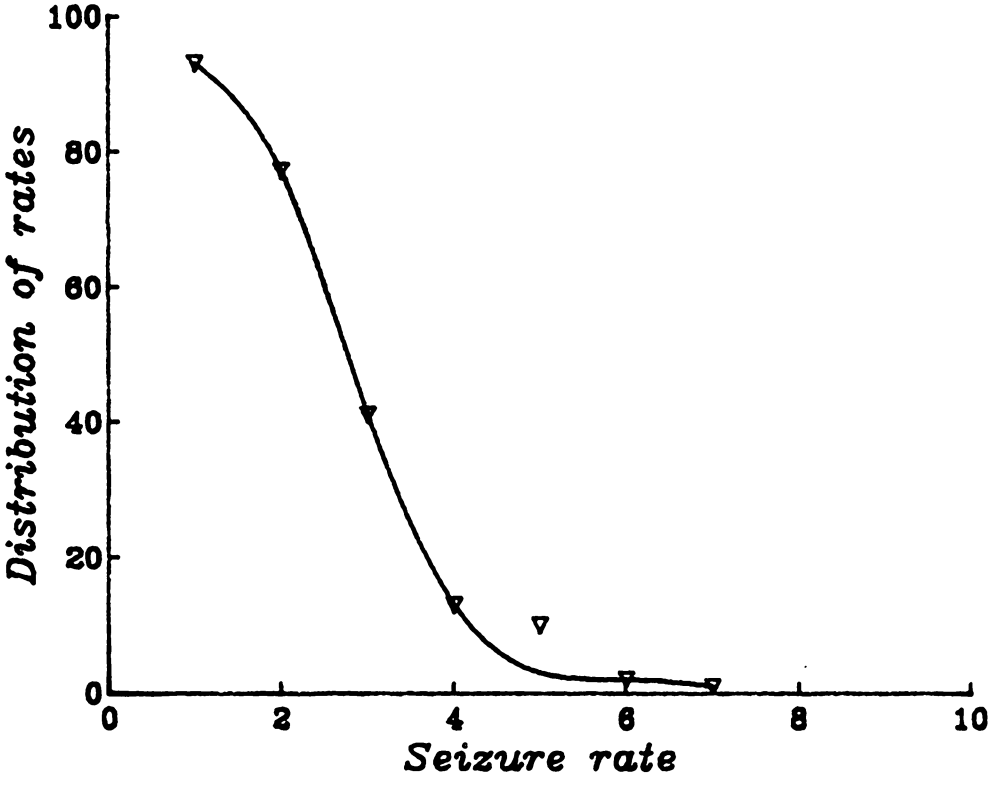

Figure 73: **Distribution of daily seizure rates as a function of seizure rate for patient CA.** The x-axis shows the daily seizure rate, and the y-axis shows the number of days on which a particular seizure rate occurred.

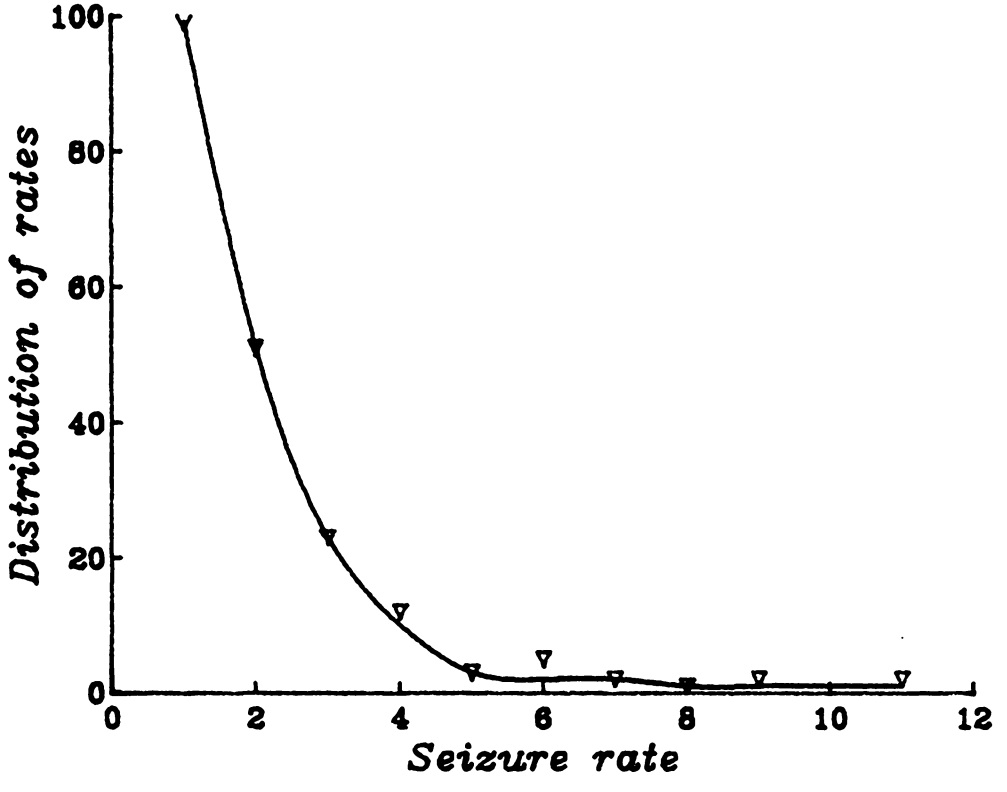

Figure 74: **Distribution of daily seizure rates as a function of seizure rate for patient ES.** The x-axis shows the daily seizure rate, and the y-axis shows the number of days on which a particular seizure rate occurred.

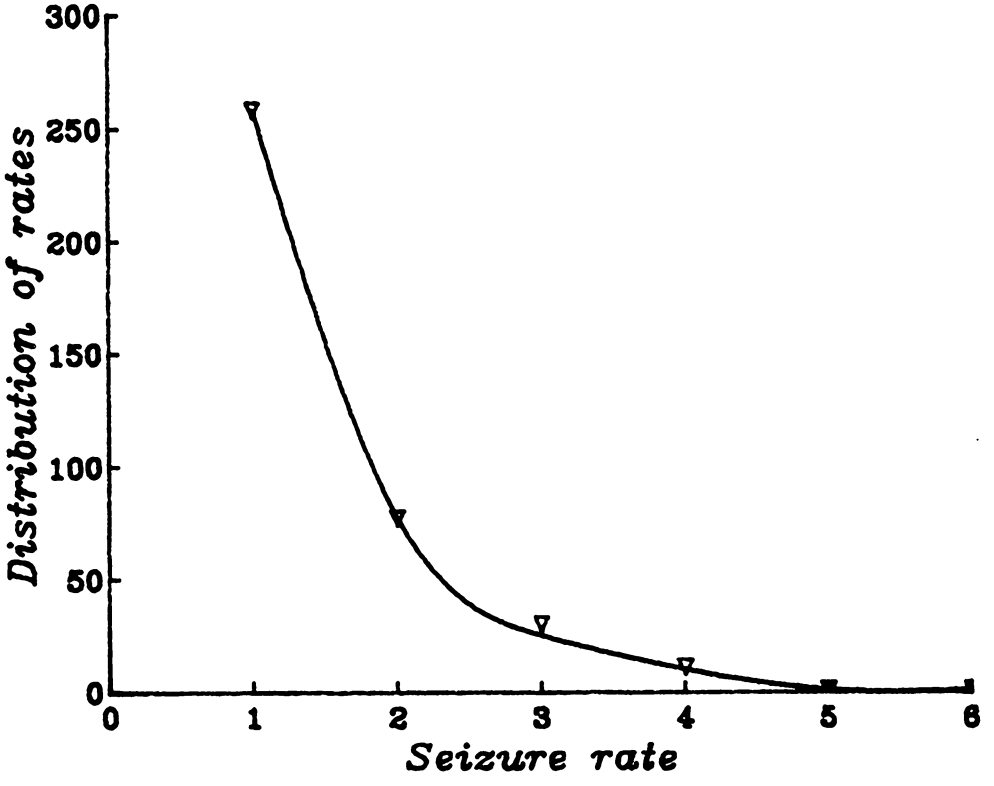

Figure 75: **Distribution of daily seizure rates as a function of seizure rate for patient JC.** The x-axis shows the daily seizure rate, and the y-axis shows the number of days on which a particular seizure rate occurred.

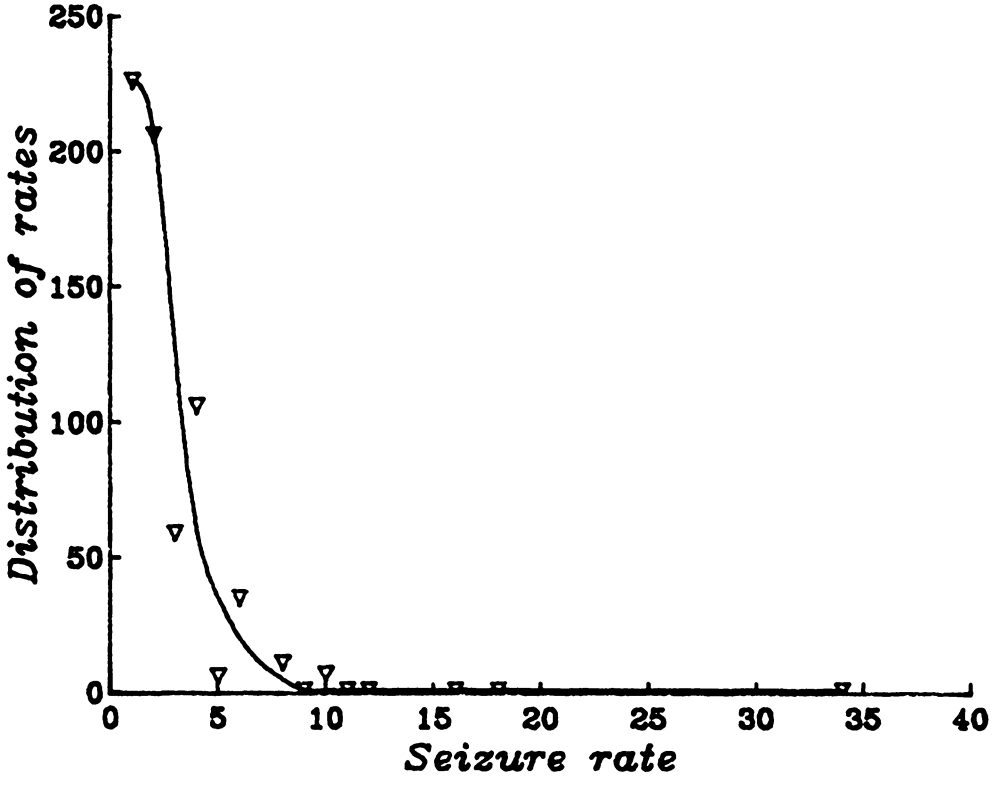

Figure 76: **Distribution of daily seizure rates as a function of seizure rate for patient JM.** The x-axis shows the daily seizure rate, and the y-axis shows the number of days on which a particular seizure rate occurred.

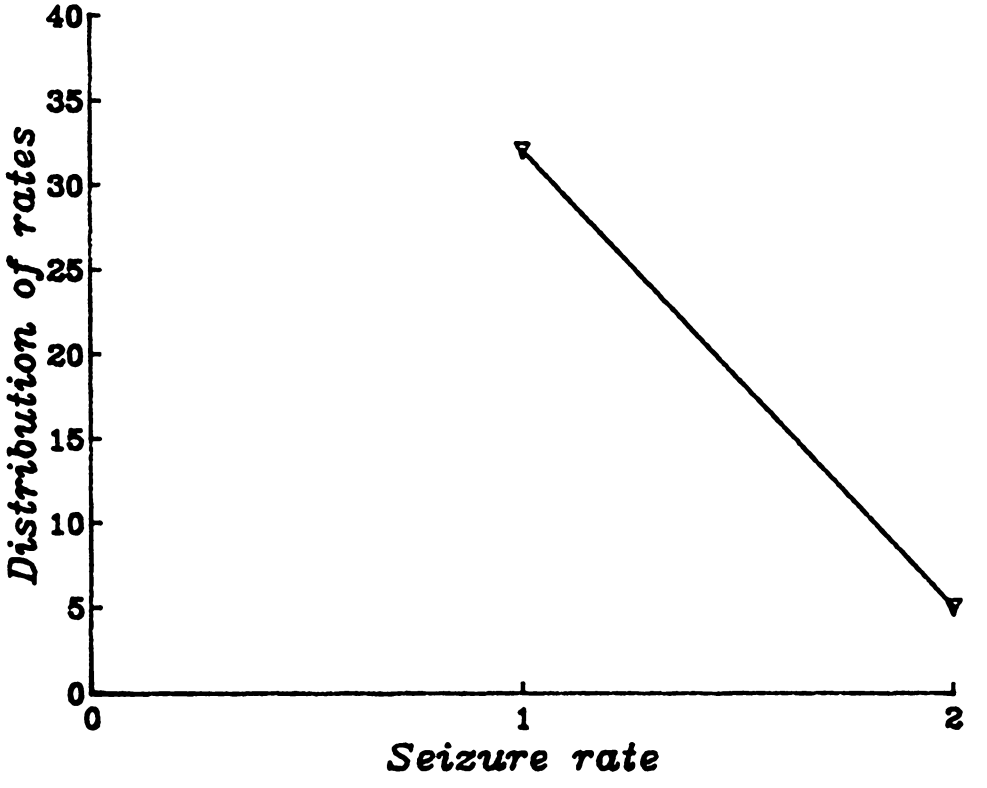

Figure 77: **Distribution of daily seizure rates as a function of seizure rate for patient KD.** The x-axis shows the daily seizure rate, and the y-axis shows the number of days on which a particular seizure rate occurred.

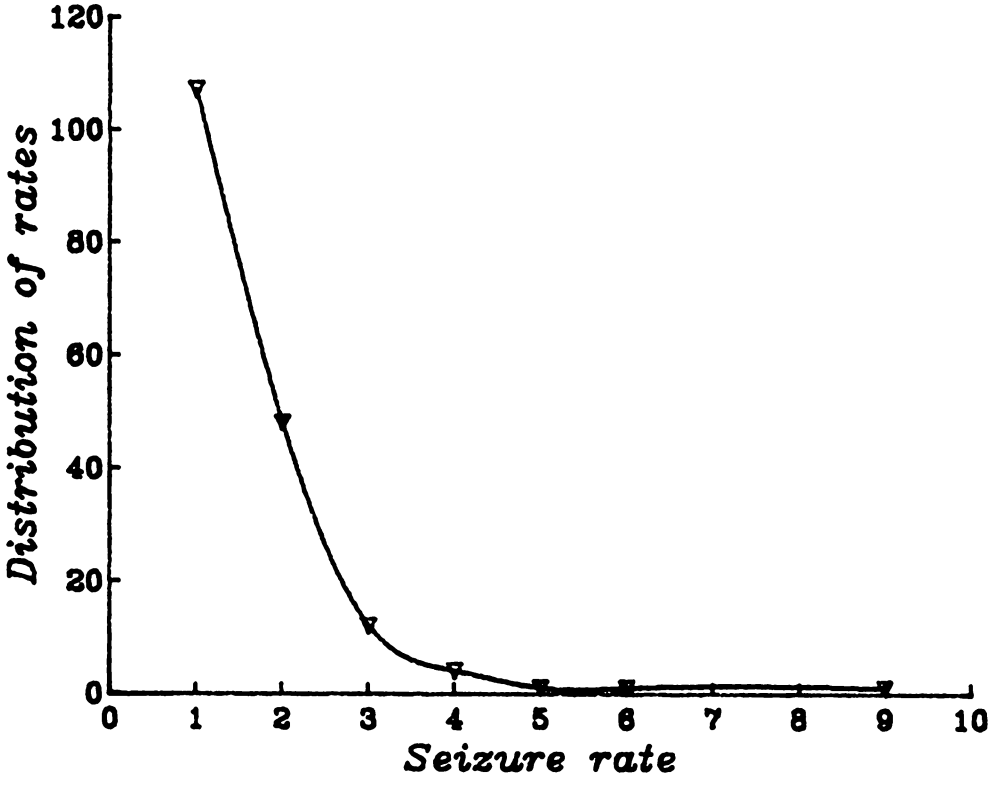

Figure 78: **Distribution of daily seizure rates as a function of seizure rate for patient MAH.** The x-axis shows the daily seizure rate, and the y-axis shows the number of days on which a particular seizure rate occurred.

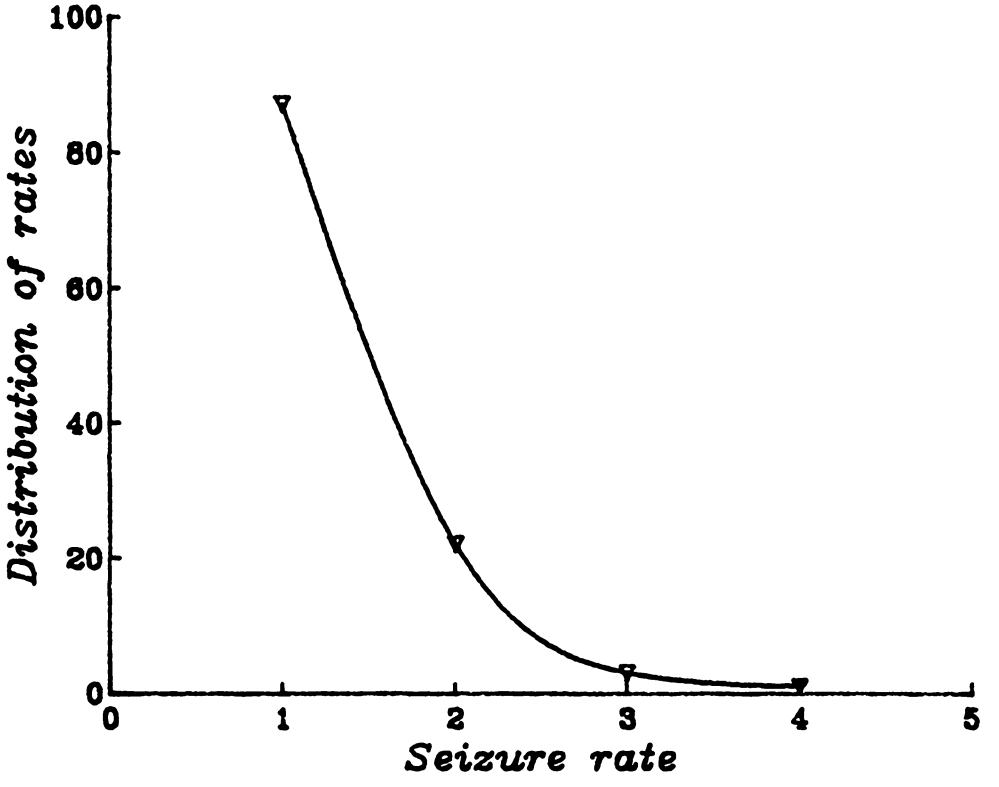

Figure 79: **Distribution of daily seizure rates as a function of seizure rate for patient RK.** The x-axis shows the daily seizure rate, and the y-axis shows the number of days on which a particular seizure rate occurred.

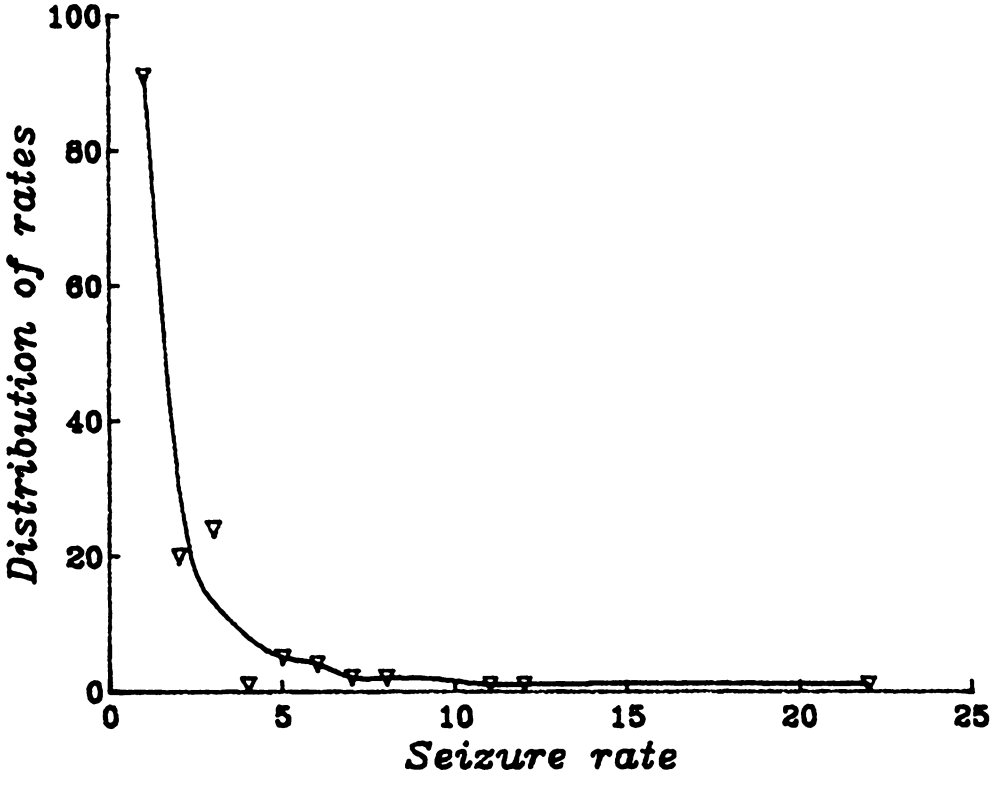

Figure 80: **Distribution of daily seizure rates as a function of seizure rate for patient TV.** The x-axis shows the daily seizure rate, and the y-axis shows the number of days on which a particular seizure rate occurred.

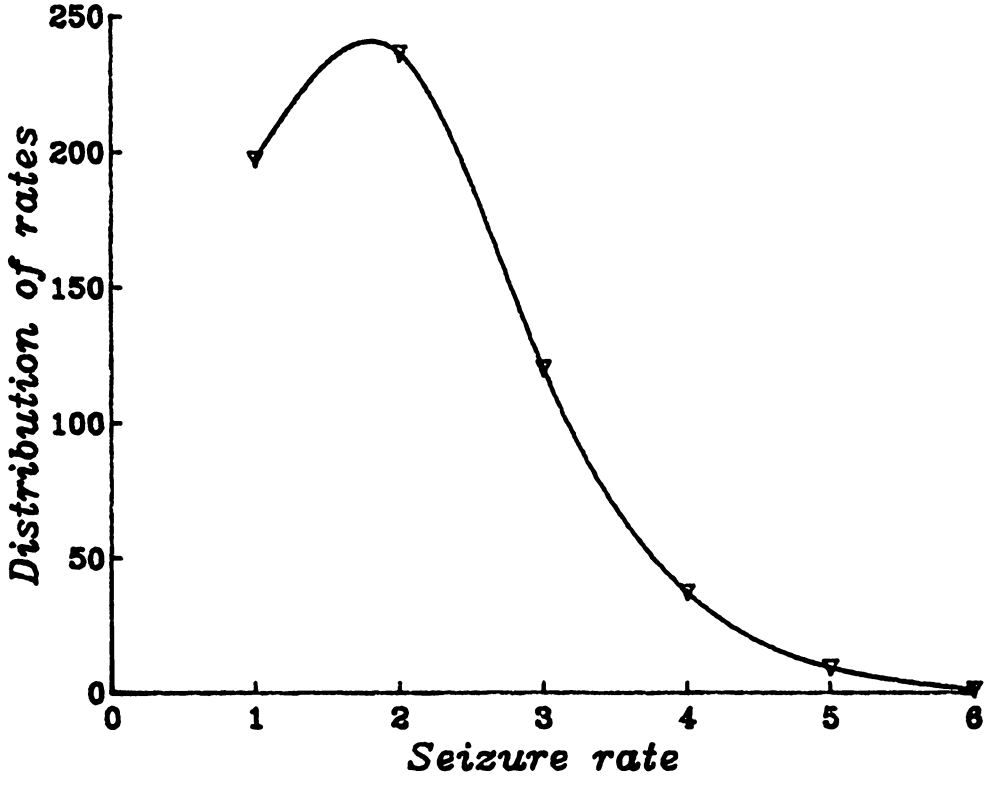

Figure 81: **Distribution of daily seizure rates as a function of seizure rate for patient WC.** The x-axis shows the daily seizure rate, and the y-axis shows the number of days on which a particular seizure rate occurred.

Appendix B

Data reduction techniques

As stated earlier, the raw data from the Epilepsies Clinic at Bowman-Gray School of Medicine is in ASCII form. Each patient's record consists of four files. The primary data reduction and display tool was a program written in C, which read the data files into memory using a simple parser [2] to translate the data into an internal representation. The representation chosen was a tree [88] in which each node was one day in the seizure calendar, and branches formed the seizure events for that day. Such a representation makes it particularly easy to compute such quantities as the average daily seizure rate and the seizure-free intervals.

Frequency histograms, such as those required for an analysis of seizure-free interval distribution, were represented as bucket and chain hash tables [2], with the bin numbers being hashed to bucket indexes and used to search for the bin on the chain. Hash tables were chosen because they permit having an indeterminate number of bins, limited only by available memory. A simple bin structure using an array referenced by bin numbers would require an a priori knowledge of the number of bins so that sufficient space could be allocated.

For analyses on the clinical data other than those programmed into the main analysis program, it was unnecessary to code complex C programs. Instead, the UNIX^{TM} utility

awk [56], which was developed particularly for such statistical analyses, was used. *Awk* can automatically parse data files into records and fields, performing operations of any desired complexity on selected records or fields. When combined with the Korn shell script language, *awk* provides a data reduction tool permitting rapid development of programs and reasonably fast execution. This was the technique used to analyze the EEG data as well.

The Monte-Carlo simulations were programmed in C instead of *awk* because the latter is too slow for such computationally intensive tasks (it is an interpreted language, whereas C is compiled). Furthermore, the UNIX™ C library contains several excellent random number generators particularly suited to Monte-Carlo simulations. Unfortunately, the microcomputer used for the simulations was slow and the Monte-Carlo simulations had to be restricted to smaller lattices. Large minicomputers such as the DEC VAX 8800 were entirely unable to perform the simulations, since the authors of their floating-point libraries thought it unnecessary to include a good random-number generator.

The primary data reduction and graphing tool will soon be available free of charge from Epilepsy Information, Inc. 819 S. Hawthorne Road, Winston-Salem, NC 27103. All other programs used in this research study can be obtained free of charge from the author.

The vita has been removed from the scanned document